PHOTOCONTROL OF ION PERMEATION IN LIPID VESICLES INCORPORATING AMPHIPHILIC DITHIENYLETHENE AND SPIROOXAZINE DERIVATIVES

A Thesis

Submitted to the Faculty of Graduate Studies and Research

In Partial Fulfillment of the Requirements

For the Degree of

Doctor of Philosophy

in

Chemistry

University of Regina

By

Yamuna Sangeetha Kandasamy

Regina, Saskatchewan

May 2016

UNIVERSITY OF REGINA

FACULTY OF GRADUATE STUDIES AND RESEARCH

SUPERVISORY AND EXAMINING COMMITTEE

Yamuna Sangeetha Kandasamy, candidate for the degree of Doctor of Philosophy in Chemistry**,** has presented a thesis titled, ***Photocontrol of Ion Permeation in Lipid Vesicles Incorporating Amphiphilic Dithienylethene and Spirooxazine Derivatives,*** in an oral examination held on April 15, 2016. The following committee members have found the thesis acceptable in form and content, and that the candidate demonstrated satisfactory knowledge of the subject material.

External Examiner:	Dr. Matthew Paige, University of Saskatchewan
Supervisor:	Dr. Scott Murphy, Department of Chemistry and Biochemistry
Committee Member:	Dr. Dae-Yeon Suh, Department of Chemistry and Biochemistry
Committee Member:	Dr. Andrew Wee, Department of Chemistry and Biochemistry*
Committee Member:	Dr. Adisorn Aroonwilas, Faculty of Engineering & Applied Science
Chair of Defense:	Dr. Andrew Cameron, Department of Biology

*Not present at defense

ABSTRACT

The photocontrol of ion permeation across a lipid bilayer membrane incorporating amphiphilic photochromic compounds, such as dithienylethenes (DTEs) and spirooxazines (SpOxs), has been investigated. In general, photochromic compounds change their molecular structure during photoisomerization. The effect of this photoisomerization on the membrane permeability of lipid vesicles has been examined. Specifically, three DTE derivatives **21**–**23** and three SpOx derivatives **24**–**26** were incorporated into a variety of lipid vesicles to study their potential as membrane disruptors. Initially, a regioselective approach was used to synthesize **21**–**23** that contain a dodecyl or hexyl chain terminated with a quaternary ammonium substituent, and methyl or phenylethynyl substituents at the reactive carbons. Similar to DTEs, SpOxs **24** and **25** contain charged tethers that differ only in the alkyl chain length, whereas **26** is the first bolaamphiphilic SpOx dimer with two large photochromic units.

Two different assays were used to assess the photocontrol of proton and potassium ion permeation in lipid vesicles. These assays examine the effect of the inclusion and photoisomerization of DTEs and SpOxs on membrane permeability. The results from the proton permeation assay showed that the open-ring isomers of DTEs **21**–**23** were more disruptive than the closed-ring isomers in the four lipid vesicle systems studied, regardless of their lamellar phase at room temperature. Also, a steric effect was clearly observed as DTEs incorporating the comparatively smaller methyl group exhibited lower rates of ion permeation than the bulkier phenylethynyl group. The inclusion of SpOxs **24**–**26** in lipid vesicles also significantly disrupts the bilayer

membrane and enhances proton permeation. The effect of chain length on membrane permeability was more pronounced for these SpOxs than the DTEs because DTEs **21** and **22** does not show any significant difference in either the rate constant of proton permeation or in the extent of proton permeation. Overall, 1,2-dioleoyl-*sn*-glycero-3-phosphatidylcholine (DOPC) vesicles incorporating **26** showed the highest permeability to protons.

Potassium ion permeation was examined in 1,2-dipalmitoyl-*sn*-glycero-3-phosphatidylcholine (DPPC) vesicles and DOPC vesicles. The rate constant for ion permeation and net change in the percentage of release were highly dependent on the lipid bilayer phase state and the alkyl chain length of the photochromic compound. In general, lipid vesicles including DTEs were less permeable to potassium ions than vesicles including SpOxs. Also, the open-ring isomers of all SpOxs were more disruptive than their closed-ring isomers. In addition, the difference in potassium ion permeability under UV and visible irradiation was more pronounced than previously reported photoresponsive membrane disruptors with reversible photocontrols. The membrane permeability of both DPPC and DOPC vesicles incorporating **24**–**26** increased in the following order of **25** < **24** < **26.** The structure-activity relationship exists for SpOxs in both lipids for the potassium ion permeation but only in DOPC vesicles for the proton permeation. A comparison of the activity of SpOxs in DPPC and DOPC vesicles revealed that **26** in DOPC vesicles exhibits good photocontrol of potassium ion permeation. All together, the proton and potassium ion permeation studies suggest that **26** in DOPC vesicles is the most photoresponsive system for the delivery of small molecules.

ACKNOWLEDGEMENTS

I am grateful to my supervisor, Dr. R. Scott Murphy, for the guidance, advice and support he provided throughout my graduate studies. The training I received during my time as a member of his research group has helped me develop better research, teaching and writing skills.

I would like to thank the other members of my supervisory committee, Dr. Renata J. Raina-Fulton, Dr. Andrew G. H. Wee, Dr. Dae-Yeon Suh, Dr. Adisorn Aroonwilas and Dr. Lynn M. Mihichuk for their suggestions and advice.

My past and present lab colleagues Mr. James Cai, Ms. Alisha Beler, Mr. John Ottaviano and Ms. Jemeli Sang are thanked for their friendship and for all help they offered over the years. Special thanks to Mr. James Cai for training me on the lab techniques. I also thank Dr. Chuanzhong Wang for his assistance with the NMR experiments.

I gratefully acknowledge the financial support from the Faculty of Graduate Studies and Research, the Department of Chemistry and Biochemistry, and the Natural Sciences and Engineering Research Council (NSERC) grant of Dr. R. Scott Murphy.

My special thanks to my husband Arumugam Jayaraman, who has been very supporting to my studies, and sharing good and bad times together with me over these years. Many thanks to my parents Kandasamy and Sethupathy, my sister Sabitha and her family, and my in-laws for their love and support throughout my time here.

To my parents, my son Ajay and my niece Ponshika

TABLE OF CONTENTS

LIST OF TABLES

LIST OF FIGURES

LIST OF SCHEMES

LIST OF ABBREVIATIONS AND SYMBOLS

A	absorbance
br	broad
BuLi	butyllithium
C_0	concentration of potassium ion at time t_0
C_f	concentration of potassium ion when the vesicles are lysed
C_t	concentration of potassium ion at time t
CF	carboxyfluorescein
d	doublet
dd	doublet of doublets
DHP	dihexadecyl phosphate
diPhyPC	1,2-diphytanoyl-*sn*-glycero-3-phosphatidylcholine
DPPC	1,2-dipalmitoyl-*sn*-glycero-3-phosphatidylcholine
DOPC	1,2-dioleoyl-*sn*-glycero-3-phosphatidylcholine
DSPE	1,2-distearoyl-*sn*-glycero-3-phosphoethanolamine
DTE	dithienylethene
δ	chemical shift in NMR
Δ	heat
E_{403}	emission intensity at wavelength 403 nm
E_{460}	emission intensity at wavelength 460 nm
EYPC	egg yolk *L*-α- phosphatidylcholine

EI	electron impact
ESI	electrospray ionization
ε	molar absorption coefficient
h	Planck constant
HPTS	8-hydroxypyrene-1,3,6-trisulfonic acid trisodium salt
HRMS	high-resolution mass spectrometry
I_0	relative emission intensity at time t_0
I_f	relative emission intensity when vesicles are lysed
I_t	relative emission intensity at time t
J	coupling constant
K_D	dissociation constant
k_{H+}	rate constant of proton permeation
k_{K+}	rate constant of potasssium ion permeation
LUV	large unilamellar vesicle
m	multiplet
MC	merocyanine
MHz	megahertz
MLV	multilamellar vesicle
m/z	mass-to-charge ratio
n	Hill coefficient
N	extent of proton permeation
NA	Avogadro's constant

NBS	*N*-bromosuccinimide
NMR	nuclear magnetic resonance
OFCP	octafluorocyclopentene
PC	phosphatidylcholine
PEG	polyethylene glycol
ppm	parts per million
PSS	photostationary state
R_f	retention factor
s	singlet
SP	spiro
SpOx	spirooxazine
SUV	small unilamellar vesicle
t	triplet
T	transmittance
THF	tetrahydrofuran
TLC	thin layer chromatography
UV	ultraviolet light
vis	visible light
ν	frequency of light
Y	fractional activity
ϕ	quantum yield
λ_{em}	emission wavelength

λ_{ex}	excitation wavelength
λ_{max}	wavelength of maximum absorption
λ_c	cut-off wavelength

CHAPTER 1

INTRODUCTION

1.1. Photochromic Compounds

Photochromic compounds are molecules that undergo a reversible chemical reaction in the presence of light of appropriate wavelength. This light induced process is called photochromism. Photochromic isomers that result from the photochemical reaction differ not only in their absorption properties, such as color but can also have different physical and chemical properties such as geometric structure, refractive index, dielectric constant, and oxidation/reduction potentials.[1] As a result, photochromic compounds have been continuously used in the development of various photoresponsive systems and materials. Some common families of photochromic compounds are azobenzenes, spiropyrans, spirooxazines (SpOxs), fulgides and dithienylethenes (DTEs) (Figure 1.1). These compounds have been applied as photoswitches[2,3] and commonly used in the field of optoelectronics[4]. The reversible photochemical reactions that take place in these compounds are mainly based on *cis-trans* isomerization and electrocyclic reactions. Specifically, the photochromic properties of azobenzenes are due to the *cis-trans* isomerization about the N=N bond (Figure 1.1). The photochromic properties of spiropyrans, SpOxs, fulgides and DTEs, on the other hand, are due to electrocyclic reactions (Figure 1.1). Photochromic compounds can be classified into two categories based on the thermal stability of their photoisomers. Thermally reversible photochromic compounds are classified as T-type, and compounds of such type are azobenzenes,

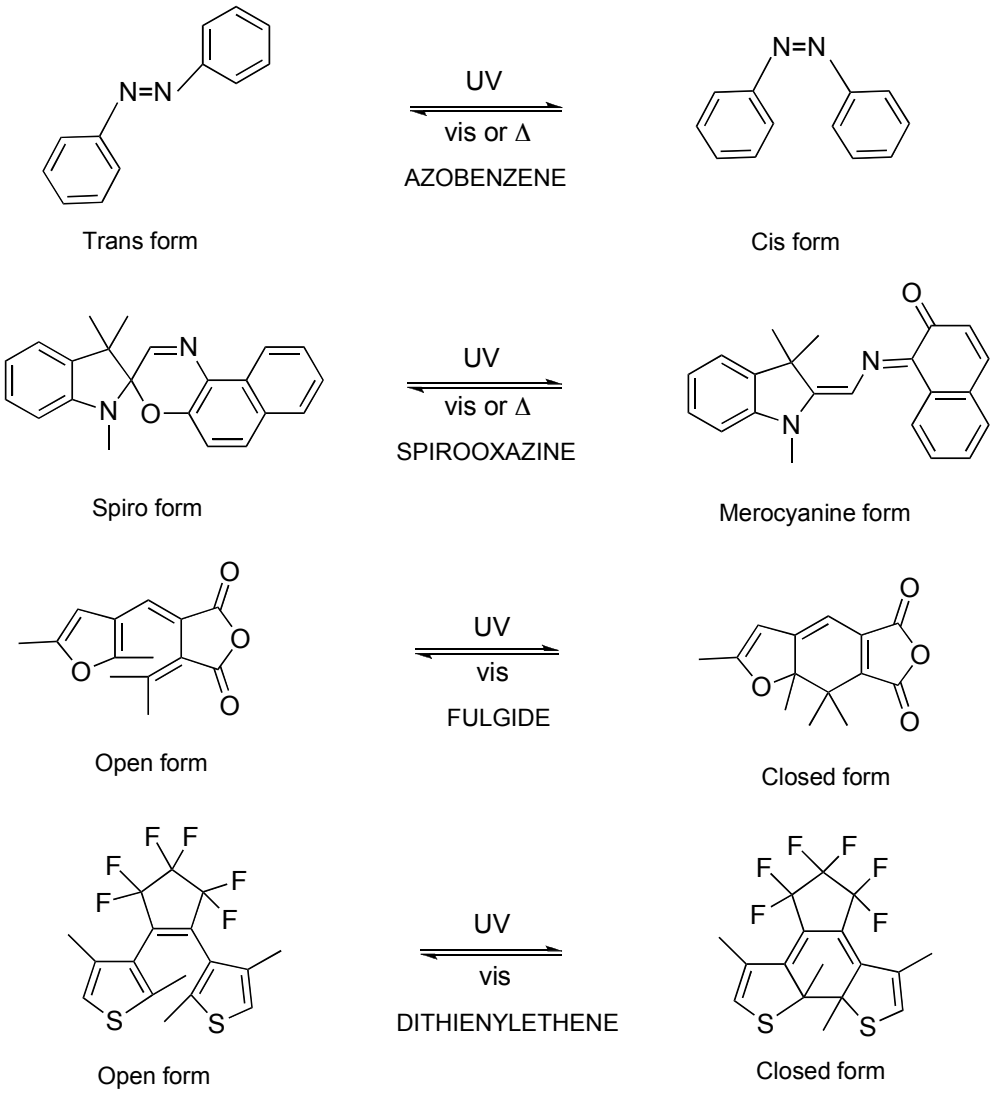

Figure 1.1. Representative examples of photochromic compounds.

spiropyrans and SpOxs; whereas thermally irreversible compounds are classified as P-type, and representative compounds of this type are fulgides and DTEs.[5] The photogenerated isomers of T-type compounds may undergo isomerization to their initial forms in the presence of light or heat, whereas the photogenerated isomers of P-type compounds are thermally irreversible and require light to isomerize to their initial forms.

Although all these compounds exhibit reversible photochromism, some have drawbacks that limit their application. For instance, many of the azobenzene derivatives show overlapping absorption bands for their two different photoisomers in the UV region, which significantly prevents selective excitation. In spiropyrans, the overlapping of absorption bands is uncommon; but their thermal reversibility is often compromised due to competing degradation processes. Since my interests are to develop photoresponsive lipid vesicles, photochromic compounds such as DTEs and SpOxs were chosen that avoid these drawbacks to certain extent. In the upcoming sections, I will describe the photochemical mechanisms for DTE and SpOx isomerization, the formation of photodegradation products and its consequences, and some important photochromic properties.

1.2. Dithienylethenes

DTEs undergo reversible isomerization between open-ring and closed-ring isomers when irradiated with light of a particular wavelength (Figure 1.2A). The photoisomerization of DTEs involve an electrocyclic reaction.[6] In this reaction, the bonds are formed or broken at the termini of a conjugated π systems (Figure 1.2B).

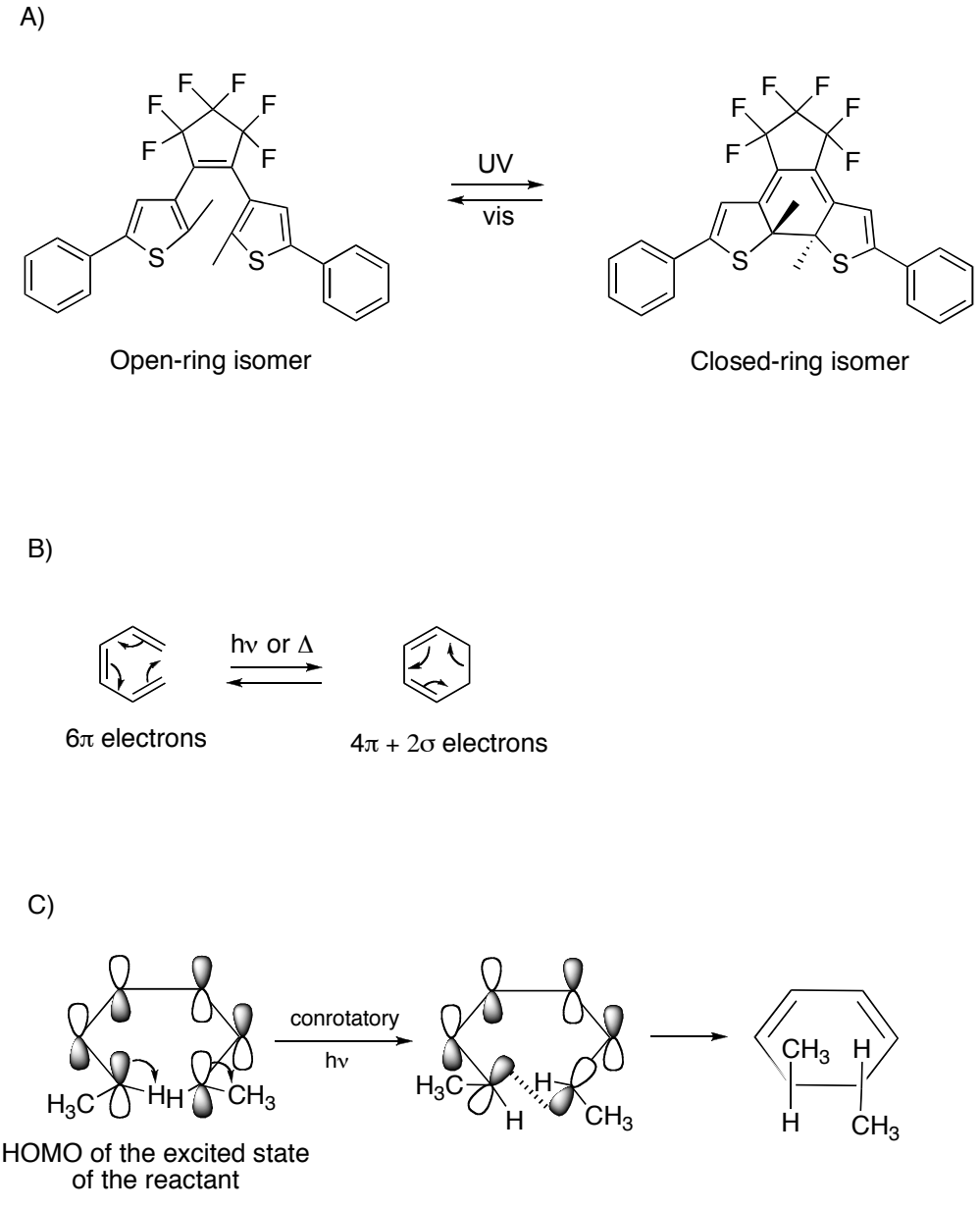

Figure 1.2. Photochromism of DTE A) Open-ring and closed-ring isomers of DTE, B) The rearrangement of 6π electrons in hexatriene via an electrocyclic reaction to give cyclohexadiene, and C) Formation of a σ bond by overlap of *p* orbitals at termini through a conrotatory mode.

During the ring-closure reaction a σ-bond is formed, at the cost of a π-bond, between the termini of a conjugated π system. In the ring-opening process, the newly formed σ-bond breaks to give back a conjugated π system.[7] The electrocyclic reaction is highly stereospecific, and the stereochemistry of the product can be predicted by Woodward-Hoffmann rules. According to the rules, the electrocyclic reactions of a 6π electron system proceeds through a conrotatory rotation under photochemical conditions. In this conrotatory mode, the bonds are formed to opposite faces of the π system. As a result, the substituents at the reactive carbons are *trans* to one another about the plane of the ring system (Figure 1.2C).[8]

The photoisomerizable open-ring and closed-ring isomers of DTE show well-separated absorption bands. In the open-ring isomer, the π-electrons of DTE are localized within the thiophene unit; whereas in the closed-ring isomer they are conjugated and delocalized throughout the molecule (Figure 1.3).[9] Thus, the open-ring isomer has absorption spectra in the UV region, and the closed-ring isomer has absorption spectra in the visible region.

The open-ring isomer of DTE has two possible conformations. They are (i) parallel conformation (C_s or mirror symmetry), and (ii) antiparallel conformation (C_2 symmetry) (Figure 1.3).[9] These conformers exist due to the free rotation of C–C single bond between the thiophene rings and the cyclopentene ring. The parallel and antiparallel conformers of most DTEs interchange on a very fast time-scale, even at -90 °C.[10] As a result, ^{1}H NMR analysis shows only one set of time-averaged signals. However, two sets of ^{1}H NMR signals were reported for the two open-ring conformers of

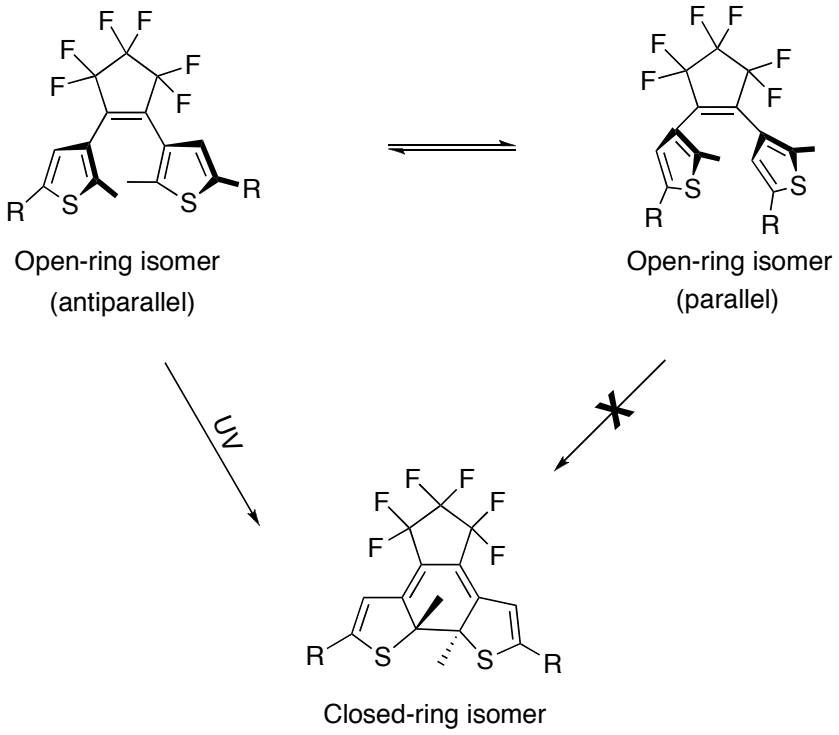

Figure 1.3. Parallel and antiparallel conformations of open-ring isomer.

a DTE that has bulky substituents at the C2 position of the thienyl groups, preventing their free rotation.[11] Among these two open-ring conformers, the photocyclization reaction proceeds only from the antiparallel conformer, as a molecule with C_2 symmetry has favorable geometry for the ring closure reaction via a conrotatory mode.[12] Therefore, the presence of parallel conformer affects the efficiency of the photocyclization reaction. Quantifying the efficiency of a photochemical reaction is represented by the quantum yield (ϕ), which is defined as the ratio of number of photons absorbed per unit time to the number of reacted molecules per unit time. An increase in the quantum yield for the ring closure reaction can be observed when bulky substituents are present at the C2 position of thienyl rings, which increases the steric strain and decreases the ratio of the parallel conformer to the antiparallel conformer.[13]

1.2.1. Fatigue Resistance

Fatigue resistance is another factor, which also affects the quantum yield of a photochemical reaction. Fatigue resistance refers to the resistance to the loss of reversibility due to competing processes such as photodegradation and photooxidation. These photochemical side reactions involve the rearrangement of chemical bonds and leads to the formation of photo and thermally irreversible photoproducts. These side reactions in turn affect the cyclization and cycloreversion quantum yields. Although DTEs are known for their fatigue-resistant properties, some can undergo photodegradation after a limited number of isomerization cycles, even in absence of oxygen.[14,15] The formation of photogenerated side products **2** and **3** from the closed-ring

isomer **1** is illustrated in Figure 1.4A. In this, compound **2** was observed mostly after a prolonged irradiation of **1** with UV light.[14] Compound **3** was observed after 500 isomerization cycles in the presence of air.[15]

One of the possible reaction routes for the formation of photodegraded product is shown in Figure 1.4B.[5,16] In the closed-ring isomer, the C_1–S_8 bond length (1.829 Å) seems lengthier than the normal C–S single bond length (1.719 Å), which could have facilitated the homolytic cleavage of the C_1–S_8 bond in the photoexcited state. In the next step, the formation of the C_1–C_5 bond takes place through the migration of radicals to form intermediate **4**. Then, the side-product **5** resulted from cleavage of the C_5–C_6 bond followed by formation of the C_6–S_8 bond. This photodegradation can be minimized by substitution of the hydrogens at C4 and C4′ positions of the thiophene rings in **1** with methyl groups or replacing the thiophene ring systems with benzothiophene systems.[4,16] It was also reported that DTEs containing a perfluorocyclopentene moiety show higher fatigue resistivity than perhydrocyclopentene in the presence of air and at temperatures over 80 °C.[3] This could be due to a difference in the electron densities of the central cyclopentene moieties.[17] The electron rich perfluorocyclopentene moiety may inhibit radical migration and the formation of photostable by-products. All of these factors were considered when designing DTEs for my studies. In the next section, the common synthetic routes to DTEs containing the perfluorocyclopentene moiety are discussed.

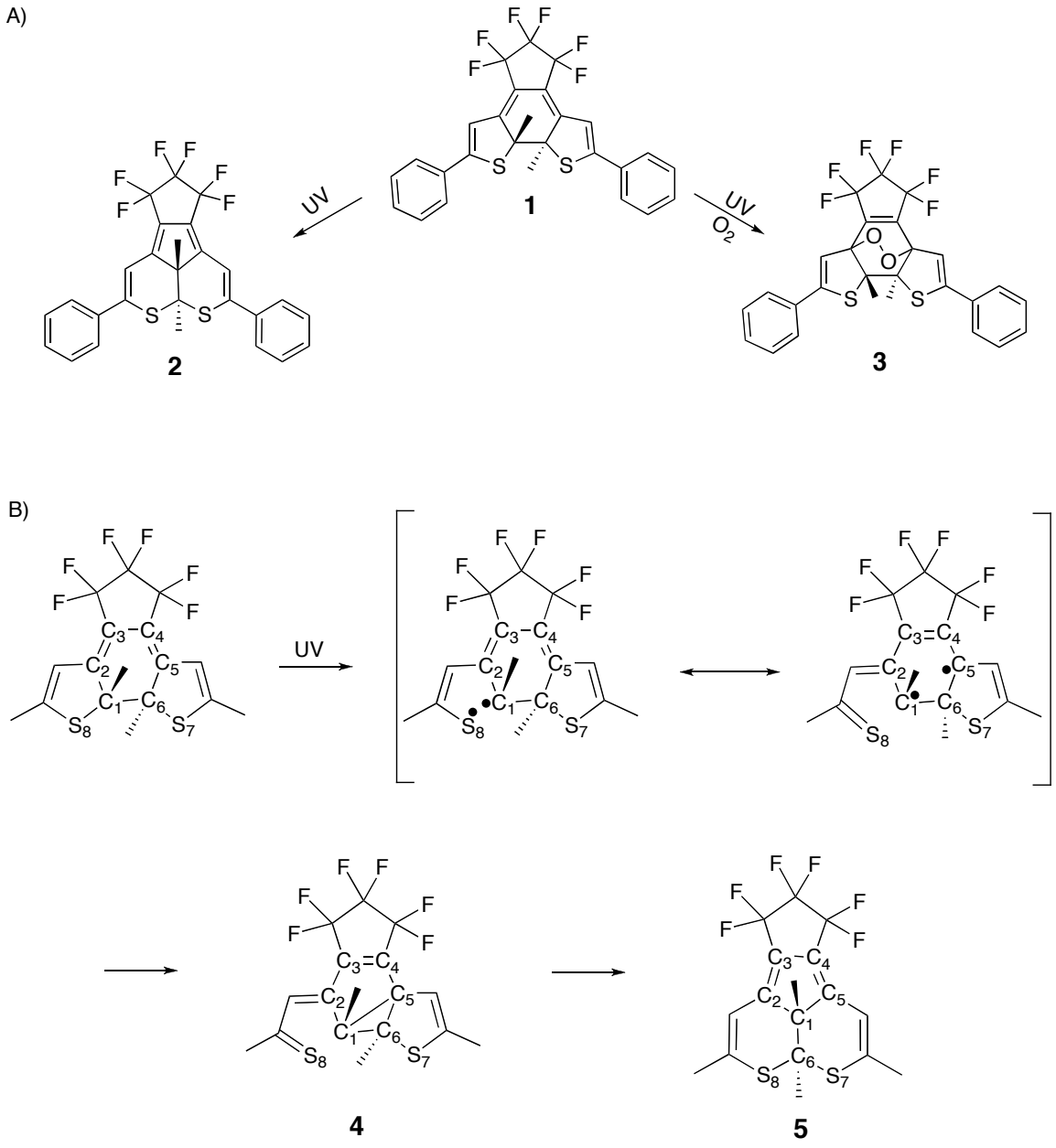

Figure 1.4. Photodegradation of DTE (A) Formation of photodegraded products from closed-ring isomer, and (B) Possible mechanism for the formation of photodegraded product.

1.2.2. General Methods of Synthesis of DTEs Containing Perfluorocyclopentene Moiety

To date, various derivatives of DTE have been synthesized, which include symmetrical, [18-20] asymmetrical,[21-23] amphiphilic,[24,25] and multiphotochromic dimers[26-28]. A number of methods have been reported for the synthesis of DTEs, and some of these are described briefly in this section. The most common method used for the synthesis of DTEs is based on the coupling of octafluorocyclopentene with lithium derivatives of thiophene. This method is used for the synthesis of both symmetrical and asymmetrical DTEs (Scheme 1.1A).[29] The treatment of bromide derivative **6** with butyl lithium gives lithiated thiophene derivative **7** followed by reaction with octafluorocyclopentene yields symmetrical DTE derivative **8**.[18-20] Asymmetrical DTE derivative can be selectively prepared by controlling the ratio of aryllithium and octafluorocyclopentenes. By using an equimolar ratio, only one of the fluorine atoms at the double bond of cyclopentene will be replaced and monosubstituted product **9** can be isolated.[23,30] Further reaction with a different substituted thiophene derivative **10** under standard conditions affords asymmetrical DTE **11**.

Another method by which both symmetrical and asymmetrical DTEs can be synthesized is based on intramolecular McMurry cyclization reaction.[31] In this method, the central DTE backbone is initially formed and followed by subsequent functionalization on thiophene units (Scheme 1.1B).[32] The synthesis of DTE involves bromination of 2-chloro-5-methylthiophene **12** to give compound **13**. The regioselectively lithiated product of **13** was then reacted with diethyl hexafluoropentanedioate **14** to form dithienyl diketone **15** followed by intramolecular

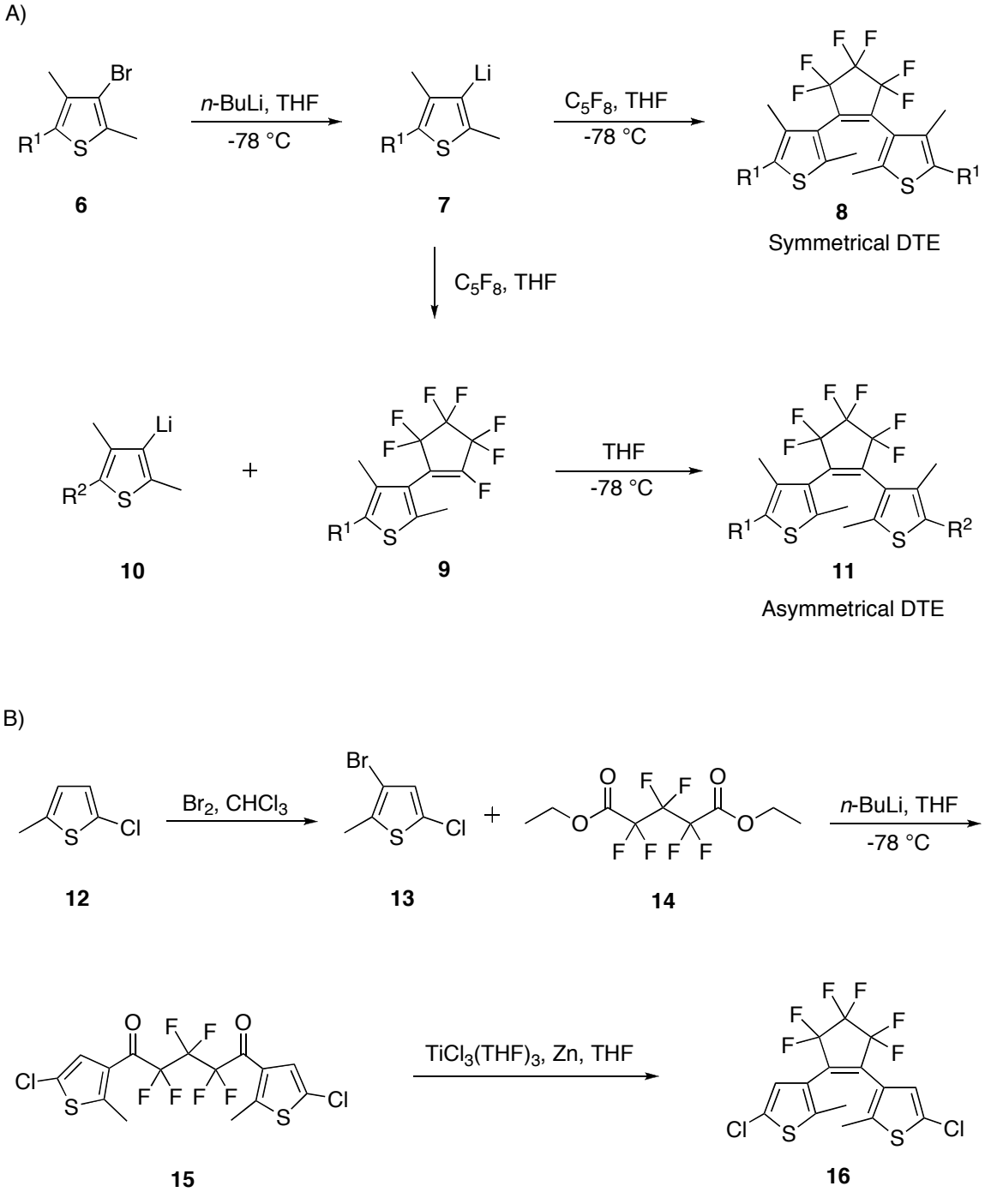

Scheme 1.1. Methods of synthesis of DTE derivatives via (A) octafluorocyclopentene coupling reaction and (B) McMurry coupling reaction.

cyclization reaction (McMurry ring-closing reaction) of **15** to give **16**. The various symmetrical and asymmetrical derivatives can be synthesized by following subsequent reaction. A Suzuki reaction of **16** with various aryl boronic acids,[33] or replacement of chlorine atoms in **16** with lithium using butyl lithium followed by coupling with various alkyl and aryl halides.[3,34] In my studies, I followed the first method to synthesize the desired DTE derivatives. In McMurry reactions central DTE backbone has to be initially prepared, which provides some limitations to the relative substitution order on thiophene because of having reactive alkynyl substituents in the central DTE backbone. Thus, first method was used with regioselective approach that introduces functional groups at periphery of the thiophene prior to the introduction of the alkynyl substituents. In the next section, a brief overview of SpOxs is presented.

1.3. Spirooxazines

SpOxs are another type of organic photochromic compound that undergo a reversible isomerization reaction when irradiated with light of appropriate wavelength or with heat. SpOxs have been mainly applied in photonic devices[35], chemo- and biosensors.[36] In addition, they have been used in drug delivery systems.[37,38] The reversible isomerization reactions of SpOxs are shown in Figure 1.5A. SpOxs exist in two isomers namely, the closed-ring spiro (SP) isomer and the open-ring merocyanine (MC) isomer.[36] The SP form undergoes heterolytic cleavage of the C_{spiro}–O bond upon irradiation with UV light followed by isomerization leads to the formation of the MC form (Figure 1.5B).[39] The MC form can be converted back to the closed-ring SP form

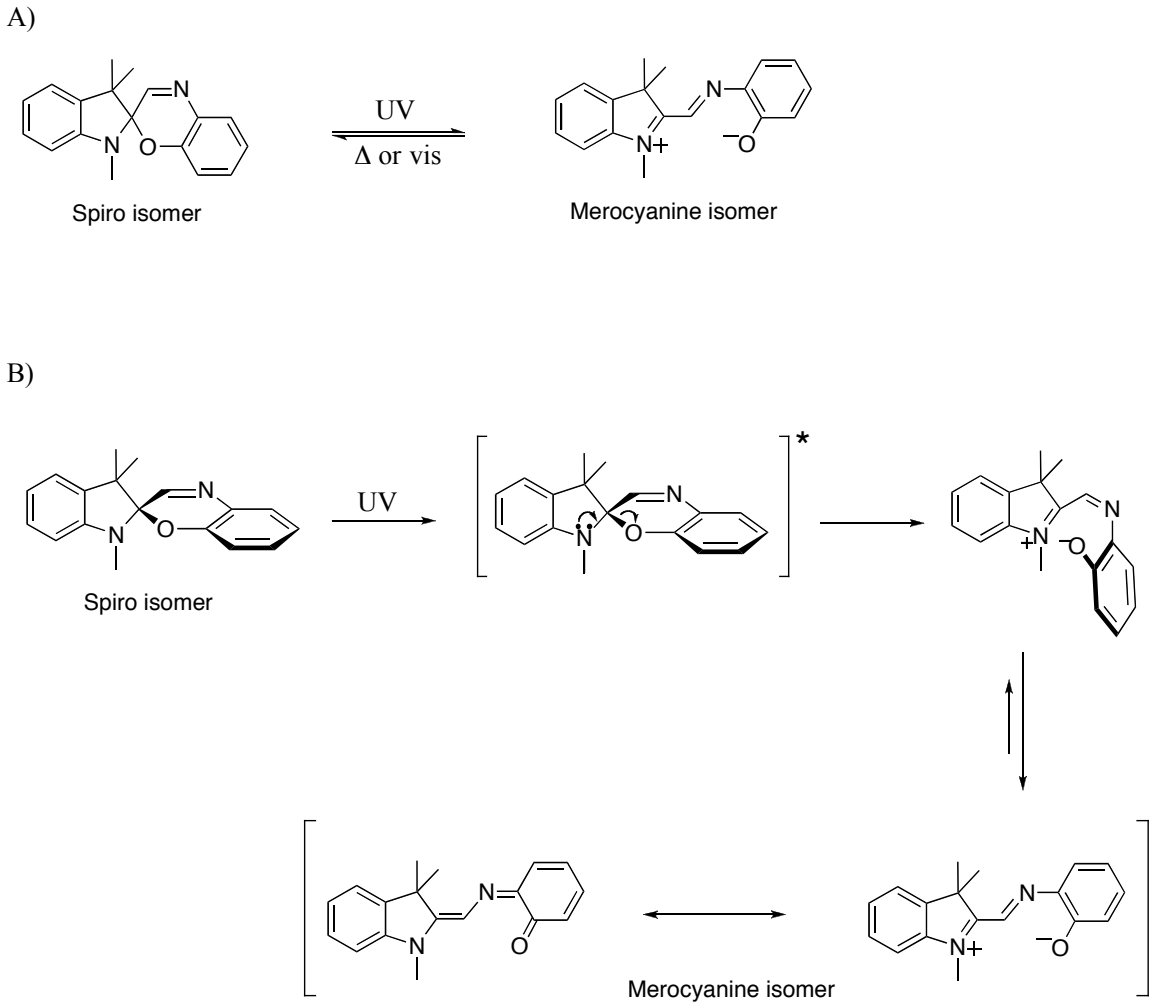

Figure 1.5. A) Reversible isomerization of a SpOx derivative, and B) Mechanism of photoisomerization of spiro isomer (This figure was adapted from reference 39).

either photochemically by irradiation with visible light or thermally. One of the resonance forms of the MC isomer is zwitterionic in nature, which results in the MC form being more polar than the SP form. The SP form consists of an indoline and an oxazine moiety connected together through a spiro junction and oriented perpendicular with respect to one another. The planar MC form with extended π-conjugation absorbs in the visible region, which is well-separated from the absorption of the SP form in the UV region.[36,40] SpOxs are well known for greater resistance to photodegradation than the structurally related spiropyrans.[40-42] The higher photodegradation resistance in SpOxs is due to the presence of the nitrogen atom in the oxazine moiety.

SpOxs are unique among other photochromic compounds due to various physical and chemical properties between two isomers.[39] First, the charge separation in the MC form leads to large dipole moment in the range of 14–18 D, whereas the dipole moment of SP form is in the range of 4–6 D.[43,44] Second, there is a significant structural difference between the SP and MC form. The molecular volume of the MC form is larger than the SP form. Also, the MC form is more basic than the SP form and its protonation results in MCH^+ form. These changes during photoisomerization have been considered when designing these photoresponsive molecules as potential membrane disruptors.[40,45]

To date, only a few SpOx amphiphiles have been synthesized[46] and characterized in lipid vesicles.[40,47] Yet, their photocontrol of ion permeability in lipid vesicles has never been examined. In addition, photochromic dimers containing two photochromic units is especially attractive due to the extensive changes in their photochromic properties.[48,49] Surprisingly, the preparation of a bolaamphiphilic SpOx dimer has never

been reported. In general, a compound that has two hydrophilic groups, one on each end of the long hydrophobic unit is termed as bolaamphiphile.[50] Previously, non-amphiphilic biphotochromic SpOx compounds[42,48,49,51-53] have been designed and investigated for their photochromic characteristics such as fatigue resistance[48], and thermal relaxation rates[51]. Recently, the photochromic reactivity of non-amphiphilic SpOx dimers in organic solution[49,54], and their photocontrol of guest binding while tethered to a polymer[55] have been examined. Although the functionality achieved by these systems is slowly improving,[56] biphotochromic systems have never been examined in lipid vesicles. The subsequent sections discussed more about the lipid vesicles and their different phases, and photocontrol of ion permeation from lipid vesicles.

1.4. Lipid Vesicles

In general, lipid vesicles are spherical structures composed of a lipid bilayers and they have been used as model systems for cellular membranes.[57] Lipid bilayers are thin polar membranes that are made up of two layers of phospholipids. Lipid vesicles play a vital role as carriers of a large variety of compounds.[58] In addition, they are biodegradable and nontoxic in nature. Each phospholipid molecule in a bilayer contains a hydrophilic polar head group and hydrophobic hydrocarbon tail group (Figure 1.6). The polar head group can be zwitterionic, cationic or anionic depending on the structure of the lipid. When these phospholipids are suspended in an aqueous medium, they aggregate to form lipid bilayer membrane.[58] The majority of the double-chain lipids with hydrocarbon tails having greater than eight carbons in length form bilayer structures.

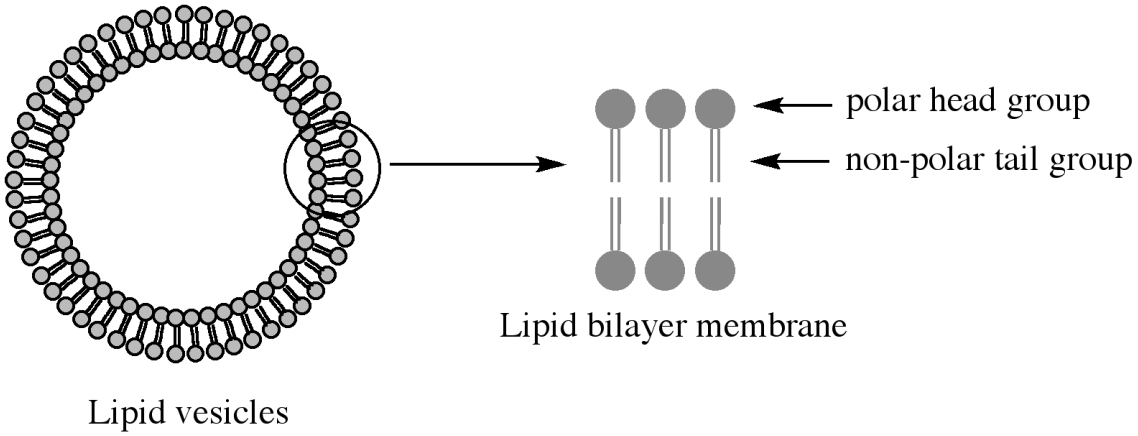

Figure 1.6. Schematic representation of a unilamellar vesicle.

Lipid vesicles having a single lipid bilayer are known as unilamellar vesicles (Figure 1.6).[59] Unilamellar vesicles can be subcategorized into small unilamellar vesicles (SUVs) and large unilamellar vesicles (LUVs) based on their diameter. SUVs range from 15-30 nm in diameter, and LUVs are 100-200 nm in diameter. The size, composition, charge, and lamellarity of lipid vesicles can be controlled.[58] Lipid vesicles with diameters ranging from nm to μm tend to encapsulate both hydrophilic and hydrophobic molecules in their self-assembled structures. The encapsulated contents of lipid vesicles can be released using a few different strategies. These strategies include pH, temperature, redox potential, or light as an external stimulus.[59-63] Among these, the use of light as an external stimuli is attractive as it provides a high degree of spatial and temporal control. Also, parameters such as the wavelength, intensity and duration of the light source can be modulated for on-demand dosing.[57,64]

1.4.1. Lipid Phases

The bilayer membrane of a lipid vesicle can exist in different phase states in aqueous media, and the phases depend on vesicle composition and temperature. Two important phase states are the gel phase and the fluid phase state. The main phase transition temperature, T_m, is the temperature at which the gel phase changes to the fluid phase (Figure 1.7A). Each phase describes the molecular order and mobility of a lipid within the bilayer.[65] In the gel phase, the hydrocarbon chains of lipids are tightly packed, and hence exhibit a slow rotational motion. In contrast to the gel phase, the fluid phase exhibits a more disordered arrangement of hydrocarbon chains with both lateral

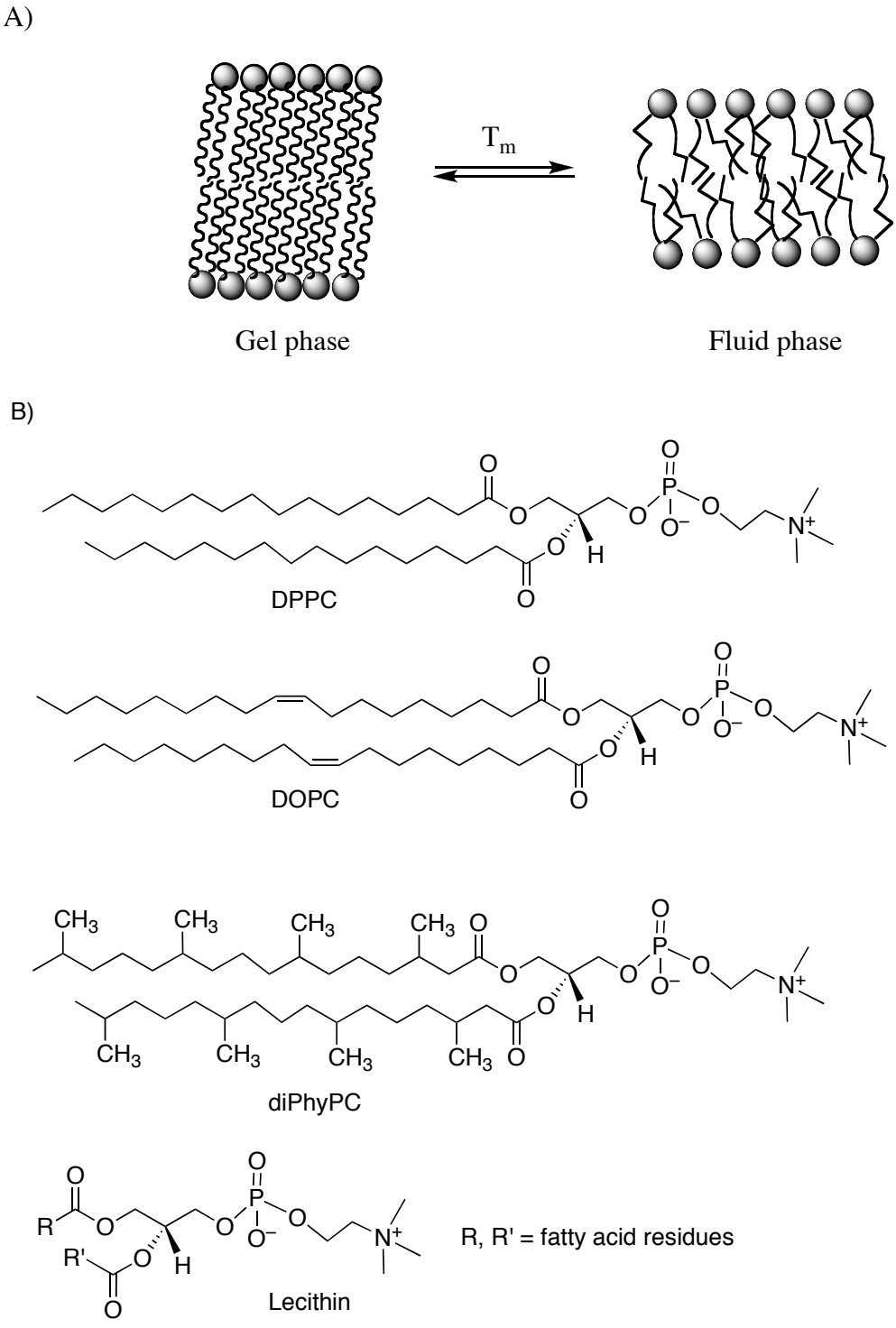

Figure 1.7. A) Gel and fluid phases of lipid bilayer membrane, and B) Chemical structure of phospholipids used in ion permeation studies.

and rotational motion.[65] In our ion permeation studies, we have prepared LUVs from four different phospholipids (Figure 1.7B), namely 1,2-dipalmitoyl-*sn*-glycero-3-phosphatidylcholine (DPPC), 1,2-dioleoyl-*sn*-glycero-3-phosphatidylcholine (DOPC), 1,2-diphytanoyl-*sn*-glycero-3-phosphatidylcholine (diPhyPC), and lecithin. At room temperature, vesicles composed of the saturated lipid DPPC are in the gel phase, whereas unsaturated lipid DOPC are in the fluid phase.[66] The lipid diPhyPC was chosen given this lipid has no detectable gel to liquid crystalline phase transition from –120 to 80 °C due to methyl branched acyl chains.[67] Lecithin is a mixed lipid system that contains the mixture of saturated and unsaturated PC lipids primarily composed of unsaturated acyl chains (e.g., linoleyl and oleyl).[68] Similar to DOPC, both diPhyPC and lecithin are in the fluid phase at room temperature.

1.5. Ion Permeation Across Lipid Vesicles

Ion transport through cell membranes is an important physiological process in living systems.[69] In this process, membrane bound proteins are naturally regulating the flow of ions and molecules across cell membranes.[70,71] Therefore, modeling natural ion transporters to develop synthetic transporters is necessary. This allows one to gain a better understanding of biological ion transport processes and to develop systems with potential applications in the fields of drug delivery and sensors.[72,73] In order to establish the photocontrol of ion permeation across a lipid bilayer membrane, photochromic compounds need to be integrated into the bilayer membrane. In this way, lipid vesicles incorporated with photochromic compounds become photoresponsive systems.[74,75]. The

conformational change accompanying photoisomerization of these compounds can disrupt the bilayer membrane and allow ions to permeate across the bilayer membrane.[76] In addition, photocontrols based on the reversible photoisomerization of photochromic molecules could be used to regulate the delivered dosage. Photoresponsive systems that perform photoinduced processes are continually being developed to improve function in applications such as drug delivery and ion transport.[61,64,77-81] The photocontrol release provides a high level of spatial and temporal control.

1.5.1. Photocontrolled Release from Lipid Vesicles Incorporated with Photochromic Compounds

Reversible photocontrol of ion permeation based on lipid analogs of photochromic compounds such as azobenzene[76,82-91], and spiropyran[37,38,92-96] have been studied in lipid vesicles. For example, photocontrol release of an amphiphilic azobenzene (Figure 1.8) incorporated in lipid vesicles containing the mixture of egg yolk *L*-α-phosphatidylcholine (EYPC) and cholesterol was investigated using a 8-hydroxypyrene-1,3,6-trisulfonic acid trisodium salt (HPTS) fluorescence assay.[76] UV or visible light irradiation induce changes in the structure and the transport activity of azobenzene in lipid vesicles. Upon irradiation of the *trans* isomer with UV light, the *cis*-isomer is produced, which enhances the permeability of ions. The ion transport activity was decreased when irradiated with visible light, which suggested the kinked structure of *cis* isomer increases the transport activity than the linear and mostly planar *trans* isomer.

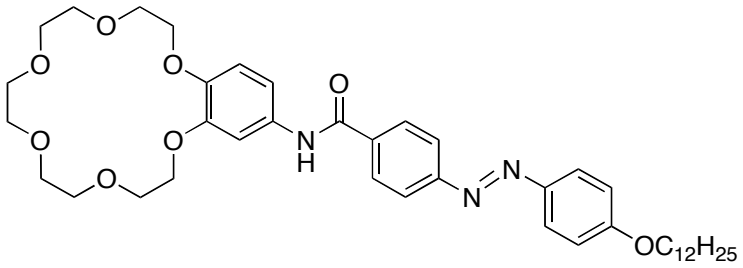

Figure 1.8. Structure of an amphiphilic azobenzene.

Studies have also shown that lipid vesicles that incorporate spiropyran derivatives undergo reversible photocontrol release of entrapped contents upon irradiation with either UV or visible light.[37,74,95] A recent study showed a photoinduced drug release in nanoparticles composed of spiropyran (Figure 1.9), 1,2-distearoyl-*sn*-glycero-3-phosphoethanolamine-*N*-carboxy(polyethylene glycol)-5000 (DSPE-PEG) and lecithin.[38] A four fold increase in percent release of encapsulated drug was observed when irradiating nanoparticles with UV light. The photoinduced release was due to the volume change in nanoparticles upon photoirradiation. The size was 143 nm when a nanoparticle contain spiropyran in SP form and reduced to 47 nm in MC form. The reason proposed for changes in the size of nanoparticles was due to the relative position of spiropyran isomers in nanoparticles. The hydrophobic SP form is most likely positioned in the hydrocarbon tail region of lipid vesicles, which causes the hydrophobic core to have a loose structure and increases the size of a nanoparticle.[38] The photoisomerization to zwitterionic MC form made them to move towards the more hydrophilic PEG layer of the nanoparticle, which tighten the hydrophobic core and decreases the size of the nanoparticle.

In another study, an amphiphilic spiropyran derivative with terminally charged quaternary ammonium group (Figure 1.10A) was studied in DPPC vesicles for the release of encapsulated dye, carboxyfluorescein (CF).[95] During UV-visible cycle, the percent release was increased when the spiropyran derivative was in the MC form, whereas the SP form decreases the percent release.[95] A mechanism was proposed for the release of CF from the lipid vesicles upon photoisomerization of spiropyran derivative (Figure 1.10B).[95] The solvatochromic properties of spiropyran derivative and the fluorescence

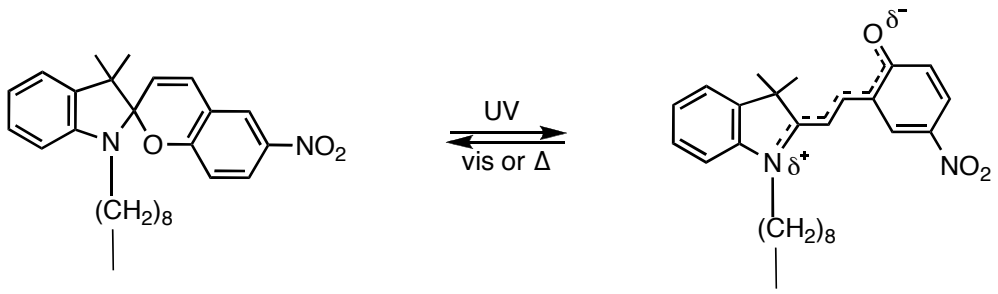

Figure 1.9. Structure of photoisomers of a spiropyran derivative.

A)

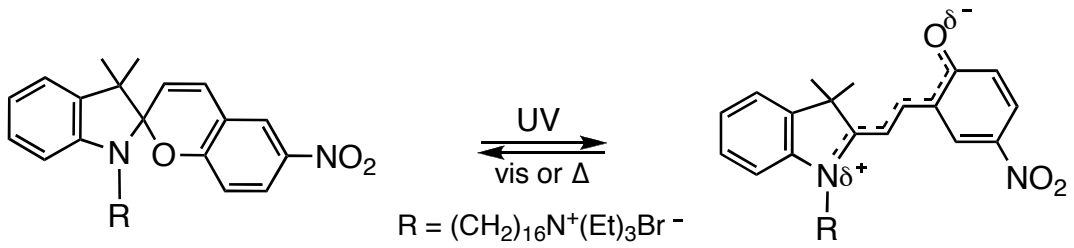

B)

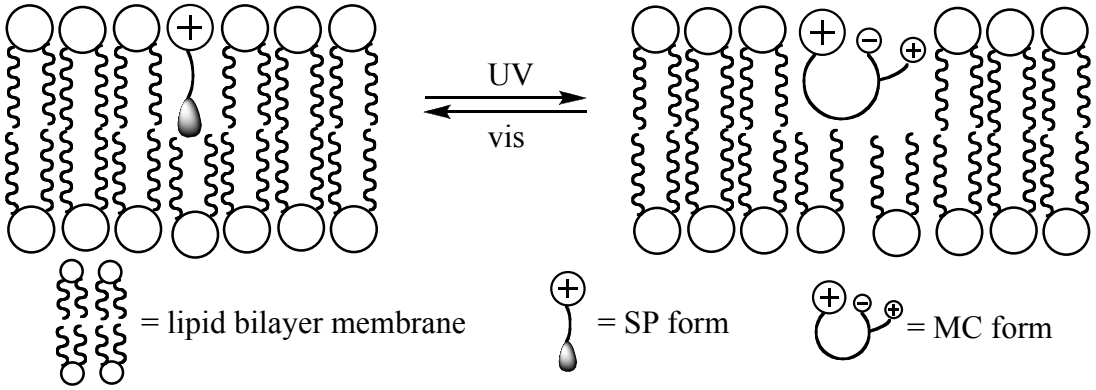

Figure 1.10. Release of CF dye from DPPC vesicles incorporated with an amphiphilic spiropyran derivative: A) Structures of the photoisomers of spiropyran derivative, and B) Proposed mechanism for the release of CF dye (This figure was adapted from reference 95).

intensity of CF were used to locate the spiropyran derivative in the region of bilayer membrane. It was suggested that the amphiphilic nature of SP form was responsible for positioning the charged ammonium ion in the head group region and the photochromic unit in the lipid tail region (Figure 1.10B).[95] Upon UV irradiation, the SP form undergoes isomerization to the more hydrophilic MC form. As a result, the more polar MC form relocates the photochromic unit closer to the hydrophilic head group region of the lipid bilayer.[95] This reorientation was proposed as the main reason for the increase in CF permeation across the bilayer membrane.[74,95] When irradiated with visible light, the open-ring MC form isomerizes back to the SP form, which places the photochromic unit back to the non-polar tail region and decreases the permeation across the bilayer membrane.

In another study, the reversible photocontrol of potassium ion permeation through dihexadecyl phosphate (DHP) and phosphatidylcholine (PC) vesicles using a spiropyran derivative containing hexadecanoyloxy group in the indoline moiety (Figure 1.11A) was reported.[37] The release of potassium ion from the bilayer membrane was measured using an ion-selective electrode. It was suggested that spiropyran derivative in the SP form have shown four fold increase in the rate of potassium ion permeation across the DHP vesicle and it was decreased to control values for the MC form. But in PC vesicles, no significant difference in the rate of potassium ion permeation was observed between the two isomeric states.[37] The mechanism for the release of potassium ion was proposed based on the location of spiropyran in the lipid bilayer membrane.[37] Given the non-polar character of the SP form, it may be located in the bilayer midplane (Figure 1.11B). Thus, the presence of SP form more likely disrupts the hydrocarbon chain packing, which

A)

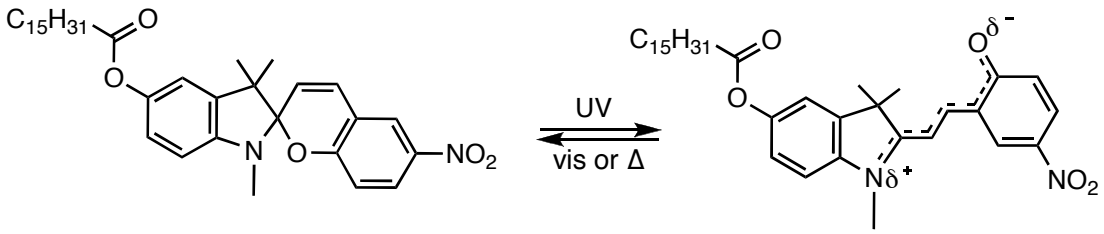

B)

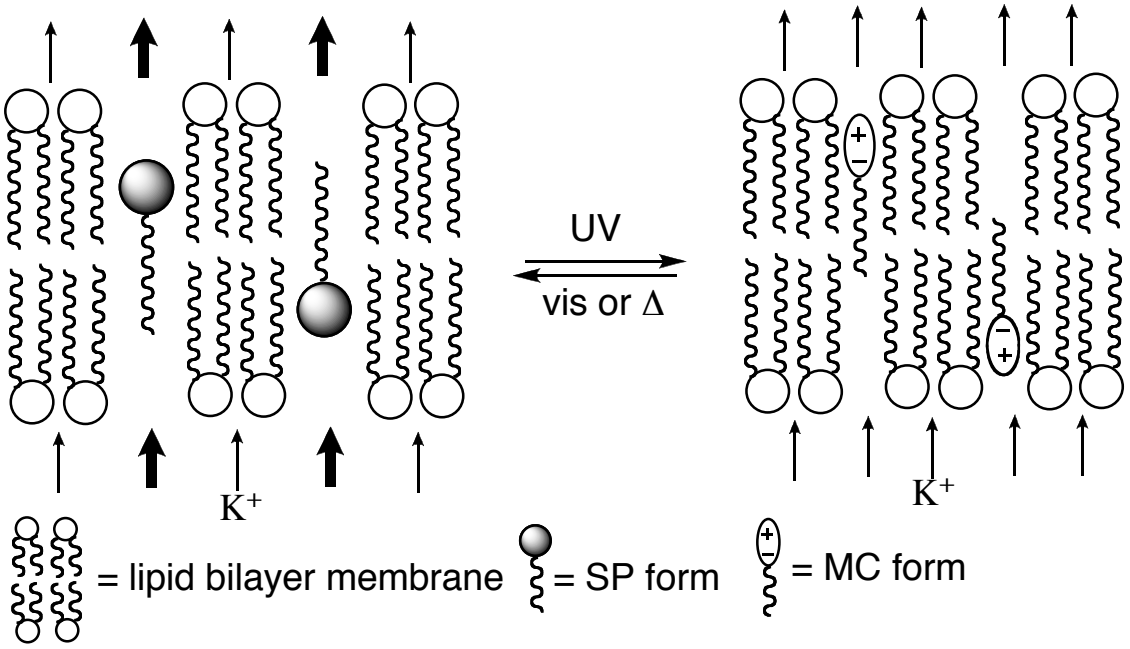

Figure 1.11. Potassium ion permeation from DHP vesicles incorporated with a spiropyran derivative: A) Structures of the photoisomers of spiropyran derivative, and B) Proposed mechanism for the potassium ion permeation (This figure was adapted from reference 37).

increases the free volume within the membrane and increases the rate of potassium ion permeation. In general, free volume is the free space present in the lipid bilayer, which improves the flexibility of hydrocarbon chain within the bilayer membrane.[97] Wohl et al. studied spiropyrans with varying alkyl chain lengths in DPPC vesicles to assess the free volume distribution in a bilayer membrane.[93] This report showed that the smallest free volume was observed in the highly ordered region of the hydrocarbon chain while the largest free volume was detected in the bilayer midplane. Upon UV irradiation, the rate of potassium ion permeation was decreased, as the SP form was isomerized to the hydrophilic MC form.[37] As a result, the MC form relocates closer to the glycerol-ester backbone region of the bilayer membrane (Figure 1.11B), which may improve the interior hydrocarbon chain packing and decreases the potassium ion permeation.[37]

In the above said examples, the photochromic molecules comprised of azobenzenes and spiropyrans have been used in photocontrol release of encapsulated contents from lipid vesicles. However, these derivatives often exhibit limited thermal stability and low fatigue resistance, which limits their applicability. As mentioned earlier, a drawback with many azobenzene systems is the overlapping absorption of photoisomers in the UV region, which hinders selective excitation. Spiropyrans are less resistant to photodegradation than the structurally similar SpOxs. Among the many photochromic compounds that have been studied in lipid vesicles for photocontrolled release of encapsulated ions/molecules, photoresponsive systems incorporating amphiphilic DTE and SpOx in lipid vesicles have been limited. As a result, it is of interest to explore the photocontrol of ion permeation across bilayer membranes using

amphiphilic DTEs and SpOxs. The following sections deals with general overview of mechanism for ion permeation, types of transporter and assays used for ion permeation.

1.5.2. Mechanism of Ion Permeation

Two major mechanisms have been proposed for the permeation of ions and small molecules across a bilayer membrane.[98,99] They are the pore mechanism and the solubility-diffusion mechanism. Protons and potassium ions are the two ions studied in our permeation assays.

In the pore mechanism, ion permeation is due to the formation of transient hydrated defects (or pores) within the bilayer membrane (Figure 1.12A).[99] These pores are produced by thermal fluctuations in the lipid vesicles. In the pore mechanism, the permeability of ions decreases with increasing ionic radius.[100] Thus, the rate of ion transport inside these hydrated pores is greater for protons than the potassium ions. For instance, the radius of a potassium ion is 1.38 Å, whereas the radius of a proton is <0.01 Å.[101] There is another mechanism called Grotthuss mechanism[102] through which protons permeates across the bilayer membrane in combination with pore mechanism. This is due to the formation of hydrogen bonds between water molecules present in the bilayer defects. This provides a pathway for protons to jump from one side of the membrane to the other side by hopping along hydrogen-bonded chains of water (i.e., proton wire), a mechanism that is not available for other cations.[102] Thus, hopping along hydrogen-bonded water molecules can increases the permeation of protons five to six times greater than other monovalent cations.

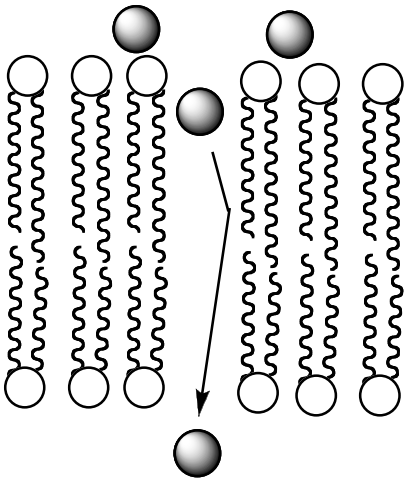

A) Pore Model

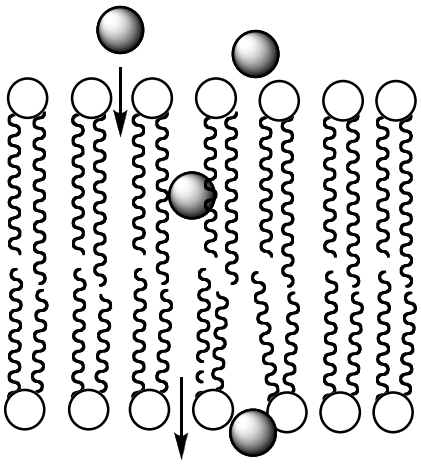

B) Solution-Diffusion Model

Figure 1.12. Ion permeation through membranes by pore and solution-diffusion model (This figure was adapted from reference 98).

In the solubility-diffusion mechanism, the lipid bilayer membrane is considered a hydrophobic barrier that separates one aqueous phase from the other. In order to cross this barrier, the permeating ions must partition into the hydrophobic region then diffuse through the hydrophobic interior before leaving out of the hydrophobic phase and dissolve into aqueous phase on other side (Figure 1.12B).[98] In the solubility-diffusion mechanism, the permeation of ions is aided by a concentration gradient. There are various types of transporters that accelerate the ion permeation across a bilayer membrane using these mechanisms are described below.

1.5.3. Types of Transporters

Ion carriers, ion channels and membrane disruptors are the three different types of transporters used to increase the rate of ion permeation across a bilayer membrane (Figure 1.13).[69,103]. Ion carriers such as valinomycin and crown ethers are used to form ion complexes on one side of the membrane, which then move across the membrane and release the ion on other side of the membrane (Figure 1.13A). Ion channels are molecules that form channel like structure across the bilayer membrane and transports the ions through these pores. A few examples of ion channels are gramicidin, amphotericin, etc. (Figure 1.13B). A membrane disruptor is a compound, which disrupts the organization of a bilayer membrane. As a result, ions permeate through the defects formed in the bilayer membrane (Figure 1.13C). Some examples of membrane disruptor are mellitin, detergents, etc. In our research, photochromic compounds incorporated into the lipid vesicles are act as transporter. The change in molecular structure of

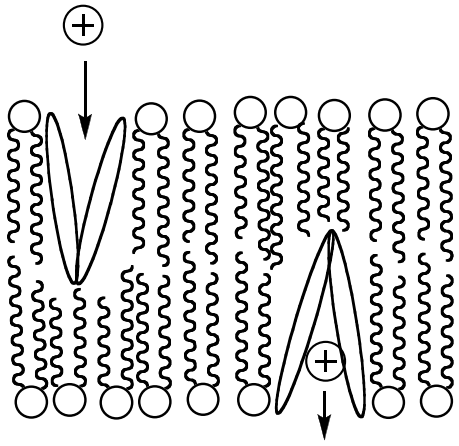

a) Ion Carrier

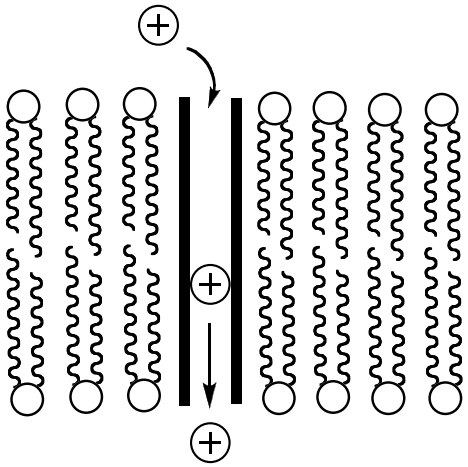

b) Ion Channel

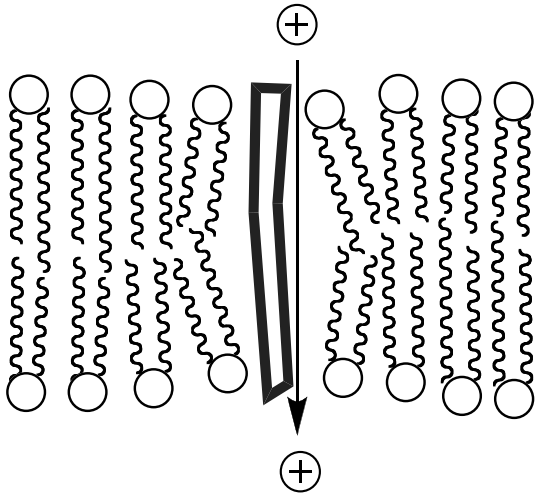

c) Membrane Disruptor

Figure 1.13. Types of ion transporter (This figure was adapted from references 69 and 103).

photochromic compounds during photoisomerization is expected to disrupt the bilayer membrane and allow for the ion permeation. In this way, the photochromic compounds behave as membrane disruptors. In the following section, a brief overview of assays used for ion permeation activity is discussed.

1.5.4. Ion Permeation Assays

In general, ion permeation activity of a photochromic compound across lipid vesicles can be studied using fluorescence spectroscopy and ion-selective electrodes. The advantages of using vesicle assays are the relative ease to conduct the experiments and the ion transporters can be tested quickly for its activity. In addition, lipid vesicles can be purified by gel permeation or centrifugation so that the encapsulated contents are found only inside the vesicles not in the external buffer medium. This difference in components between the external and internal medium provides a transmembrane chemical potential gradient across a bilayer membrane, which results in ion permeation. The rate of ion permeation increases in presence of a transporter. This change can be detected through a change in an indicator within or outside the vesicles. A disadvantage of using vesicle assays is the batch-to-batch variability, which may differ the background leakage.

In the fluorescence assay, proton permeation through the lipid bilayer membrane is determined using internal fluorescent pH probes. Fluorescent pH probes are molecules that are highly sensitive to pH changes in its microenvironment.[104] A few examples of fluorescent pH indicators are HPTS, fluorescein, and carboxyfluorescein. HPTS is a highly water soluble, weak organic acid with a pK_a value of 7.3 (Figure 1.14).[105,106]

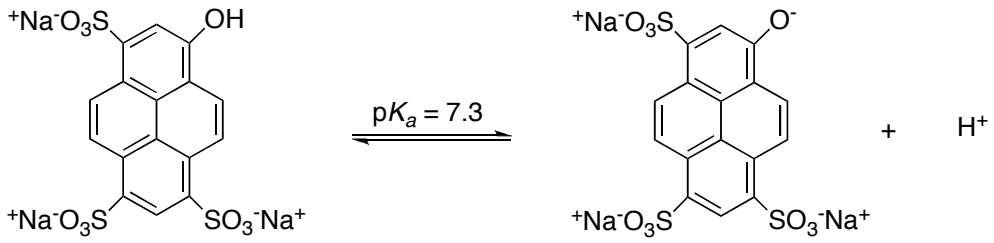

Figure 1.14. Chemical structures of HPTS in acidic and basic form.

HPTS and its conjugate base have different excitation wavelengths (λ_{ex}), 403 and 460 nm, respectively. However, they have a similar emission wavelength (λ_{em} = 510 nm). That is, the wavelength of emission does not change as the concentration of each form is varied, but the fluorescence intensity does.[106] As the pH is increased (pH > 7.5), acid-base equilibrium is shifted towards the dissociated form, and in the excitation spectrum there is an increase in intensity at 460 nm, and a concomitant decrease in intensity at 403 nm. These changes are due to the pH-dependent ionization of the hydroxyl group.[106]

In this research, HPTS was encapsulated inside the lipid vesicles to measure proton permeation across a bilayer membrane. When a base is added to the external medium, a pH gradient is established, which initiates proton from HPTS to permeate across the bilayer membrane. This change in pH can be measured by monitoring the changes in fluorescence intensity of acid and conjugate base forms of HPTS by alternating the excitation wavelength during the assay.[107]

Potassium ion permeation in lipid vesicles can be monitored using a potassium ion-selective electrode. In this assay, KCl was encapsulated inside the lipid vesicles. The amount of potassium ion that permeates to external medium is measured using ion-selective electrode.[37] Thus, photocontrol of ion permeation in lipid vesicles were studied in my research using these two assays.

1.6. Development of Amphiphilic Photochromic Compounds

A previous member of our research group examined the photoisomerization of a symmetrical DTE **17** in DPPC vesicles and the release of HPTS under self-quenching conditions (Figure 1.15).[108] In these studies, photoisomerization was shown to be

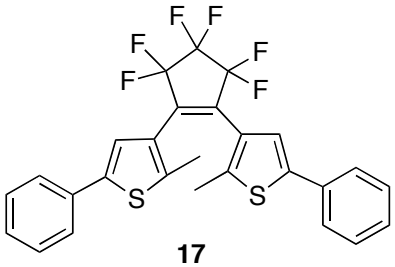

17

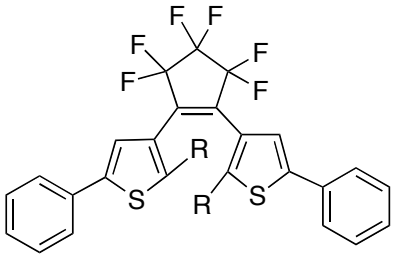

18: R = CCPh

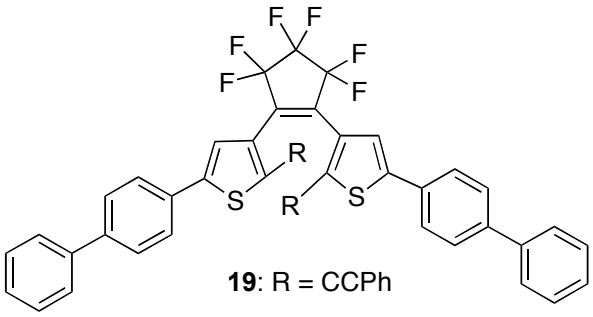

19: R = CCPh

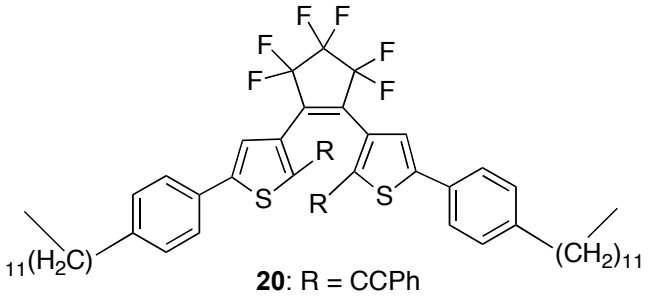

20: R = CCPh

Figure 1.15. Chemical structure of symmetrical DTEs.

completely reversible, but the release of encapsulated HPTS upon photoisomerization was not significant. It was hypothesized that the change in molecular structure upon photoisomerization was not large enough to disrupt the lipid bilayer packing, and the size of the HPTS dye is too large to release. To address the small change in structure, three symmetrical DTEs **18**–**20** (Figure 1.15) were synthesized that include bulky phenylethynyl substituents at the C2 and C2′ positions in the thiophene rings.[19] A DTE incorporating a rigid and bulky phenylethynyl substituent has been shown to undergo a large change in the molecular structure upon photoisomerization.[18] In addition, the cyclization quantum yield for **20** was four fold lower than **18**. It was hypothesized that this large decrease was due to the presence of the dodecyl chains. Further, the dodecyl chains may interact, favoring the photoinert parallel conformer and decreasing the relative percentage of photoactive antiparallel conformers available for cyclization.[109] To increase the quantum yields, and to study the effect of ion permeation in lipid vesicles, three new asymmetrical and amphiphilic DTEs **21**–**23** (Figure 1.16) were synthesized. To introduce asymmetry, DTEs that contain different substituents at the C5 and C5′ positions were produced. Furthermore, to improve the lipid complementary nature of DTEs, a charged quaternary ammonium substituent was introduced at the end of the alkyl chain. These derivatives are expected to have better organization with the lipid bilayer membrane through favorable intermolecular interactions. DTEs **21** and **22** contain bulky phenylethynyl substituents that undergo larger changes in molecular geometry upon photoisomerization than the analogous methyl derivatives. Thus, in my photocontrolled ion permeation studies, the inclusion and photoisomerization of these DTEs in a lipid bilayer membrane are expected to show significant effect on ion permeation.

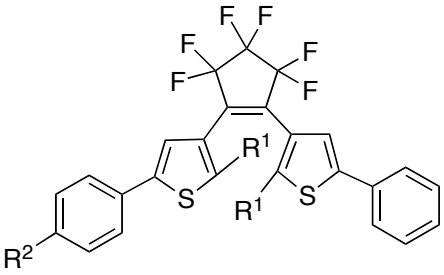

21–23

21: R^1 = —C≡C— 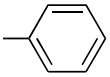

$R^2 = (CH_2)_{12}N^+(CH_3)_3I^-$

22: R^1 = —C≡C— 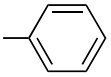

$R^2 = (CH_2)_6N^+(CH_3)_3I^-$

23: $R^1 = CH_3$

$R^2 = (CH_2)_6N^+(CH_3)_3I^-$

Figure 1.16. Chemical structure of amphiphilic DTE monomers.

In addition, three derivatives of SpOx photochromic compounds were previously synthesized by members of our research group (Figure 1.17).[110] They are two phenanthryl-based SpOx monomers **24** and **25**, and a bolaamphiphilic bis-SpOx dimer **26.** Similar to the DTEs, all of these SpOx derivatives contain a charged quaternary ammonium cation at the end of the alkyl chain. In my research, photocontrolled ion permeation in lipid vesicles using these SpOx derivatives was studied. Previously, the orientation of amphiphilic spiro compounds in lipid vesicles was studied based on solvatochromic properties.[37,40,47,95] These studies revealed that the charged group on spiro compound interacts with the polar head group region, and the remaining photochromic unit resides in the less polar hydrophobic tail region. Consistently, the thermal isomerization of **24** in organic solvents and lipid vesicles showed that the wavelength of maximum absorption (λ_{max}) of the open-ring isomer underwent a small bathochromic shift with increasing solvent polarity.[47] Upon inclusion of **24** in DPPC vesicles, the λ_{max} for the open-ring isomer underwent a hypsochromic shift relative to toluene, which suggested that the photochromic moiety of **24** is most likely located in the less polar aliphatic region of the bilayer membrane.[47] Therefore, we anticipate that the remaining SpOx derivatives **25** and **26** could also have similar organization in a bilayer membrane. The dimer may have two types of orientations in lipid vesicles. The dimer may orient in such a way that the charged groups on both ends of the dimer could anchor the hydrophilic head group on both ends of a bilayer membrane by elongating throughout the bilayer membrane. However, it is also possible that the dimer may have U-shaped or folded orientation by spanning one side of the bilayer membrane. Thus, these SpOx derivatives may act as membrane disruptors for ion permeation in lipid vesicles. Overall,

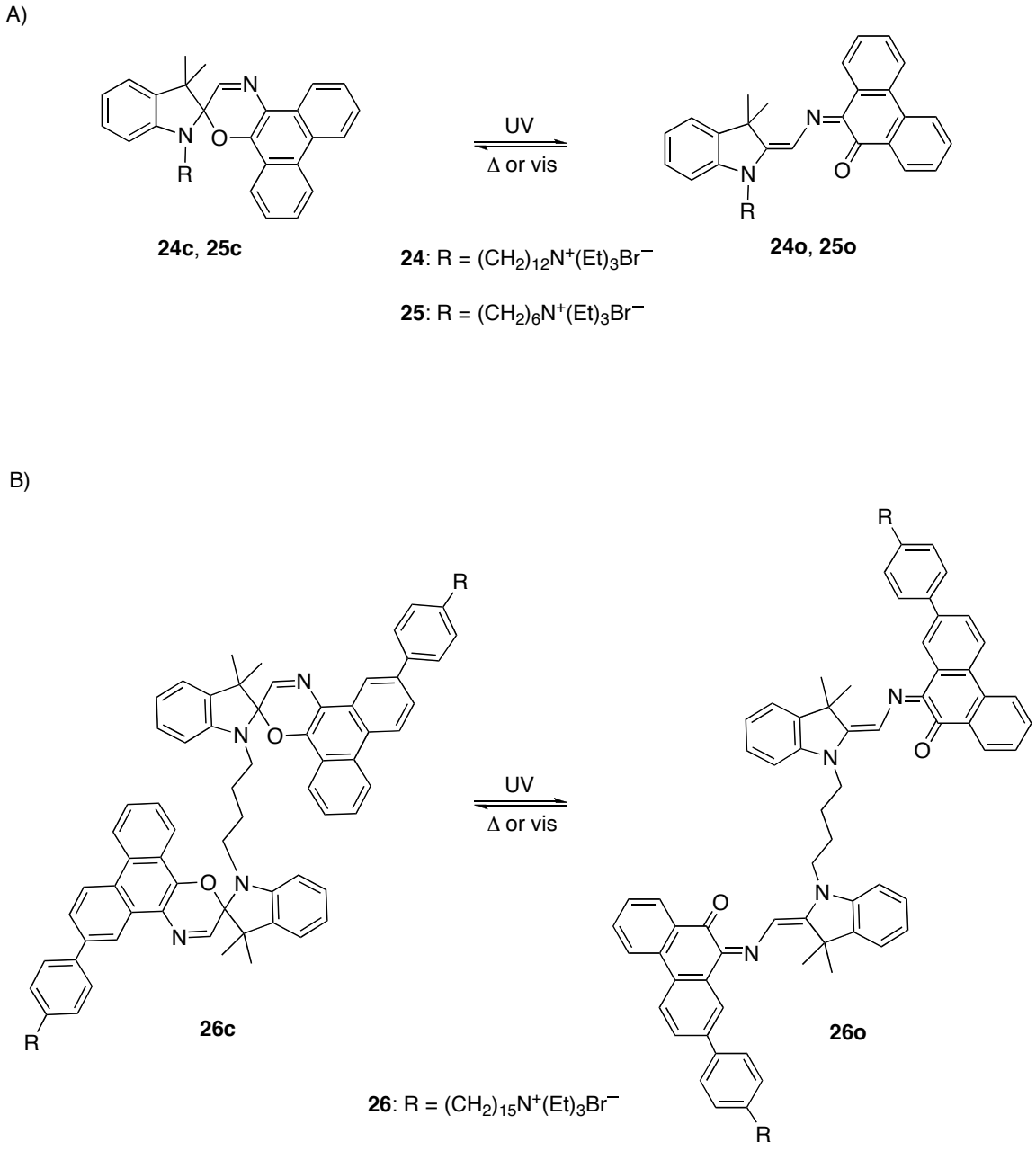

Figure 1.17. Structures of the photoisomers of SpOx derivatives A) amphiphilic monomers **24** and **25**, and B) bolaamphiphilic dimer **26**.

in my thesis research, proton and potassium ion permeation abilities of both the isomeric states of two photochromic families **21**–**26** at various mole ratios in a bilayer membrane will be examined using the appropriate technique for each ion.

1.7. Research Objectives and Outline

The main objective of my thesis research is to develop photoresponsive lipid-based systems using photochromic compounds and to examine the photocontrol of ion permeation in lipid vesicles. The photoresponsive systems are expected to undergo reversible changes in their membrane bilayer structure in response to light. As a result, these changes in the local lipid order can be exploited to release encapsulated contents in a controlled manner.[61,64,79] To develop photoresponsive lipid-based systems, amphiphilic photochromic compounds are required. Therefore, for this purpose, amphiphilic DTEs **21**–**23** and SpOxs **24**–**26** were chosen for this study.

To accomplish this objective, initially **21**–**23** will be synthesized and their photochromic properties will be characterized. These photochromic properties include photoinduced cyclization and cycloreversion quantum yields, and photoconversion yields at the photostationary state (PSS). Upon completion of this work, **21**–**23** will be studied in four different lipid systems having different lamellar phases at room temperature. A proton permeation assay will be used to examine the effect of the inclusion and the photoisomerization of DTEs, at various mole ratios, on proton permeation in lipid vesicles. In particular, the rate constants for proton permeation and the extent of proton permeation will be determined. Subsequently, the photocontrol of potassium ion

permeation in DPPC and DOPC vesicles incorporating DTEs will be investigated. Specifically, this assay will be used to measure the rate constant for potassium ion permeation of both the isomeric states of DTEs within the same experiment and the overall percentage of potassium ion release.

Similar to DTE studies, the photocontrol of proton and potassium ion permeation in DPPC and DOPC vesicles incorporating amphiphilic SpOxs **24**–**26** will be examined. All together, ion permeation in lipid vesicles for both photochromic families will be compared in order to determine which photoresponsive system has the greatest potential for the photocontrolled delivery of small molecules.

In summary, *Chapter 2* will present the details of experimental procedure. *Chapter 3* will discuss the synthesis of **21**–**23**, their absorption and photochromic properties, and their photostability. *Chapter 4* will present and discuss the results from the proton permeation studies. *Chapter 5* will present and discuss the results from the potassium ion permeation studies. Further, all photoresponsive systems studied will be compared to assess their relative efficacy with respect to the photocontrol of ion permeation. To conclude, *Chapter 6* will propose the next steps for this research.

CHAPTER 2

EXPERIMENTAL

2.1. Instrumentation

^{1}H, ^{19}F, and ^{13}C NMR spectra were recorded at 300.18, 282.46, and 75.48 MHz, respectively, on a Varian Mercury plus spectrometer (Palo Alto, CA, USA). Chemical shifts are referenced to solvent signals. ^{19}F NMR spectra were recorded without ^{1}H decoupling. ^{13}C NMR spectra were recorded with ^{1}H decoupling. High-resolution mass spectral analyses were carried out by the University of Calgary or University of Saskatchewan on a VG 70SE mass spectrometer (Manchester, UK) or API Qstar XL mass spectrometer (Carlsbad, US), respectively, which was operated in electrospray ionization mode or electron impact mode. HPLC analyses were performed on a HP 1090 Series II liquid chromatograph (Santa Clara, CA, USA). A guard column containing SecurityGuard ULTRA pentafluorophenyl (PFP) cartridges was connected to a Kinetex 2.6 μm PFP analytical column (150 mm × 4.6 mm i.d.) from Phenomenex (Torrance, CA, USA). An isocratic elution was run for **23** in which the flow rate was 1.4 mL min^{-1} and the mobile phase was 8:92 water/methanol with each solvent containing 0.1% trifluoroacetic acid.

Steady-state absorption spectra were obtained at constant temperature (e.g., 21.0 ± 0.1 °C) on a Cary 300 Bio UV–Vis spectrophotometer (Mississauga, ON, Canada) equipped with a dual cell Peltier circulator accessory. The absorption spectra were recorded at a scan rate, step size, and integration time of 300 nm min^{-1}, 0.5 nm, and 0.1 s, respectively.

Steady-state fluorescence spectra were obtained at constant temperature (e.g., 21.0 ± 0.5 °C) with a PTI QuantaMaster spectrofluorometer (Birmingham, NJ, USA), and the excitation and emission slits were set such that the bandwidths were 2 nm. Excitation ratio experiments using HPTS were performed with excitation wavelengths of 403 and 460 nm and an emission wavelength of 510 nm. The integration time was 2 seconds. For quantum yield and the HPTS ion permeation studies, all samples were irradiated with a 300 W xenon light source from Luzchem (Ottawa, ON, Canada), measured in a 10 mm × 10 mm quartz Suprasil fluorescence cell from Hellma (Concord, ON, Canada) and stirred. For UV irradiations, the xenon light source was filtered with a bandpass filter (Hoya U-340, λ_c = 340 ± 42 nm) and an aqueous solution of potassium chromate (λ_c = 313 ± 7 nm[123] circulated through a 50 mm × 22 mm cylindrical cell from Hellma (A_{313} = 0.040 ± 0.005). For visible irradiations, a bandpass filter (Thorlabs FB530-10, λ_c = 530 ± 5 nm) was used.

Potassium ion permeation was monitored using a MI-442 K+ ion microelectrode and a MI-402 Ag/AgCl micro-reference electrode from Microelectrodes (Bedford, NH, USA), which were connected to a Thermo Scientific Orion Star A325 meter (Beverly, MA, USA). The electrode potentials were recorded once per minute. All samples were measured in quartz test tube (14mm OD, 12mm ID, 100 mm long) from Luzchem, which was kept in a water-filled and water-jacketed beaker at constant temperature (i.e., 21.0 ± 0.1 °C). For potassium ion assay, and for photophysical studies such as molar absorptivity, photoconversion and photostability, UV irradiations of all samples were performed with a 6 W UVA (λ_c = 365 nm) UltraLum TLC lamp. Visible irradiations in potassium ion assay and photostability studies were carried out with a 300 W Osram

EXR halogen photooptic lamp of Kodak Ektagraphic III E Plus projector with a longpass filter (Schott GG-495, $\lambda_c = 495 \pm 6$ nm).

2.2. General Laboratory Equipment

A SB20 pH meter from VWR was used to measure the pH of buffer stock solutions. Sample dilutions and transfers were performed using Eppendrof Research series 2100 pipettes. The Mini-extruder, modified 1 mL Hamilton gas tight syringes, 100 nm polycarbonate membrane filters, and filter supports used for liposome preparation were purchased from Avanti Polar Lipids.

2.3. Materials

Starting materials (99+% purity) used in organic synthetic reactions were commercially available from Sigma-Aldrich and used without further purification. The catalysts *trans*-dichlorobis(triphenylphosphine)palladium(II) [$PdCl_2(PPh_3)_2$]; $\geq$ 99.9% purity and tetrakis(triphenylphosphine)palladium(0) [$Pd(PPh_3)_4$]; $\geq$ 99.9% purity from Strem Chemicals, and octafluorocyclopentene (99+% purity) from SynQuest Laboratories were purchased and used as received. Carbon tetrachloride, copper iodide, diethyl ether, 1,4-dioxane, tetrahydrofuran, and triethylamine were purified following literature procedures.[124] Flash column chromatography was performed using silica gel (200-400 mesh, 60 Å) and alumina (150 mesh, 58 Å) from Silicyle. For lipid vesicle preparation, lecithin (refined, Alfa Aesar, Ward Hill, MA, USA), Triton X-100 (scintillation grade, Eastman Kodak Company, Rochester, NY, USA), buffer salts

(99+%, Sigma-Aldrich and Alfa Aesar), 1,2-dioleoyl-*sn*-glycero-3-phosphatidylcholine (DOPC; >99%, Avanti Polar Lipids, Alabaster, AL, USA), 1,2-dipalmitoyl-*sn*-glycero-3-phosphatidylcholine (DPPC; >99%, Avanti Polar Lipids) and 1,2-diphytanoyl-*sn*-glycero-3-phosphatidylcholine (diPhyPC; >99%, Avanti Polar Lipids) were purchased and used as received. 8-Hydroxypyrene-1,3,6-trisulfonic acid trisodium salt (HPTS; dye content ca. 75%, Sigma-Aldrich) was recrystallized from ethanol five times. PD-Miditrap desalting columns with Sephadex G-25 medium used to remove unencapsulated HPTS or potassium ion. Deionized water was obtained from a Milli-Q Gradient A10 water system (Millipore Corp., Mississauga, ON, Canada). All aqueous solutions were prepared in phosphate buffer (10 mM Na_3PO_4, 100 mM NaCl, pH adjusted to 6.4 using H_3PO_4). The organic solvents used for photophysical measurements were spectrophotometric grade.

2.4. Procedures for the Synthesis of Photochromic DTEs

The synthesis of **21** and **22** have been adapted from previously reported procedures.[108] However, purification procedures have been improved. Silica gel was used as stationary phase in flash chromatography unless otherwise mentioned. Another member of our group synthesized **23**, and I used it in my photophysical and lipid studies. Therefore, the synthetic procedure for **23** is not reported in this thesis.

2.4.1. 12-(*N,N*-Dimethylamino)dodecanoic acid (30)

A 37% aqueous solution of formaldehyde (14 mL, 0.187 mol) was added dropwise to a stirred suspension of a mixture of 12-aminododecanoic acid **28** (10 g, 0.046 mol) and palladium on charcoal (10.0 g of 10 wt.%) in water (400 mL) at room temperature under an atmosphere of hydrogen gas. After stirring for 12 h under gas, the mixture was filtered through celite (methanol), washed with methanol and concentrated under reduced pressure. Purification of the crude product by flash column chromatography (methanol) gave pure **30** as a colorless solid (5 g, 45%). ^{1}H NMR ($CDCl_3$, δ): 1.29 (m, 14H, CH_2), 1.58 (m, 4H, CH_2), 2.23 (t, J = 8.1 Hz, 2H, CH_2), 2.45 (s, 6H, CH_3), 2.56 (t, J = 8.0 Hz, 2H, CH_2), 12.01 (br m, 1H, COOH). ^{13}C NMR ($CDCl_3$, δ): 25.4, 25.9, 26.7, 28.5, 28.6, 28.9, 29.0, 29.1, 36.4, 43.5, 58.3, and 179.4.

2.4.2. 6-(*N,N*-Dimethylamino)hexanoic acid (31)

This method is similar to that used for **30**. Compound **31** was obtained as a colorless solid (95%). ^{1}H NMR ($CDCl_3$, δ): 1.31 (m, 2H, CH_2), 1.57 (m, 4H, CH_2), 2.18 (t, J = 7.3 Hz, 2H, CH_2), 2.44 (s, 6H, CH_3), 2.61 (t, J = 8.0 Hz, 2H, CH_2), 12.0 (br m, 1H, COOH). ^{13}C NMR ($CDCl_3$, δ): 25.2, 25.6, 26.9, 36.1, 43.2, 58.0, and 179.0.

2.4.3. 1-(4-Bromophenyl)-12-(*N,N*-dimethylamino)dodecan-1-one (34)

Thionyl chloride (27.0 mL) was added dropwise to compound **30** (5.00 g, 20.5 mmol). The reaction mixture was refluxed for 2 h under an atmosphere of argon. The unreacted, residual thionyl chloride was removed under reduced pressure. Compound

12-(*N,N*-Dimethylamino)hexanoyl chloride **32** was obtained as a yellow solid (5.37 g, 100%) and was used for the next step without further purification.

Anhydrous aluminum chloride (8.2 g, 0.062 mol) was added to a stirred solution of **32** (5.37 g, 0.021 mol) in bromobenzene (30 mL) at 0 °C. After stirring at 50 °C for 2 h, icy water (50 mL) and hydrochloric acid (6.0 mL of a 6.0 M aqueous solution) was added to the reaction mixture and stirred at room temperature for 12 h. After adjusting the pH of the mixture to above 12 with sodium hydroxide (2.0 M aqueous solution), the mixture was extracted with dichloromethane (3 × 100 mL), washed with a saturated aqueous solution of sodium chloride (100 mL), dried over anhydrous sodium sulfate, filtered and concentrated under reduced pressure. Purification of the crude product by flash column chromatography (4:1:0.1 petroleum ether/dichloromethane / triethylamine) gave pure **34** as an off-white solid (4.49 g, 56 %). ^{1}H NMR ($CDCl_3$, δ): 1.20–1.41 (br m, 14H, CH_2), 1.47 (m, 2H, CH_2), 1.68 (m, 2H, CH_2), 2.25 (s, 6H, CH_3), 2.29 (t, J = 7.6 Hz, 2H, CH_2), 2.91 (t, J = 7.4 Hz, 2H, CH_2), 7.56–7.62 (m, 2H, Ar H), 7.78–7.84 (m, 2H, Ar H). ^{13}C NMR ($CDCl_3$, δ): 24.5, 27.7, 29.5, 29.7, 29.8, 38.8, 45.5, 60.0, 128.2, 129.8, 132.1, 136.0, and 199.7.

2.4.4. 1-(4-Bromophenyl)-6-(*N,N*-dimethylamino)hexan-1-one (35)

This method is similar to that used for **34**. Purification of the crude product by flash column chromatography (10:1:0.2 ethyl acetate/methanol/triethylamine) gave pure **35** as a pale yellow solid (57%). ^{1}H NMR ($CDCl_3$, δ): 1.38 (m, 2H, CH_2), 1.50 (m, 2H, CH_2), 1.73 (m, 2H, CH_2), 2.20 (s, 6H, CH_3), 2.26 (t, J = 7.3 Hz, 2H, CH_2), 2.92 (t, J = 7.4

Hz, 2H, CH_2), 7.55–7.61 (m, 2H, Ar H), 7.76–7.83 (m, 2H, Ar H). ^{13}C NMR ($CDCl_3$, δ): 23.8, 26.0, 26.8, 38.3, 44.3, 58.9, 128.4, 129.8, 132.1, 135.8, and 199.2. HRMS-EI (*m*/*z*): $[M]^+$ calcd for $C_{14}H_{20}{}^{79}BrNO$, 297.0722; found 297.0724.

2.4.5. 12-(4-Bromophenyl)-*N*,*N*-dimethyldodecan-1-amine (36)

Compound **34** (4.49 g, 11.74 mmol) and hydrazine monohydrate (2.94 g, 58.8 mmol) were added to a stirred suspension of KOH (2.64 g, 47.1 mmol) in triethylene glycol (44 mL). The reaction mixture was stirred at 135 °C for 3 h and then at 195 °C for 4 h. Water produced during this reaction was removed using a Dean-Stark trap. After allowing the mixture to cool to room temperature, the viscous mixture was diluted with water (40 mL), and stirred overnight. After adjusting the pH of the mixture to above 11 with a saturated aqueous solution of sodium carbonate, the mixture was extracted with ethyl acetate (3 × 80 mL). The combined organic extracts were washed with a saturated aqueous solution of sodium chloride (80 mL), dried over anhydrous sodium sulfate, filtered and concentrated under reduced pressure. Purification of the crude product by column chromatography (2:1:0.1 petroleum ether/dichloromethane/triethylamine) gave pure compound **36** as pale yellow oil (3.0 g, 69 %). ^1H NMR ($CDCl_3$, δ): 1.19–1.38 (m, 16H, CH_2), 1.45 (m, 2H, CH_2), 1.57 (m, 2H, CH_2), 2.22 (s, 6H, CH_3), 2.24 (t, J = 7.3 Hz, 2H, CH_2), 2.45 (t, J = 7.7 Hz, 2H, CH_2), 7.00–7.06 (m, 2H, Ar H), 7.35–7.41 (m, 2H, Ar H). ^{13}C NMR ($CDCl_3$, δ): 27.5, 27.6, 29.4, 29.7, 29.8, 31.5, 35.6, 45.3, 59.9, 119.4, 130.4, 131.5, 142.1.

2.4.6. 6-(4-Bromophenyl)-*N,N*-dimethylhexan-1-amine (37)

This method is similar to that used for **36.** Purification of the crude product by flash column chromatography using a neutral alumina column (7:1 petroleum ether/diethyl ether) gave pure **37** as pale yellow oil (81%). ^{1}H NMR ($CDCl_3$, δ): 1.32(m, 4H, CH_2), 1.44 (m, 2H, CH_2), 1.59 (m, 2H, CH_2), 2.20 (s, 6H, CH_3), 2.26 (t, J = 7.3 Hz, 2H, CH_2), 2.55 (t, J = 7.6 Hz, 2H, CH_2), 7.00–7.08 (m, 2H, Ar H), 7.34–7.42 (m, 2H, Ar H). ^{13}C NMR ($CDCl_3$, δ): 27.2, 27.4, 29.2, 31.4, 35.5, 45.2, 59.7, 119.5, 130.4, 131.5, 141.8.

2.4.7. 4-(12-*N,N*-Dimethylamino)dodecyl)phenylboronic acid (38)

n-BuLi (9.80 mL of a 2.5 M solution in hexanes, 24.5 mmol) was added dropwise to a solution of **36** (3.0 g, 8.143 mmol) in THF (60 mL) at –78 °C under an atmosphere of argon. After stirring for 60 min, trimethoxyborane (2.80 mL, 24.5 mmol) was added drop wise to the reaction mixture at –78 °C and then the mixture was allowed to warm to room temperature. After stirring for 12 h, hydrochloric acid (40 mL of a 2.0 M aqueous solution) was added and the mixture was stirred for another 20 min. The mixture was basified to a pH of 9 with saturated aqueous solution of sodium bicarbonate and was extracted with ethyl acetate (3 × 100 mL). The combined organic extracts were washed with a saturated aqueous solution of sodium chloride (100 mL), dried over anhydrous sodium sulfate, filtered and concentrated under reduced pressure. Compound **38** was obtained as pale yellow oil (2.71 g, 100%) and was used for the next step without further purification.

2.4.8. 4-(6-(*N,N*-Dimethylamino)hexyl)phenylboronic acid (39)

This method is similar to that used for **38**. Compound **39** was obtained as pale yellow oil (100%) and was used for the next step without further purification.

2.4.9. 12-(4-(4-Bromothiophen-2-yl)phenyl)-*N,N*-dimethyldodecan-1-amine (41)

2,4-Dibromothiophene **40** (2.5 g, 10.3mmol) and sodium carbonate (20 mL of a 2 M aqueous solution) were added dropwise to a stirred mixture of compound **38** (2.71 g, 8.67 mmol) and $Pd(PPh_3)_4$ (0.250 g, 0.217 mmol) in 1,4-dioxane (120 mL) under an atmosphere of argon. After stirring at 100 °C for 4.5 h, the reaction mixture was allowed to cool to room temperature, diluted with water (200 mL) and the mixture was extracted with ethyl acetate (3 × 100 mL). The combined organic extracts were washed with a saturated aqueous solution of sodium chloride (100 mL), dried over anhydrous sodium sulfate, filtered and concentrated under reduced pressure. Purification of the crude product by flash column chromatography (4:1:0.1 petroleum ether/dichloromethane/ triethylamine) gave pure **41** as an off-white solid (3.04 g, 78%). ^{1}H NMR ($CDCl_3$, δ): 1.19–1.40 (m, 16H, CH_2), 1.53 (m, 2H, CH_2), 1.62 (m, 2H, CH_2), 2.31 (s, 6H, CH_3), 2.36 (t, J = 7.3 Hz, 2H, CH_2), 2.61 (t, J = 7.7 Hz, 2H, CH_2), 7.13 (d, J = 1.4 Hz, 1H, H3), 7.16 (d, J = 1.4 Hz, 1H, H5), 7.17–7.22 (m, 2H, Ar H), 7.43–7.49 (m, 2H, Ar H). ^{13}C NMR ($CDCl_3$, δ): 27.8, 28.0, 29.5, 29.7, 29.8, 29.9, 31.6, 35.9, 45.8, 60.2, 110.6, 121.6, 125.4, 125.9, 129.3, 130.9, 143.6, and 145.9.

2.4.10. 6-(4-(4-Bromothiophen-2-yl)phenyl)-*N*,*N*-dimethylhexan-1-amine (42)

This method is similar to that used for **41**. Purification of the crude product by flash column chromatography (8:1 chloroform/methanol) gave pure compound **42** as pale yellow oil (73%). ^{1}H NMR ($CDCl_3$, δ): 1.36 (m, 4H, CH_2), 1.46 (m, 2H, CH_2), 1.63 (m, 2H, CH_2), 2.21 (s, 6H, CH_3), 2.24 (t, J = 7.2 Hz, 2H, CH_2), 2.62 (t, J = 7.7 Hz, 2H, CH_2), 7.13 (d, J = 1.4 Hz, 1H, H3), 7.16 (d, J = 1.4 Hz, 1H, H5), 7.16–7.22 (m, 2H, Ar H), 7.43–7.49 (m, 2H, Ar H). ^{13}C NMR ($CDCl_3$, δ): 27.5, 27.8, 29.4, 31.5, 35.8, 45.6, 60.0, 110.6, 121.6, 125.4, 125.9, 129.3, 130.9, 143.4, and 145.8.

2.4.11. 12-(4-(4,5-Dibromothiophen-2-yl)phenyl)-*N*,*N*-dimethyldodecan-1-amine (43)

NBS (0.839g, 99%, 4.67 mmol) was added to a solution containing **41** (1.87 g, 4.167 mmol) in a mixture of acetic anhydride (16.0 mL) and glacial acetic acid (2.60 mL). After stirring at 80 °C for 80 min, the reaction mixture was allowed to cool to room temperature, diluted with water (100 mL), basified to a pH above 11 with a saturated aqueous solution of sodium carbonate and extracted with ethyl acetate (3 × 50 mL). The combined organic extracts were washed with a saturated aqueous solution of sodium chloride (100 mL), dried over anhydrous sodium sulfate, filtered and concentrated under reduced pressure. Purification of the crude product by alumina column chromatography (7:1 petroleum ether/diethyl ether) gave pure compound **43** as an off-white solid (1.67 g, 76%). ^{1}H NMR ($CDCl_3$, δ): 1.26 (m, 16H, CH_2), 1.44 (m, 2H, CH_2), 1.61 (m, 2H, CH_2), 2.21 (s, 6H, CH_3), 2.23 (t, J = 7.4 Hz, 2H, CH_2), 2.61 (t, J = 7.6 Hz, 2H, CH_2), 7.05 (s, 1H, H3), 7.15–7.22 (m, 2H, Ar H), 7.35–7.42 (m, 2H, Ar H). ^{13}C NMR ($CDCl_3$, δ): 27.3,

27.6, 29.5, 29.7, 29.8, 31.5, 35.9, 45.2, 60.0, 109.6, 114.7, 125.2, 125.6, 129.4, 130.4, 144.0, and 145.8.

2.4.12. 6-(4-(4,5-Dibromothiophen-2-yl)phenyl)-*N,N*-dimethylhexan-1-amine (44)

This method is similar to that used for **43**. Purification of the crude product by alumina column chromatography (7:1 petroleum ether/diethyl ether) gave pure compound **44** as pale yellow oil (83%). ^{1}H NMR ($CDCl_3$, δ): 1.36 (m, 4H, CH_2), 1.45 (m, 2H, CH_2), 1.63 (m, 2H, CH_2), 2.20 (s, 6H, CH_3), 2.23 (t, J = 7.2 Hz, 2H, CH_2), 2.61 (t, J = 7.6 Hz, 2H, CH_2), 7.05 (s, 1H, H3), 7.15–7.22 (m, 2H, Ar H), 7.35–7.42 (m, 2H, Ar H). ^{13}C NMR ($CDCl_3$, δ): 27.3, 27.4, 29.3, 31.4, 35.8, 45.3, 59.8, 109.7, 114.7, 125.3, 125.6, 129.4, 130.5, 143.7, and 145.8.

2.4.13. 12-(4-(4-Bromo-5-phenylethynyl)thiophen-2-yl)phenyl)-*N,N*-dimethyldodecan-1-amine (45)

Ethynylbenzene (0.356 g, 3.489 mmol) in triethylamine (6 mL) was added dropwise to a stirred mixture of **43** (1.67 g, 3.162 mmol) in triethylamine (12 mL) followed by the addition of $PdCl_2(PPh_3)_2$ (7.5 mg, 0.011 mmol) and triphenylphosphine (2.80 mg, 0.011 mmol) under an atmosphere of argon. After stirring at 35 °C for 15 min, copper iodide (4.1 mg, 0.021 mmol) was added and the reaction mixture was stirred at 60 °C for 3.5 h. After allowing the reaction mixture to cool to room temperature, it was diluted with ethyl acetate (50 mL) and poured into water (50 mL) to give a biphasic mixture. This mixture was extracted with ethyl acetate (3 × 50 mL), dried over

anhydrous sodium sulfate, filtered and concentrated under reduced pressure. Purification of the crude product by alumina column chromatography (7:1 petroleum ether/diethyl ether) gave pure compound **45** as a pale yellow solid (1.34 g, 49%). ^{1}H NMR ($CDCl_3$, δ): 1.26 (m, 16H, CH_2), 1.45 (m, 2H, CH_2), 1.62 (m, 2H, CH_2), 2.22 (s, 6H, CH_3), 2.24 (t, J = 7.4 Hz, 2H, CH_2), 2.62 (t, J = 7.6 Hz, 2H, CH_2), 7.16 (s, 1H, H3), 7.17–7.24 (m, 2H, Ar H), 7.32–7.40 (m, 3H, Ar H), 7.42–7.49 (m, 2H, Ar H), 7.52–7.60 (m, 2H, Ar H). ^{13}C NMR ($CDCl_3$, δ): 27.7, 28.0, 29.5, 29.7, 29.8, 29.9, 31.5, 35.9, 45.7, 60.2, 81.7, 97.7, 116.8, 119.4, 122.9, 125.5, 125.8, 128.6, 128.9, 129.4, 130.4, 131.7, 144.2, 145.7.

2.4.14. 6-(4-(4-Bromo-5-phenylethynyl)thiophen-2-yl)phenyl)-*N*,*N*-dimethylhexan-1-amine (46)

This method is similar to that used for **45**. Purification of the crude product by alumina column chromatography (7:1 petroleum ether/diethyl ether) gave pure compound **46** as a waxy pale yellow solid (72%). ^{1}H NMR ($CDCl_3$, δ): 1.36 (m, 4H, CH_2), 1.48 (m, 2H, CH_2), 1.64 (m, 2H, CH_2), 2.24 (s, 6H, CH_3), 2.27 (t, J = 7.3 Hz, 2H, CH_2), 2.62 (t, J = 7.6 Hz, 2H, CH_2), 7.16 (s, 1H, H3), 7.17–7.24 (m, 2H, Ar H), 7.32–7.40 (m, 3H, Ar H), 7.42–7.49 (m, 2H, Ar H), 7.53–7.60 (m, 2H, Ar H). ^{13}C NMR ($CDCl_3$, δ): 27.0, 27.4, 29.3, 31.4, 35.8, 45.0, 59.6, 81.7, 97.7, 116.9, 119.4, 122.9, 125.5, 125.8, 128.6, 128.9, 129.4, 130.5, 131.7, 143.9, and 145.6.

2.4.15. 4-Bromo-2-phenylthiophene (47)

Phenylboronic acid (3.9 g, 32 mmol) and sodium carbonate (50 mL of a 2 M aqueous solution) were added dropwise to a stirred mixture of 2,4-dibromothiophene (6.15 g, 25.4 mmol), $Pd(PPh_3)_4$ (0.734 g, 0.635 mmol) and dioxane (250 mL) under an atmosphere of argon. After stirring at 100 °C for 4.5 h, the reaction mixture was allowed to cool to room temperature, diluted with diethyl ether (80 mL) and poured into water (80 mL) to give a biphasic mixture. This mixture was extracted with diethyl ether (3 × 80 mL). The combined organic extracts were washed with a saturated aqueous solution of sodium chloride (3 × 30 mL), dried over anhydrous sodium sulfate, filtered and concentrated under reduced pressure. Purification of the crude product by column chromatography (petroleum ether) gave pure **47** as a colorless solid (4 g, 66%). ^{1}H NMR ($CDCl_3$, δ): 7.18 (d, J = 1.5 Hz, 1H, H3), 7.22 (d, J = 1.5 Hz, 1H, H5), 7.30–7.45 (m, 3H, Ar H), 7.54–7.61 (m, 2H, Ar H). ^{13}C NMR ($CDCl_3$, δ): 110.8, 122.2, 125.9, 126.0, 128.5, 129.3, 133.4, 145.7.

2.4.16. 2,3-Dibromo-5-phenylthiophene (48)

NBS (2.135 g, 99%, 11.99 mmol) was added to a solution containing **47** (2.549 g, 10.71mmol) in a mixture of acetic anhydride (21 mL) and glacial acetic acid (3.5 mL). After stirring at 80 °C for 80 min, the reaction mixture was allowed to cool to room temperature, diluted with water (150 mL), basified to a pH above 11 with a saturated aqueous solution of sodium carbonate and extracted with dichloromethane (3 × 80 mL). The combined organic extracts were washed with a saturated aqueous solution of sodium

chloride (80 mL), dried over anhydrous sodium sulfate, filtered and concentrated under reduced pressure. Purification of the crude product by column chromatography (petroleum ether) gave pure **48** as a colorless solid (2.8 g, 83%, mp 81 °C). ^{1}H NMR ($CDCl_3$, δ): 7.10 (s, 1H, H4), 7.30–7.43 (m, 3H, Ar H), 7.45–7.51 (m, 2H, Ar H). ^{13}C NMR ($CDCl_3$, δ): 110.1, 114.6, 125.5, 125.6, 128.6, 129.1, 132.7, and 145.4.

2.4.17. 3-Bromo-5-phenyl-2-phenylethynylthiophene (49)

Ethynylbenzene (1.0 g, 9.8 mmol) in triethylamine (20 mL), [$Pd(PPh_3)_2Cl_2$] (26.6 mg, 0.038 mmol) and triphenylphosphine (13.3 mg, 0.051 mmol) were added dropwise to a stirred mixture of **48** (2.814 g, 8.91 mmol) in triethylamine (7 mL) under an atmosphere of argon. After stirring at 35 °C for 15 min, copper iodide (24 mg, 0.127mmol) was added to the reaction mixture and stirred at 60 °C for 5 h. After allowing the reaction mixture to cool to room temperature, it was diluted with ethyl acetate (75 mL) and poured into water (50 mL) to give a biphasic mixture. This mixture was extracted with ethyl acetate (3 × 75 mL). The combined organic extracts were washed with a saturated aqueous solution of sodium chloride (80 mL), dried over anhydrous sodium sulfate, filtered and concentrated under reduced pressure. Purification of the crude product by column chromatography (petroleum ether) gave pure **49** as a colorless solid (1.8 g, 60%, mp 110.0–110.6 °C). ^{1}H NMR ($CDCl_3$, δ): 7.21 (s, 1H, H4), 7.31–7.45 (m, 6H, Ar H), 7.52–7.62 (m, 4H, Ar H). ^{13}C NMR ($CDCl_3$, δ): 81.6, 98.0, 117.0, 120.2, 122.9, 125.9, 126.0, 128.7, 128.9, 129.0, 129.4, 131.8, 133.0, and 145.4.

2.4.18. 3-(Perfluorocyclopent-1-enyl)-5-phenyl-2-(phenylethynyl)thiophene (50)

n-BuLi (2.8 mL of a 2.5 M solution in hexanes, 7.02 mmol) was added dropwise to a solution of **49** (2.26 g, 6.69 mmol) in THF (50 mL) at –78 °C under an atmosphere of argon. After stirring for 40 min, the reaction mixture was added dropwise via cannula to a solution of OFCP (15 g, 70 mmol) in THF (25 mL) at –78 °C. The mixture was stirred for another 4 h at –78 °C and then allowed to warm to room temperature. After 2 h, hydrochloric acid (10 mL of a 6.0 M aqueous solution) was added. Following 10 min of vigorous stirring, THF was removed under reduced pressure. After neutralization of the acid with a saturated aqueous solution of sodium bicarbonate, the mixture was extracted with dichloromethane (3 × 60 mL), dried over anhydrous sodium sulfate, filtered and concentrated under reduced pressure. Purification of the crude product by flash column chromatography (petroleum ether) gave **50** as a light yellow solid. The product was recrystallized from hot methanol (1.5 g, 70%). ^{1}H NMR (CD_3Cl, δ): 7.30–7.47 (m, 6H, Ar H), 7.47–7.54 (m, 2H, Ar H), 7.56–7.64 (m, 3H, Ar H). ^{19}F NMR ($CDCl_3$, δ): –108.1 (m, 2F), –118.4 (m, 2F), –122.1 (m, 1F), –130.8 (m, 2F). ^{13}C NMR (CD_3Cl, δ): 80.8, 101.0, 122.2, 122.3, 128.1, 127.0, 128.8, 129.2, 129.5, 131.6, 132.7, and 148.1.

2.4.19. 12-(4-(4-(3, 3, 4, 4, 5, 5-Hexafluoro-2-(5-phenyl-2-(phenylethynyl)thiophen-3-yl)cyclopent-1-enyl)-5-(phenylethynyl)thiophen-2-yl)phenyl)-*N,N*-dimethyldodecan-1-amine (51)

n-BuLi (0.65 mL of a 2.5 M solution in hexanes, 1.62 mmol) was added dropwise to a solution of **45** (0.85 g, 1.54 mmol) in THF (23 mL) at –78 °C under an atmosphere of

argon. After stirring for 20 min, a solution of **50** (0.765 g, 0.11 mmol) in THF (15.0 ml) was added dropwise via cannula to the reaction mixture at –78 °C. The mixture was stirred for another 4 h at –78 °C and then allowed to warm to room temperature. After 2 h, hydrochloric acid (4 mL of a 1.0 M aqueous solution) was added. Following 10 min of vigorous stirring, THF was removed under reduced pressure. The reaction mixture was diluted with water (25 mL), basified to a pH above 11 with a saturated aqueous solution of sodium carbonate and extracted with ethyl acetate (3 × 75 mL). The combined organic extracts were washed with a saturated aqueous solution of sodium chloride (100 mL), dried over anhydrous sodium sulfate, filtered and concentrated under reduced pressure. Purification of the crude product by alumina column chromatography (7:1 petroleum ether/diethyl ether) gave pure compound **51** as an off white solid (531 mg, 39%). ^{1}H NMR ($CDCl_3$, δ): 1.28 (m, 16H, CH_2), 1.45 (m, 2H, CH_2), 1.65 (m, 2H, CH_2), 2.22 (s, 6H, CH_3), 2.24 (t, J = 1.5 Hz, 2H, CH_2), 2.59 (t, J = 1.5 Hz, 2H, CH_2), 7.02–7.14 (m, 8H, Ar), 7.15–7.21 (m, 6H, Ar H), 7.21–7.28 (m, 7H, Ar H). ^{19}F NMR ($CDCl_3$, δ): –109.7 (m, 4F), –131.6 (m, 2F). ^{13}C NMR ($CDCl_3$, δ): 28.1, 26.8, 28.2, 28.5, 28.6, 30.4, 34.6, 44.5, 59.0, 79.9, 80.1, 98.7, 98.9, 121.2, 121.3, 121.8, 122.3, 122.8, 124.7, 124.8, 127.3, 127.4, 127.5, 127.8, 128.0, 129.2, 130.3, 130.4, 130.5, 131.4, 131.5, 131.7, 142.5, 144.6, 145.0.

2.4.20. 6-(4-(4-(3, 3, 4, 4, 5, 5-Hexafluoro-2-(5-phenyl-2-(phenylethynyl)thiophen-3-yl)cyclopent-1-enyl)-5-(phenylethynyl)thiophen-2-yl)phenyl)-*N,N*-dimethylhexan-1-amine (52)

This method is similar to that used for **51**. Purification of the crude product by alumina column chromatography (7:1 petroleum ether/diethyl ether) gave pure compound **52** as pale yellow oil (42%). ^{1}H NMR ($CDCl_3$, δ): 1.36 (m, 4H, CH_2), 1.48 (m, 2H, CH_2), 1.63 (m, 2H, CH_2), 2.24 (s, 6H, CH_3), 2.29 (t, J = 7.3 Hz, 2H, CH_2), 2.60 (t, J = 7.6 Hz, 2H, CH_2), 7.02–7.14 (m, 8H, Ar H), 7.14–7.21 (m, 6H, Ar H), 7.21–7.28 (m, 7H, Ar H). ^{19}F NMR ($CDCl_3$, δ): –109.7 (m, 4F), –131.6 (m, 2F). ^{13}C NMR ($CDCl_3$, δ): 27.6 27.8, 29.4, 31.6, 35.8, 45.6, 60.1, 81.2, 81.3, 100.0, 100.1, 122.4, 122.5, 123.0, 125.9, 126.0, 128.5, 128.7, 129.0, 129.2, 130.5, 131.6, 131.6, 132.6, 132.7, 133.0, 143.6, 145.8, 146.2.

2.4.21. 12-(4-(4-(3, 3, 4, 4, 5, 5-Hexafluoro-2-(5-phenyl-2-(phenylethynyl)thiophen-3-yl)cyclopent-1-enyl)-5-(phenylethynyl)thiophen-2-yl)phenyl)-*N,N,N*-trimethyldodecan-1-ammonium iodide (21)

Iodomethane (0.301 g, 99%, 2.12mmol) was added to a solution of **52** (0.126 g, 0.139mmol) in dry dichloromethane (12 mL) and then stirred for 24 h at room temperature. The dichloromethane was removed under reduced pressure and the residue was washed with diethyl ether (2 × 6 mL). Recrystallization of the precipitate from dichloromethane/diethyl ether to gave pure **21** as a yellow solid (120 mg, 82%). ^{1}H NMR ($CDCl_3$, δ): 1.18–1.45 (m, 16H, CH_2), 1.58 (m, 2H, CH_2), 1.75 (m, 2H, CH_2), 2.59

(t, J = 7.5 Hz, 2H, CH_2), 3.44 (s, 9H, CH_3), 3.58 (m, 2H, CH_2), 7.02–7.14 (m, 8H, Ar), 7.14–7.20 (m, 6H, Ar H), 7.20–7.28 (m, 7H, Ar H). ^{19}F NMR ($CDCl_3$, δ): –109.6 (m, 4F), –131.6 (m, 2F). ^{13}C NMR ($CDCl_3$, δ): 23.4, 28.1, 29.4, 29.6, 29.7, 29.8, 31.6, 35.9, 54.0, 67.6, 81.2, 81.3, 100.0, 100.1, 122.4, 123.0, 125.9, 126.0, 128.5, 128.7, 129.0, 129.1, 129.3, 130.4, 131.6, 132.6, 132.9,143.7, 145.9, 146.2.

2.4.22. 6-(4-(4-(3, 3, 4, 4, 5, 5-Hexafluoro-2-(5-phenyl-2-(phenylethynyl)thiophen-3-yl)cyclopent-1-enyl)-5-(phenylethynyl)thiophen-2-yl)phenyl)-*N,N,N*-trimethylhexan-1-ammonium iodide (22)

This method is similar to that used for **21**. Compound **22** was obtained as a yellow solid (72%). ^{1}H NMR (CD_3OD, δ): 1.42 (m, 4H, CH_2), 1.68 (m, 2H, CH_2), 1.78 (m, 2H, CH_2), 2.62 (t, J = 7.5 Hz, 2H, CH_2), 3.30 (s, 9H, CH_3), 3.38 (m, 2H, CH_2), 7.06–7.18 (m, 8H, Ar H), 7.18–7.32 (m, 13H, Ar H). ^{19}F NMR ($CDCl_3$, δ): –109.7 (m, 4F), –131.6 (m, 2F). ^{13}C NMR (CD_3OD, δ): 22.8, 26.0, 28.5, 31.0, 35.2, 52.4, 66.7, 80.2, 80.3, 100.0, 100.1, 122.0, 122.5, 125.6, 125.8, 128.5, 128.8, 128.9, 129.0, 130.2, 131.1, 131.2, 132.4, 132.5, 143.6, 148.1, 148.1.

2.5. Procedure for the Photophysical Studies

2.5.1. Photocyclization and Cycloreversion Studies

A solution of **23** in ethyl acetate was prepared at a concentration of 2.00×10^{-5} mol/L. The UV-vis absorption spectra of cyclization reaction (i.e., closed-ring isomer)

were measured by irradiating the solution with UV light (λ = 365 nm) at specific interval of time, until PSS was reached. Then, the same solution was irradiated with visible light (λ = 530 nm) to measure the absorption spectra of cycloreversion process (i.e., open-ring isomer), until no changes were observed in the UV-vis spectra.

2.5.2. Quantum Yield Studies

The cyclization and cycloreversion quantum yields of **23** in ethyl acetate was determined using Aberchrome 540 (A540) as a chemical actinometer. The procedure used to determine the quantum yields of DTE has been previously described in detail.[10] Briefly, the absorbance of the solution containing A540 was matched to a solution containing **23**. The absorbances were matched at 313 nm and 530 nm for the cyclization and cycloreversion quantum yields, respectively. The matched solutions were irradiated with either UV or visible light for a known period of time under identical experimental conditions. After irradiation, the absorbance of each solution was measured immediately. From the change in absorbance for the solution containing A540, the photon rate ($h\nu/t$) was calculated using Eq. 1 when not all the incident light is absorbed,[125]

$$\frac{h\nu}{t} = \left[\frac{\log T_0}{(1-T_0)} - \frac{\log T_t}{(1-T_t)}\right] \times \frac{V}{\phi \times N_A \times \varepsilon_{max} \times l \times t} \qquad (1)$$

where $T = 10^{-A}$, A is the absorbance at 494 nm before irradiation, A_t is the absorbance at 494 nm after irradiation, V is the irradiated volume (L), ϕ is the quantum yield for the cyclization of A540 at the irradiation wavelength used (ϕ = 0.2[126]), N_A is the Avogadro constant, ε_{max} is the molar absorptivity of A540 at 494 nm (ε_{max} = 7874 M^{-1} cm^{-1} [126]), l is the optical pathlength of the quartz cell, and t is the irradiation time.

To determine the cyclization quantum yield of **23**, the change in absorbance for the DTE solution before and after irradiation with UV light was measured at the wavelength of maximum absorption (λ_{max}) in the visible region. From the change in absorbance, the ϕ was calculated using Eq. 2,

$$\phi = \left[\frac{\log T_0}{(1 - T_0)} - \frac{\log T_t}{(1 - T_t)} \right] \times \frac{V}{N_A (h\nu / t) \times \varepsilon_{max} \times l \times t} \quad (2)$$

where T_0 is the transmittance at λ_{max} before irradiation, T_t is the transmittance at λ_{max} after irradiation, $h\nu/t$ is the photon rate determined from A540 in ethyl acetate[126], ε_{max} is the molar absorptivity at λ_{max} in the visible region. The cycloreversion quantum yield was determined in a similar manner. Before the solutions containing A540 and the DTE were matched, they were irradiated with UV light for 12–15 min to their PSS. The absorbance of each solution was measured following irradiation with visible light. Given that the cycloreversion quantum yield of A540 in ethyl acetate at 530 nm has not been reported, the quantum yield of A540 in *n*-hexane[126] was used as a primary standard. The cycloreversion quantum yield of A540 in ethyl acetate was determined to be 0.032 ± 0.004.

2.5.3. Photoconversion Studies

The percentage of closed-ring isomers in the photostationary state was determined for **23** from HPLC studies. Cyclization to the closed-ring isomer was performed by irradiation with UV light (λ = 365 nm). The integrated area for the peak representing the

closed-ring isomer was divided by the sum of the integrated areas for the peaks representing both isomers and was calculated as a percentage.

2.5.4. Photostability Studies

The photostability of **21**–**23** in ethyl acetate, in presence of air, at a concentration of 0.07 μM was measured using a UV-vis absorption spectrometer. Changes in absorbance were measured for at least five cycles of photoinduced cyclization and cycloreversion. Cyclization to the closed-ring isomer was performed by irradiation with UV light (λ = 365 nm) until PSS was reached (3 min for **21** and **22**, and 10 min for **23**, respectively). Cycloreversion to the open-ring isomer was performed by irradiation with visible light (λ = 530 nm) until no absorption was observed in the visible region (2 min for **21** and **22**, and 3 min for **23**, respectively). The absorbance at λ_{max} in the visible region was measured for both the cyclization and cycloreversion processes. That is, the absorbance was recorded at 585 nm for **21** and **22**, and at 588 nm for **23**.

2.6. Procedure for Ion Permeation Studies

2.6.1. Proton Permeation Assay

The protocol to prepare lipid vesicles and the proton permeation assay has been adapted from a previously published procedure.[127] The preparation of large unilamellar vesicles (LUVs) with or without **21**–**26** followed similar procedures. Generally, the preparation protocol requires two days to obtain LUVs for further study (Figure 2.1).

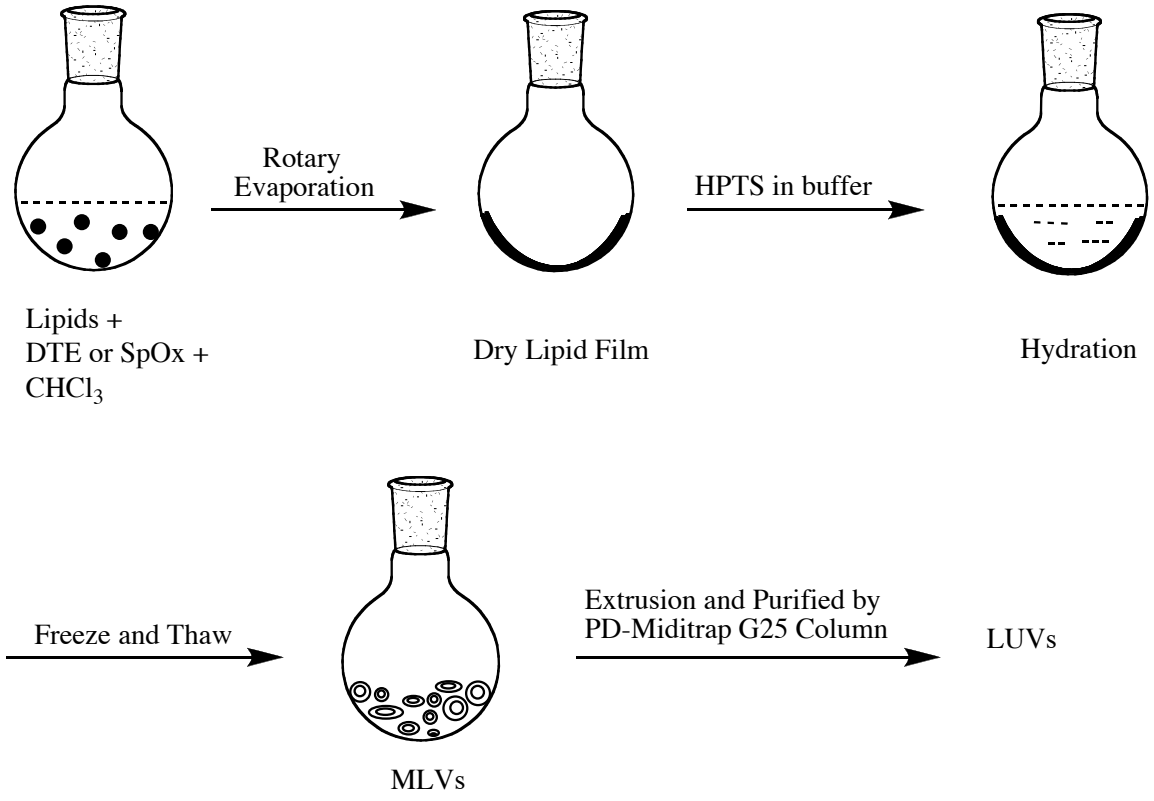

Figure 2.1. Schematic representation of the procedure used in the preparation of LUVs.

The first day involved the formation of a dry lipid film, which was left under reduced pressure for at least 3 h and followed by hydration of the lipid film with HPTS in phosphate buffer solution for at least 3 h. The next day the hydrated lipid vesicles were extruded through polycarbonate membrane filters with a pore size of 0.1 μm to give LUVs of uniform size. After extrusion the samples were eluted through PD-Miditrap desalting columns to remove the unencapsulated HPTS. These columns are commonly used for the separation of high molecular weight substances (MW > 5000 g/mol) such as lipid vesicles from low molecular weight substances (MW < 1000 g/mol) such as HPTS.

Lipid stock solutions (2 mg/mL) of DOPC, DPPC, diPhyPC, and lecithin were prepared in $CHCl_3$, respectively. Separate stock solutions of DTE **21**–**23** and SpOx **24**–**26** in $CHCl_3$ (1 mM), and 8-hydroxypyrene-1,3,6-trisulfonic acid trisodium salt (HPTS; 10 μM) in phosphate buffer were prepared. The phosphate buffer contains 10 mM Na_3PO_4 and 100 mM NaCl in deionized nanopure water. The pH of the buffer solution was adjusted to 6.4 using H_3PO_4.

The same procedure was followed to prepare all lipid vesicles except the volume of DTE or SpOx used to get different molar ratios. For example, to prepare DOPC vesicles containing **21** at a mole ratio of 1:20 (**21**/DOPC), a stock solution of **21** (127 μL) and DOPC (1 mL) were added to a 10 mL round bottom flask. The $CHCl_3$ was evaporated under reduced pressure to deposit a lipid film. The lipid film was dried under vacuum for more than 3 h to remove all organic solvents. Then the dry lipid film was hydrated with internal HPTS buffer solution (1 mL) at 50.0 ± 0.1 °C for a minimum of 3 h. The lipid suspension was left to stand overnight at 4 °C in the refrigerator. The hydrated lipid suspension underwent 5 freeze and thaw cycles by placing the sample in a

dry ice/acetone bath, followed by a warm water bath and vortexed for 30 s. The Mini extruder was placed on a hot plate and the temperature was measured to be 50.0 ± 0.5 °C using a thermometer inserted into a well on the stand. The suspension was extruded 21 times in 1 mL gas tight syringes using 0.1 μm polycarbonate membrane filters to get uniform LUVs. After extrusion the samples were filtered through PD MidiTrap G-25 desalting columns. The disposable column contains pre-packed Sephadex G-25 as a stationary phase and a mobile phase used was phosphate buffer. Each column was equilibrated with 15 mL of buffer solution prior to use. The extruded samples were loaded onto the column and eluted with 1.5 mL of buffer to remove extravesicular HPTS. The first 5 drops of eluent from the column were discarded to obtain a purified lipid vesicle sample (ca. 1.2 mL, ca. 91 μM).

The protocol for the proton permeation assay has been adapted from a previously published procedure.[113] The modulated emission intensity of HPTS at 510 nm was monitored at excitation wavelengths 403 and 460 nm. For non-irradiated samples, 2 mL of phosphate buffer, and 100 μL of the lipid vesicle sample were added to a fluorescence cell and stirred. Following a 150 s equilibration period, 50 μL of 0.5 M NaOH was added. After ca. 700 s, the vesicles were lysed with 50 μL of a 5% Triton X-100 solution. For irradiated samples, after 70 s of equilibrated period, the sample was irradiated with UV light for 3 min followed by equilibration for 80 s, and at 150 s, 50 μL of 0.5 M NaOH was added. All samples were measured at 21.0 ± 0.1 °C. All data collected during the 150 s equilibration period and ca. 30 s after the addition of base was ignored when fitting the data . The relative emission intensity E_{403}/E_{460} (I) was calculated. The extent of proton permeation (N) was calculated using Eq. 3,

$$N = \frac{(I_t - I_0)}{(I_f - I_0)} \tag{3}$$

where I_t is the relative emission intensity at time t, I_0 is the relative emission intensity at t_0, and I_f is the relative emission intensity when the vesicles are lysed. The extent of ion permeation was plotted against time, and the slope from the linear fit represents the rate constant for proton permeation. The results obtained for the vesicles incorporating photochromic compounds were compared with control vesicles composed of only lipids. These comparisons help to ensure that the changes observed are due to the effect of inclusion and photoisomerization of photochromic compounds on the permeability of the lipid vesicles. T-tests were performed at a 95% confidence interval to confirm that our comparisons were statistically significant. Even with well-controlled protocols, replicates conducted from a single batch of vesicles under optimal conditions have been shown to vary by a factor of ± 20%.[113] In plots of N vs. time, the data was often randomly scattered about the linear fit. As a result, the R^2 values obtained from these fits varied from 0.6 to 0.8 for DPPC vesicles, yet the R^2 values were greater than 0.9 for DOPC vesicles. In addition, upon irradiation of vesicles incorporating DTEs some quenching of the HPTS emission was observed because the closed-ring isomers do absorb at 510 nm. This quenching resulted in an apparent increase in the extent of ion permeation before the addition of base. In these cases, the extent of ion permeation prior to lysis was corrected by subtraction of this experimental artifact.

To assess aggregation behavior, the extent of ion permeation (N) at 700 s for the various mole ratios of DTE in DPPC vesicles was used. The mole ratios that gave the minimal and maximal extent of ion permeation (i.e., N_{min} and N_{max}) were used to

recalibrate for a fractional activity (Y) using Eq. (4)

$$Y = \frac{(N - N_{\min})}{(N_{\max} - N_{\min})} \tag{4}$$

A plot of Y as a function of the concentration of DTE yielded a sigmoidal curve. The Hill coefficient n was obtained from the curve fit using the Hill equation (5)[128].

$$Y = Y_{\infty} + (Y_0 - Y_{\infty})/(1 + (c/K_D)^n) \tag{5}$$

where Y_0 = Y without DTE; Y_{∞} = Y with excess DTE; c = concentration of DTE; n = Hill coefficient; K_D = dissociation constant.

2.6.2. Potassium Ion Permeation Assay

The protocol to prepare lipid vesicles for the potassium ion permeation assay has been adapted from a previously published procedure.[34,127] The preparation of LUVs with or without SpOxs **24**–**26** and DTEs **21** and **22** followed similar procedures to those prepared for the proton permeation assay studies. In potassium ion assay, the internal aqueous compartment of LUVs was encapsulated with 0.2 M KCl. Also, the concentration of a lipid used for the preparation of LUVs in each sample was 4 mg/mL.

Potassium ion that permeates across a bilayer membrane was monitored using K^+ specific ion microelectrode and reference electrode connected to a pH/conductivity meter, which measures the potential of a solution. In a quartz test tube, 2 mL of phosphate buffer, and 100 μL of the lipid vesicle sample were added and stirred. After a stable potential was observed, the samples were alternatively irradiated with UV and visible light for 6 min. The permeation of potassium ion, in terms of potential, was

continuously measured during the irradiations. After 3.5 cycles, the potential for the total concentration of potassium ion in the lipid vesicle was then determined by adding 50 μL of 5% Triton X-100. The measured potential in mV was then converted to concentration of potassium ion using the calibration plot.[129] The potassium ion-selective electrode was calibrated with serial dilutions of 0.01–5.00 mM KCl in phosphate buffer. A calibration curve was prepared from the electrode potentials recorded at various concentrations of potassium chloride in phosphate buffer. A strong linear correlation was observed (i.e., R^2 = 0.9954, Figure 2.2). The slope of the calibration curve was used for the conversion of mV to potassium ion concentration. The concentration of potassium ion that permeates across a bilayer membrane was plotted against the irradiation time, and the slope from the linear fit represents the rate constant for potassium ion permeation. The rate constants determined in these studies are for a zero order process, expressed with units of M/s for our experimental conditions. The percent release was calculated using Eq. 6,

$$\%\text{release} = \frac{(C_t - C_0)}{(C_f - C_0)} \times 100 \tag{6}$$

where C_t is the concentration of potassium ion at time t (t was taken during irradiation with UV and visible light), C_0 is the concentration of potassium ion at t_0, and C_f is the concentration of potassium ion when the vesicles are lysed after 3.5 cycles of alternating irradiation with UV and visible light.

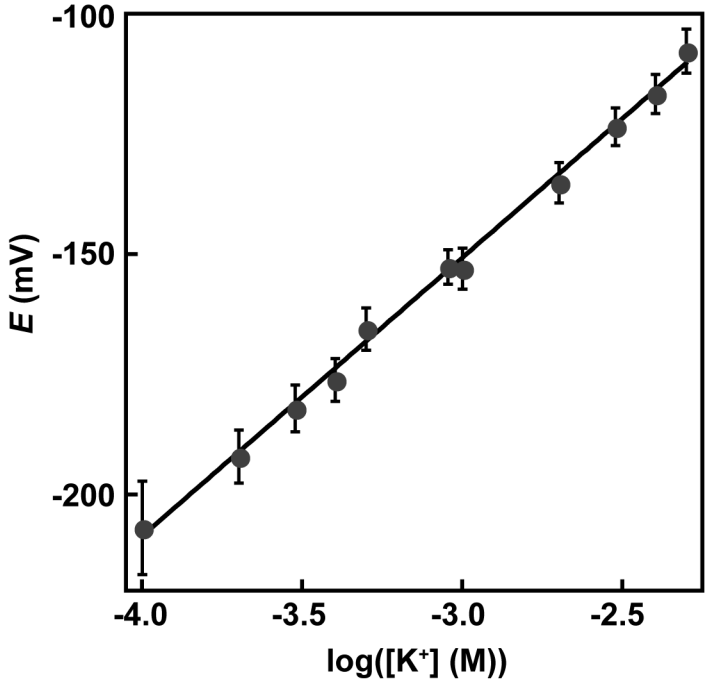

Figure 2.2. Calibration curve for the electrode potential of potassium ions in phosphate buffer.

CHAPTER 3

SYNTHESIS AND PHOTOPHYSICAL CHARACTERIZATION OF ASYMMETRICAL AMPHIPHILIC DTEs

In this chapter, the following sections are discussed in order. First, the synthesis of **21**–**23** is discussed. Then, the absorption properties and the photochromic reactivity of **21**–**23** are described. Subsequently, the photostability of **21**–**23** is presented.

3.1. Synthesis of Asymmetrical Amphiphilic DTEs

To carry out the photophysical studies and the lipid vesicle studies, three asymmetrical, amphiphilic of DTEs were synthesized. The synthesis of these DTEs was achieved by following the procedures previously reported by past research group members.[111] However, slight modifications to the purification procedures will be described.

DTEs **21** and **22** contain rigid phenylethynyl substituents at their reactive carbons. Specifically, these are the C2 and C2′ positions situated on the thiophene ring systems. These phenylethynyl substituents are bulky when compared with methyl substituents found at the reactive carbons of **23**. Also, these DTEs include a cationic quaternary ammonium group at the end of alkyl chain to improve their amphiphilicity when compared with previously reported parent DTE derivative.[19] As a result, this 'charged tether' will most likely promote a favorable organization in a lipid bilayer membrane

where the ammonium group will interact within the polar headgroup region of a lipid bilayer, while the photochromic moiety will reside in the non-polar aliphatic region.

A regioselective approach was used for the synthesis of these asymmetrical DTEs. This approach circumvents the undesired reactivity of phenylethynyl substituents as reported previously.[19] That is, the substitution at the C5 and C5′ positions of the thiophene rings were introduced first prior to coupling the phenylethynyl substituents to the reactive carbons. The synthesis of **21** and **22** begins with amino acids as starting materials (Scheme 3.1). The first step is the conversion of primary amines in **28** and **29** to tertiary alkyl amines **30** and **31** by reductive amination using 37% formaldehyde and hydrogen gas over 10% palladium on carbon as a catalyst in aqueous solution. Carboxylic acids in **30** and **31** were then reacted with thionyl chloride to produce acid chlorides **32** and **33**. These acid chlorides **32** and **33** were used, without further purification, in the Friedel-Crafts acylation reaction with bromobenzene to form ketones **34** and **35**, respectively. In the subsequent step, the Wolff-Kishner reduction of these ketones at high temperature gave the reduced products **36** and **37** as pale yellow oils. Then, the compounds **36** and **37** were converted to the corresponding boronic acids **38** and **39**. In the next steps, Suzuki and Sonogashira cross coupling reactions were employed to introduce various substituents at the reactive C2 position of thiophene derivatives. A Suzuki coupling reaction of **38** and **39** with 2,4-dibromothiophene **40** afforded the intended coupled products **41** and **42**, respectively. In the next step, the electrophilic bromination of **41** and **42** using *N*-bromosuccinimide (NBS) yields **43** and **44**. Then, the phenylethynyl substituent was introduced using a Sonogashira reaction by coupling phenylacetylene to the bromo-substituted products to give intermediates **45** and **46** in good yields.

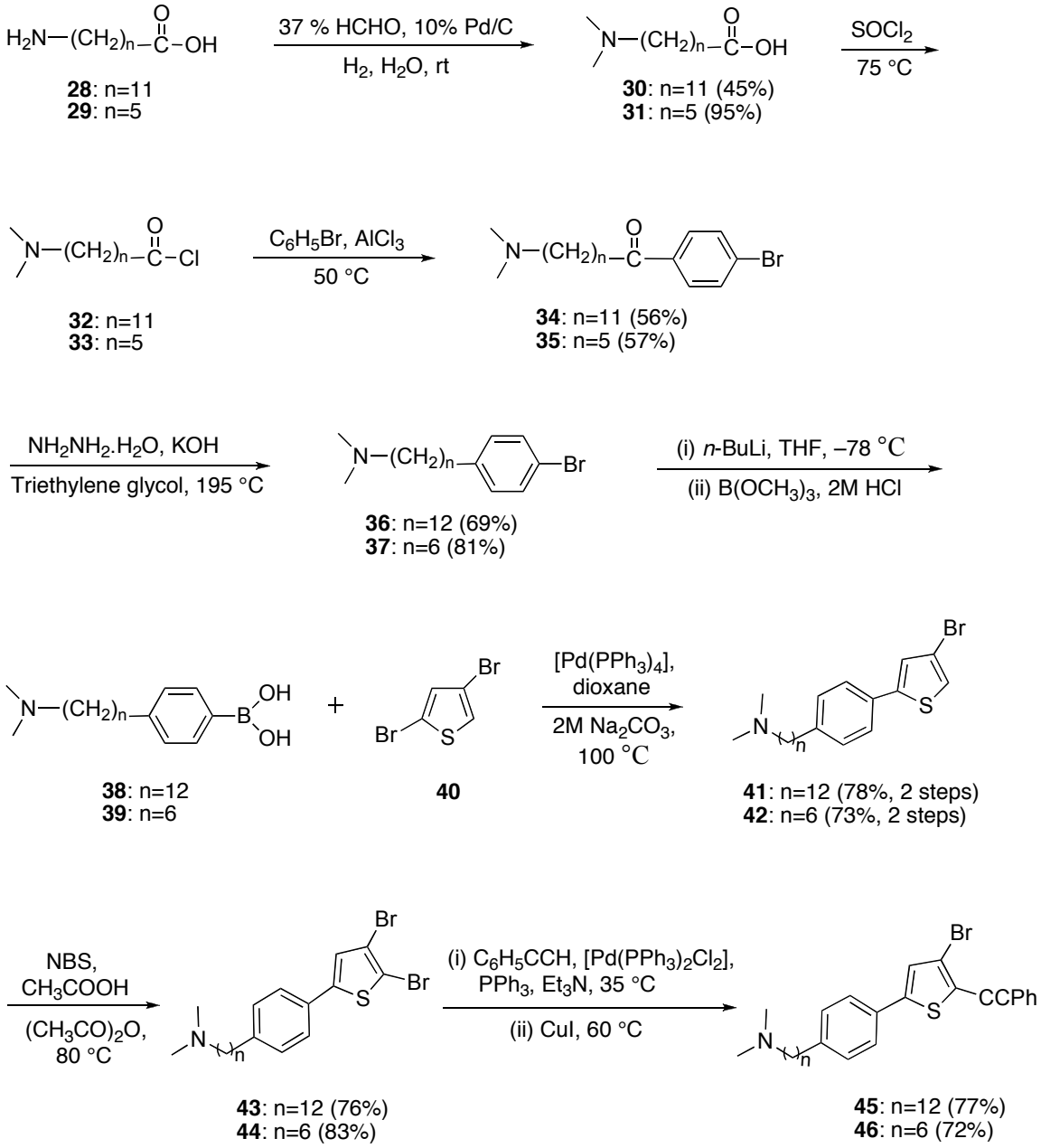

Scheme 3.1. Synthesis of **45** and **46**.

A Suzuki coupling reaction between 2,4-dibromothiophene and phenylboronic acid formed the coupled product **47** in a moderate yield (Scheme 3.2). The brominated product **48** obtained from **47** was subjected to a Sonogashira coupling reaction with phenylacetylene to give a colorless solid **49**. The reaction of **49** with ten equivalents of octafluorocyclopentene (OFCP) using *n*-BuLi produced shiny yellow crystals of **50** after recrystallization. The reason for using excess equivalents of OFCP is to minimize the formation of symmetrical DTE. The coupling of the lithiated intermediates **45** and **46** with compound **50** gave the precursors **51** and **52** of the final product **21** and **22**, respectively. Compounds **43**–**46**, **51** and **52** were purified by column chromatography using neutral alumina as the stationary phase and 1:7 diethyl ether/petroleum ether solvent mixture as the mobile phase. On silica gel TLC plates, the retention factor (R_f) values for these compounds are very close to the R_f value of their respective side products. A better separation of these compounds from side products was achieved only when alumina was used as the stationary phase in column chromatography. Conversion of tertiary amine in **51** and **52** to their respective quaternary ammonium group was achieved by reacting them with iodomethane, which afforded the final products **21** and **22**, respectively. A synthetic route of **22** was adapted to prepare **23** in which the 3,5-dibromo-2-methylthiophene was used to introduce the methyl substituents at the reactive carbons (Scheme 3.3). These synthesized DTEs were examined using photophysical methods to determine their absorption properties, cyclization and cycloreversion quantum yields, photoconversion, and photostability. These photophysical properties were measured using UV-vis absorption spectroscopy. Photoconversion studies were carried

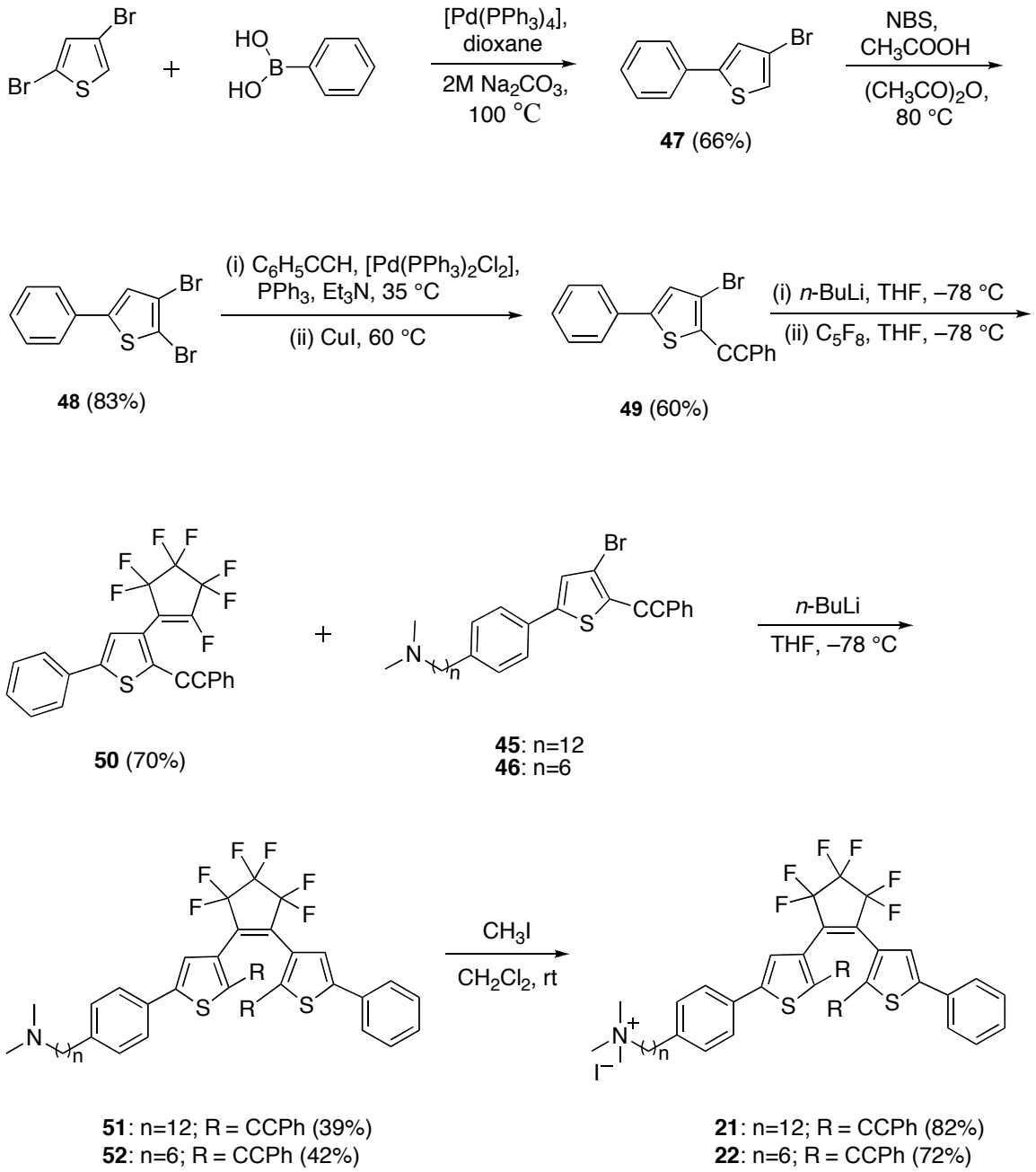

Scheme 3.2. Synthesis of **21** and **22**.

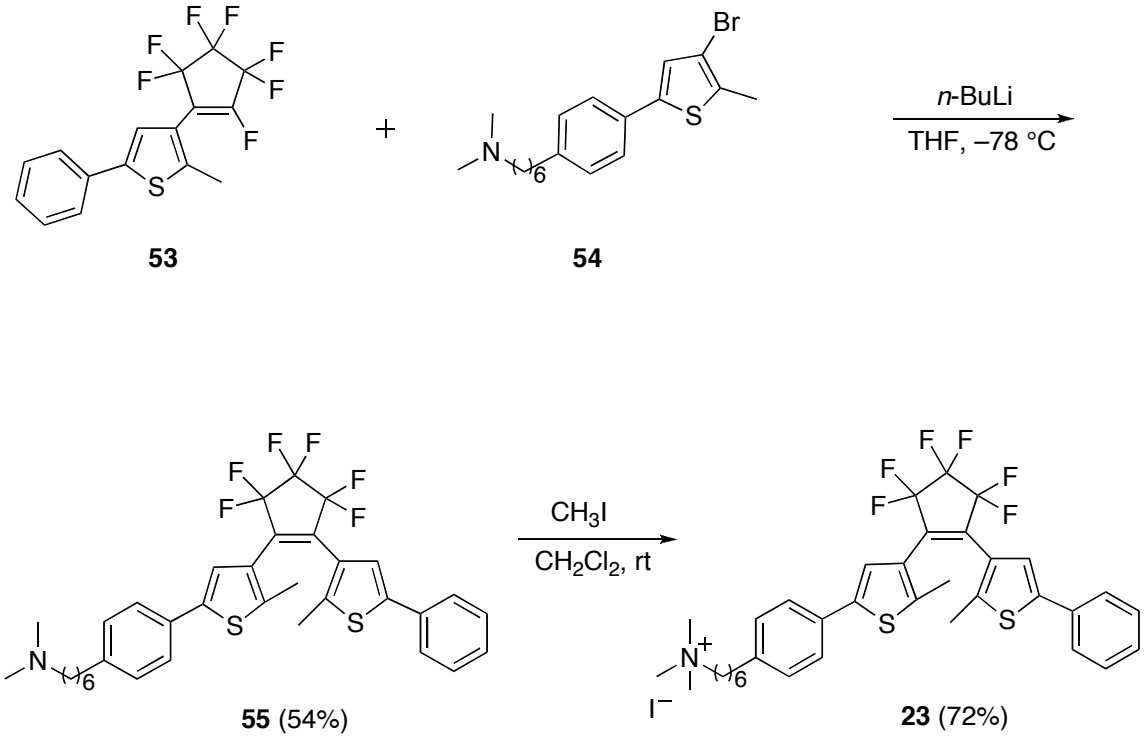

Scheme 3.3. Synthesis of **23**.

out using HPLC, which separates the open-ring and closed-ring isomers of DTEs. The results of these studies are described in the following sections.

3.2. Absorption Properties of 21–23

Photochromism of **21**–**23** was observed in ethyl acetate (Figure 3.1). The open-ring and closed-ring isomers of **21**–**23** show well-separated absorption bands (Figure 3.2 and Table 3.1). The open-ring isomer has an absorption maximum in the UV region while the closed-ring isomer also has an absorption maximum in the visible region. Prior to irradiation of **23** with UV light, the open-ring isomer **23o** was predominant with its absorption maximum at 288 nm and no absorption due to closed-ring isomer **23c** was observed. Following irradiation with UV light (λ = 365 nm), the yellow solution of **23o** turned blue, and an increase in absorbance at 588 nm was observed with a concomitant decrease in absorbance at 288 nm. The absorption band at 588 nm signifies the formation of **23c**. Additional irradiation of **23** with UV light for 10 min brought the system to a PSS of the open-ring and closed-ring isomers. An isosbestic point was also observed at ca. 310 nm, which represents the presence of only two interconverting isomers in solution.[112] Further, the absorbance of **23** at λ_{max} in the visible region decreases to a minima following irradiation with visible light (λ = 530 nm) for 180 s (Figure 3.3). The molar absorptivity for both open-ring and closed-ring isomers was measured to calculate the cyclization and cycloreversion quantum yields. Similar absorption properties were also observed for **21** and **22**. Also, the closed-ring isomers of **21c**–**23c** show no evidence of thermal isomerization to **21o**–**23o** after 24 h in the dark at room temperature.

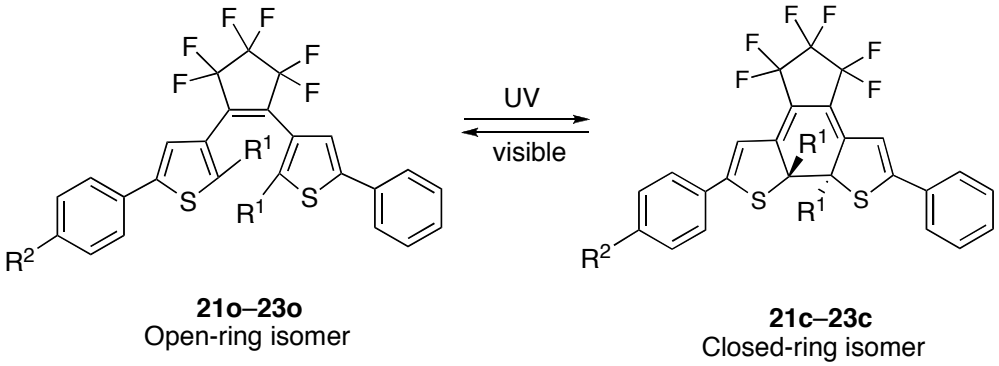

21o–23o
Open-ring isomer

21c–23c
Closed-ring isomer

21: R^1 = CCPh; R^2 = $(CH_2)_{12}N^+(CH_3)_3I^-$

22: R^1 = CCPh; R^2 = $(CH_2)_6N^+(CH_3)_3I^-$

23: R^1 = CH_3; R^2 = $(CH_2)_6N^+(CH_3)_3I^-$

Figure 3.1. Photoisomers of amphiphilic DTEs.

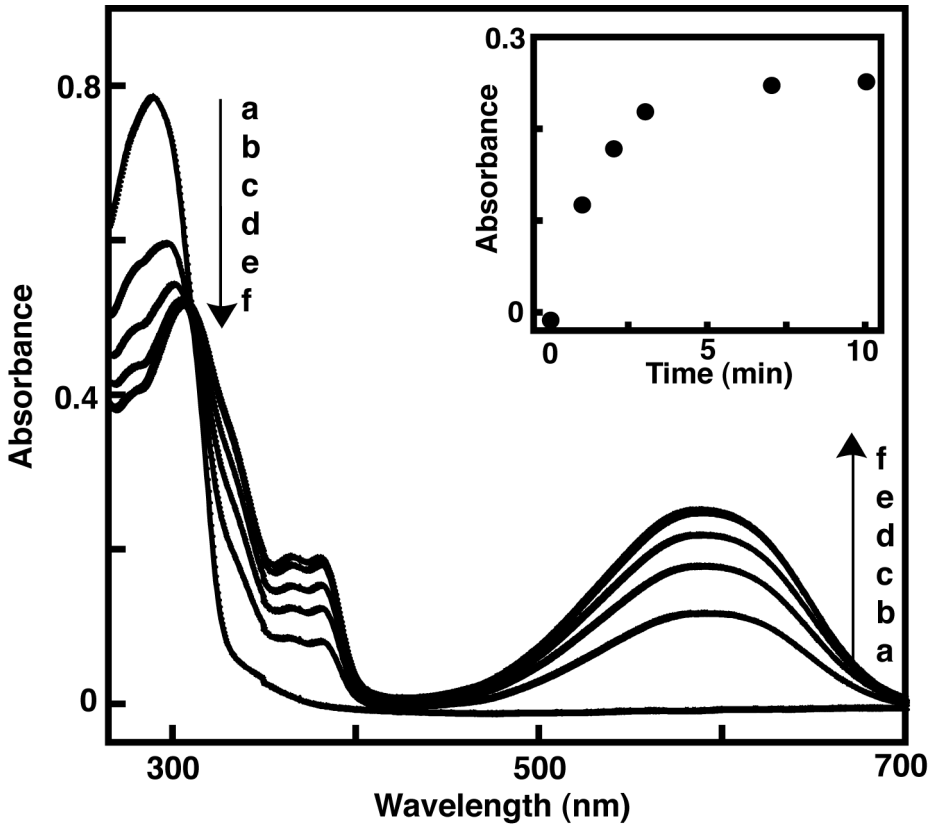

Figure 3.2. Absorption spectra of **23** in ethyl acetate a) prior to irradiation, and after irradiation with UV light in the following sequence: b) 1 min, c) 2 min, d) 3 min, e) 7 min, and f) 10 min. The inset is a plot of absorbance at λ = 588 nm as a function of total irradiation time.

Table 3.1. Absorption properties and quantum yields of **21**–**23** in ethyl acetate[a]

DTE	λ_{max} (nm)[b]	ε (10^4 M^{-1} cm^{-1})	ϕ
21o	310	1.93 ± 0.09	0.28 ± 0.03[c]
22o	312	4.17 ± 0.50	0.10 ± 0.02[c]
23o	288	3.85 ± 0.18	0.46 ± 0.02[c]
21c	585	0.47 ± 0.01	0.38 ± 0.08[d]
22c	585	0.98 ± 0.08	0.15 ± 0.01[d]
23c	588	1.64 ± 0.04	0.008 ± 0.001[d]

[a] The error is the standard deviation of the mean taken from a minimum of three independent measurements.
[b] The error is ± 1 nm.
[c] Cyclization quantum yield.
[d] Cycloreversion quantum yield.

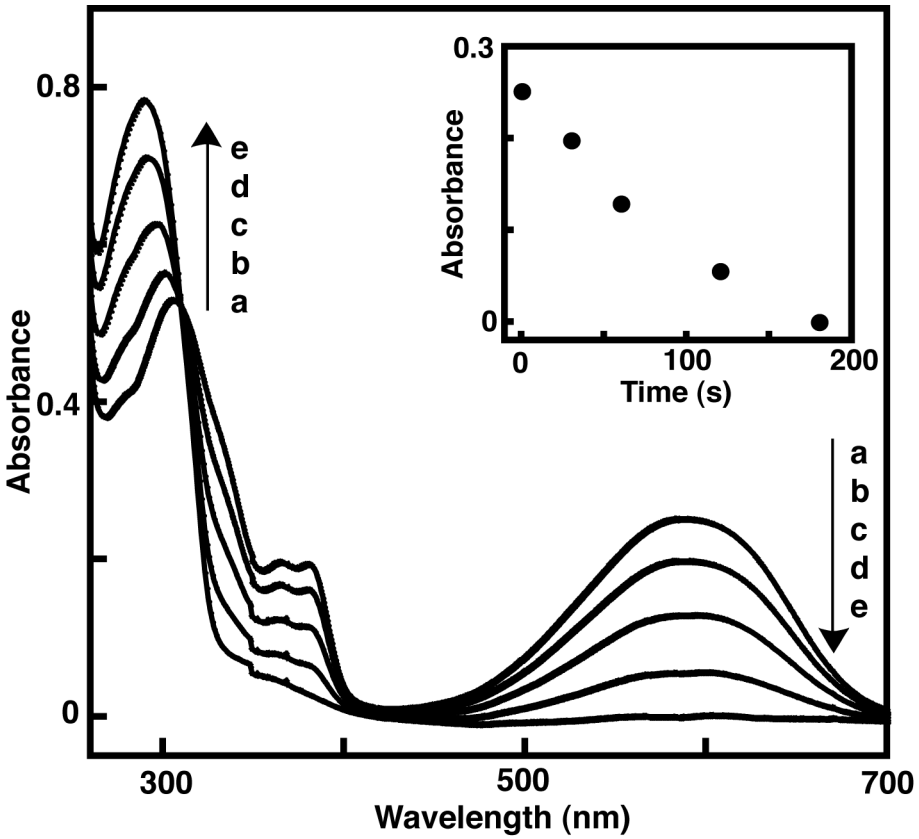

Figure 3.3. Absorption spectra of **23** in ethyl acetate a) at the PSS, and after irradiation with visible light in the following sequence: b) 30 s, c) 60 s, d) 120 s, and e) 180 s. The inset is a plot of absorbance at λ = 588 nm as a function of total irradiation time.

UV-vis absorption properties for **21**–**23** were also measured in DPPC vesicles to ensure that DTEs are included in the lipid bilayer membrane, and photoisomerization does occur. For example, the absorption spectrum of **21** incorporated in DPPC vesicles at 1:20 mole ratio (**21**/DPPC) shows an absorbance maximum at 310 nm (Figure 3.4). Following UV irradiation, an increase in absorbance at 600 nm was observed with a concomitant decrease in absorbance at 310 nm. Also, the spectrum for pure DPPC vesicles does show moderate light scattering, which increases at shorter wavelengths. These results suggest that DTEs are incorporated into the bilayer membrane of lipid vesicles and undergo photoisomerization upon UV irradiation.

3.3. Quantum Yields and Photoconversion of 21–23

The cyclization and cycloreversion quantum yields of **21**–**23** were also determined in ethyl acetate (Table 3.1). The open-ring isomer of DTEs has two conformations; parallel, and antiparallel conformations. These two conformers undergo interconversion in solution. The conrotatory photocyclization reaction can proceed only from the antiparallel conformation.[4] As a result, the cyclization quantum yield is dependent on the ratio of the two conformers. When the concentration of the photoactive antiparallel conformation is increased, the quantum yield is expected to increase. The cyclization quantum yield for **23o** was found to be five fold higher than its phenylethynyl analog **22o** (Table 3.1). This result suggests that the bulky phenylethynyl substituents may decrease the relative concentration of the photoactive antiparallel conformer when compared with methyl substitution. Notably, the cycloreversion quantum yield of **23c**

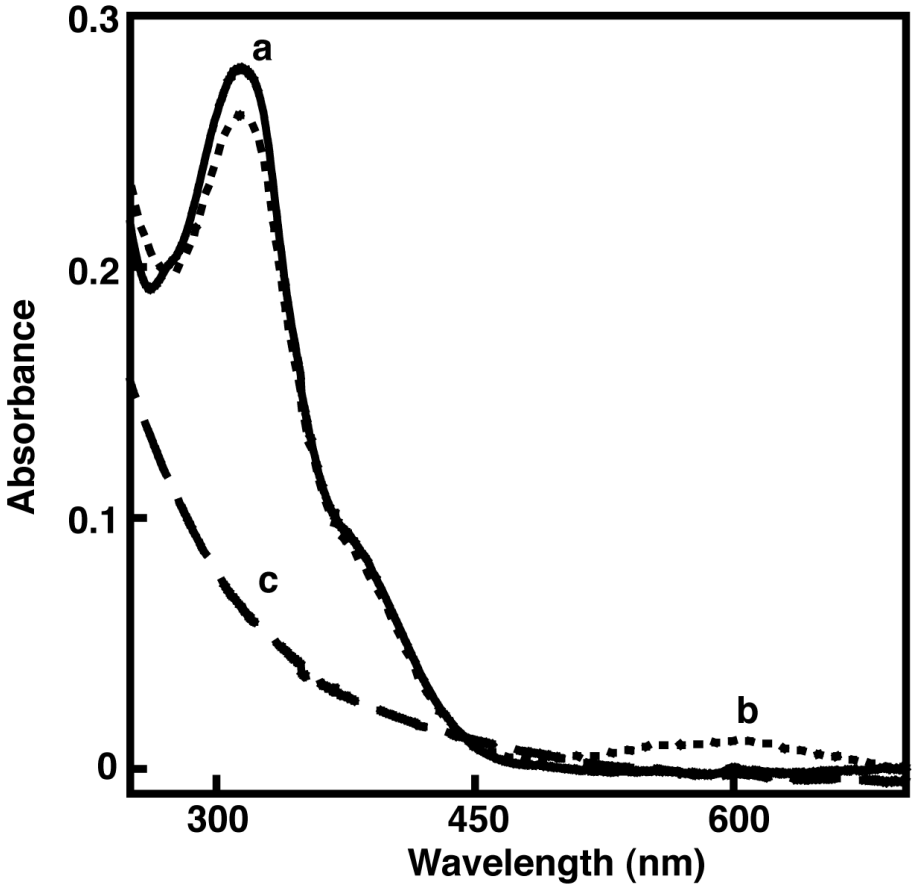

Figure 3.4. Absorption spectra of **21** in DPPC vesicles at a mole ratio of 1:20 (**21**/DPPC) a) open-ring isomer, b) closed-ring isomer, and c) pure DPPC vesicles.

was 18-fold lower than **22c**. In general, the introduction of phenylethynyl substituents at the reactive carbons of DTEs show an enhancement in the efficiency of the cycloreversion reaction relative to the cyclization reaction.[18,19] Upon irradiation with UV light, the conversion from **23o** to **23c** at the PSS was 82 ± 0.3%. This result agrees well with previously reported DTEs that contain methyl substituents at the reactive carbons.[113] The conversion efficiency of **23** was significantly higher than **21** and **22** (52 ± 0.4% and 48 ± 0.5%, respectively). This result further suggests that the presence of methyl substituents increased the conversion of open-ring to the closed-ring isomer when compared to the phenylethynyl substituents. The next section describes how the substituents affect the photostability of DTEs under continuous irradiation of alternate UV and visible light.

3.4. Photostability of 21–23

The photostability of **21**–**23** was measured in ethyl acetate. This property was determined by monitoring changes in absorbance at the λ_{max} of the closed-ring isomer in the visible region, as the photochromic compounds were switched between their isomeric states with UV and visible light (Figure 3.5). After five complete cycles of alternating UV and visible irradiation, DTEs **21**, **22**, and **23** underwent 17%, 14%, and 5% degradation, respectively. As a result, the photostability was found to increase in the order of **21** < **22** < **23**. These results suggest that the presence of phenylethynyl substituents lowers the photostability of DTEs when compared with those

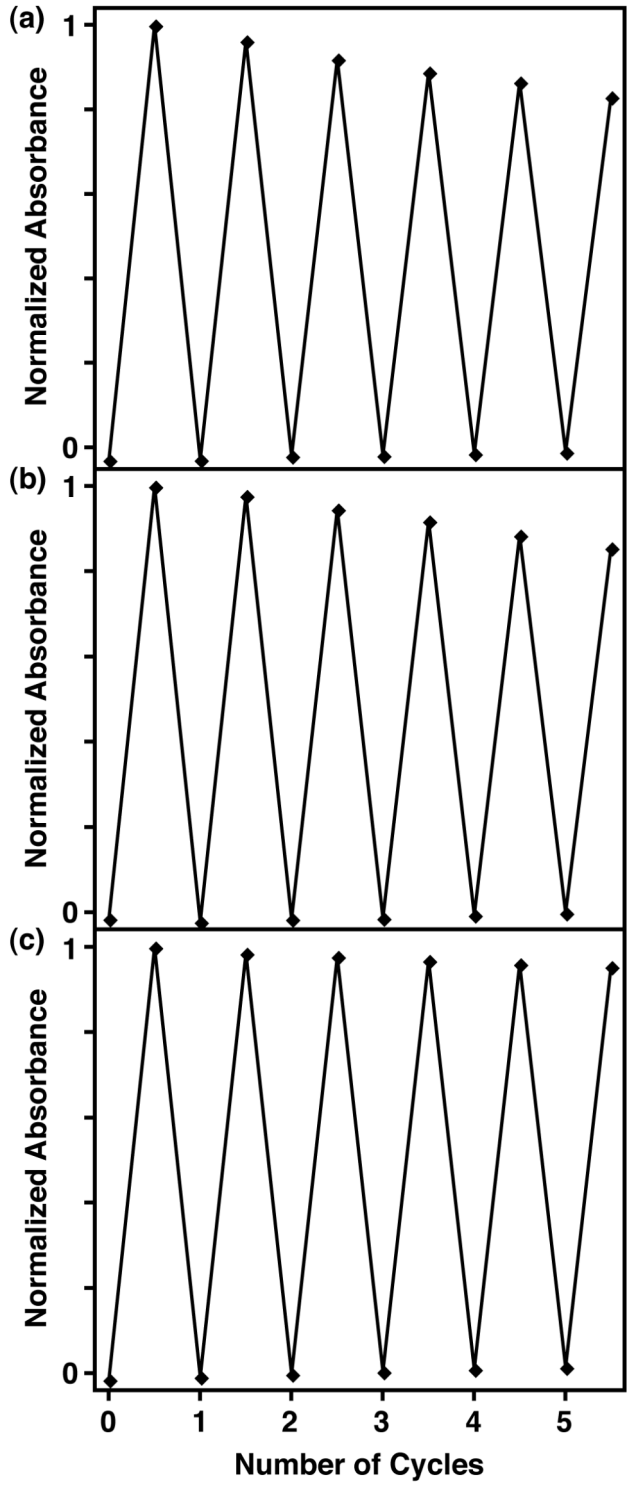

Figure 3.5. Changes in the absorbance at the λ_{max} for **21c**–**23c** (a–c, respectively) in ethyl acetate, upon alternating irradiation with UV and visible light.

containing methyl substituents. This irreversible photodegradation is consistent with the previous reports on the photostability of DTEs.[19] This degradation stems from prolonged UV irradiation of the closed-ring isomers to an isomeric photostable by-product **21b**–**23b** (Scheme 3.4). Moreover, the thiophene rings in a closed-ring isomer are converted into a fused ring system with two six membered heterocyclic rings. The ^{1}H NMR spectrum for **21b** shows two new signals at 6.67 ppm and two signals at 6.83 ppm upon prolonged irradiation of **21o** with UV light (Figure 3.6). The two singlets at 6.83 ppm can be assigned to the thiophene hydrogens (H_a) on the closed-ring isomer (**21c**), while the two singlets at 6.67 ppm can be assigned to the hydrogens (H_b) of the photostable by-product (**21b**). The signal at 6.67 ppm of **21b** continues to increase with continuous UV irradiation. This clearly suggests that **21b** is a product of the photolysis of **21c**, which is consistent with previous reports.[5,14,114] The formation of the photostable by-product in DTEs may involve a methylcyclopentene diradical as a possible intermediate.[16,115] The phenylethynyl substituents in **21** and **22** may increase the stability of the diradical intermediates through delocalization. Thus, increased degradation was observed in the case of phenylethynyl derivatives **21** and **22** when compared with the methyl derivative **23**.

3.5. Summary

Three asymmetrical amphiphilic DTEs **21**–**23** have been synthesized through a regioselective approach. In particular, the coupling of phenylacetylene with a thiophene derivative under Sonogashira reaction conditions was always carried out as the final

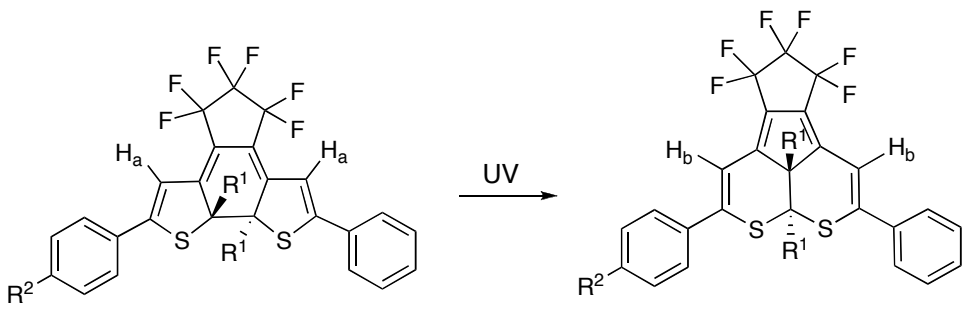

21c–23c
Closed-ring Isomer

21b–23b
Photostable by-product

21: R^1 = CCPh; R^2 = $(CH_2)_{12}N^+(CH_3)_3I^-$

22: R^1 = CCPh; R^2 = $(CH_2)_6N^+(CH_3)_3I^-$

23: R^1 = CH_3; R^2 = $(CH_2)_6N^+(CH_3)_3I^-$

Scheme 3.4. Photostable by-product formed upon prolonged irradiation of closed-ring isomer with UV light.

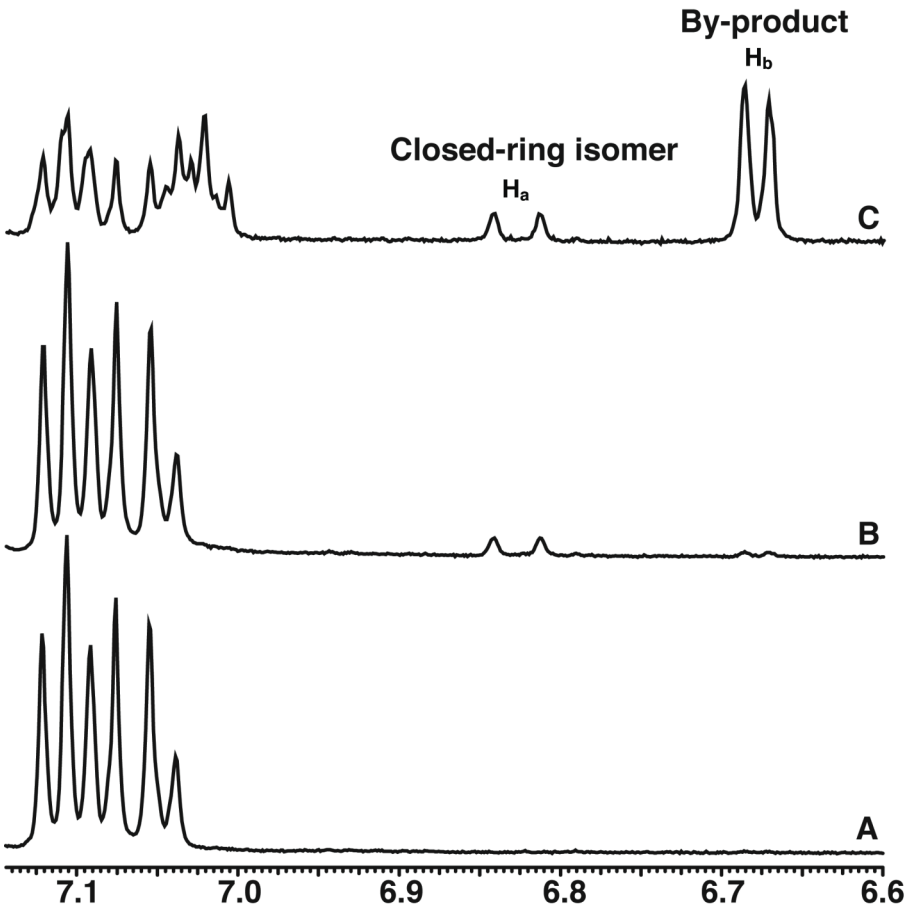

Figure 3.6. ^{1}H NMR spectra of **21**: A) prior to irradiation; B) after irradiation with UV light for 45 min; C) after irradiation with UV light for 8 h.

substitution to avoid unwanted reactivity of the labile alkynyl substituent during bromination reactions. The absorption properties and photochromic reactivity of **21**–**23** were studied in ethyl acetate. The open-ring and closed-ring isomers of **21**–**23** have well separated absorption bands. The open-ring isomers have absorption maximum in the UV region while the closed-ring isomers have the absorption maximum in both the UV and visible regions. The cyclization quantum yield and photoconversion of **23** are higher than **21** and **22** due to differences in substitution at the reactive carbons. However, DTEs **21** and **22** exhibit higher cycloreversion quantum yields. Further, DTE **23** is more photostable than **21** and **22**. The decrease in photostability of **21** and **22** is due to the presence of phenylethynyl substituents, which enhances the formation of a photostable by-product upon UV irradiation.

CHAPTER 4

PHOTOCONTROL OF PROTON PERMEATION IN LIPID VESICLES

In this chapter, studies on the photocontrol of proton permeation across lipid bilayer membrane incorporating DTEs and SpOxs are presented. First, the assay used for proton permeation studies is discussed. Then, the rate constant of proton permeation and the extent of proton permeation obtained for the pure lipid vesicles are discussed. This is followed by a discussion of the effect of inclusion and photoisomerization of DTEs **21**–**23** on proton permeation in lipid vesicles. Finally, a similar study will be presented for SpOx derivatives **24**–**26** in lipid vesicles. Then, these series of photochromic compounds will be compared to identify the photoresponsive system that exhibits good photocontrol of proton permeation.

4.1. Proton Permeation Assay

Proton permeation across a bilayer membrane incorporating photochromic compounds was assessed using a common ratiometric fluorescence technique. In this assay, photochromic compounds were incorporated into the bilayer membrane during the preparation of lipid vesicles. Also, HPTS was encapsulated inside the internal aqueous compartment of the lipid vesicles (Figure 4.1).[120,121] HPTS is a highly water soluble pH-sensitive fluorophore. The acid and the conjugate base forms of HPTS have the same wavelength of maximum emission (i.e., λ_{em} = 510 nm), whereas the wavelengths of

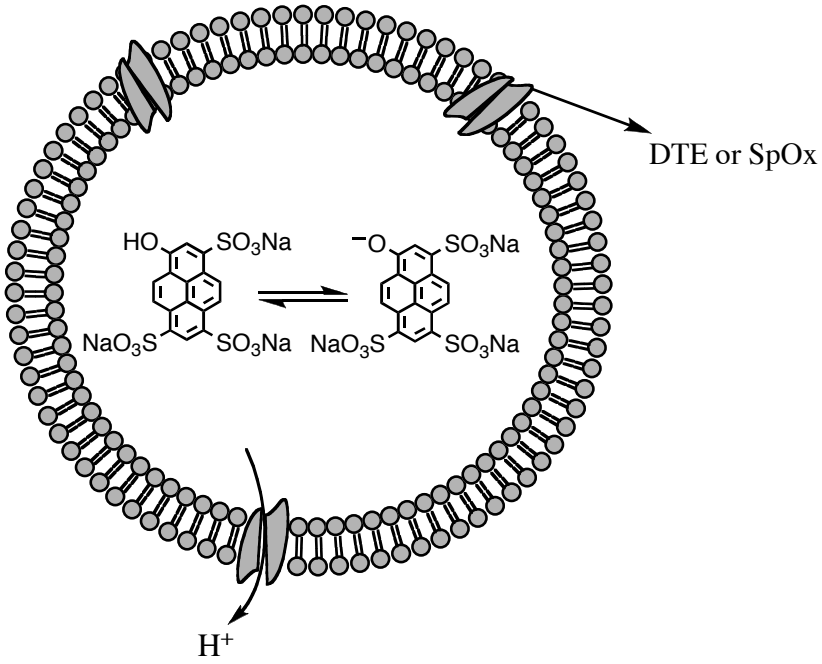

Figure 4.1. Schematic representation of proton permeation across bilayer membrane.

maximum excitation (λ_{ex}) differ for the acid and conjugate base form (i.e., 403 and 460 nm, respectively). The fluorescence of these vesicles is stable prior to the addition of a base to the external buffer. Further, the permeation of protons across the bilayer membrane is initiated by this addition of the base, which creates a transmembrane pH gradient. This increase in pH increases the concentration of the conjugate base form of HPTS inside the lipid vesicles. Consequently, the emission of the conjugate base form increases relative to the emission of the acid form. Therefore, the acid/base ratio can be determined from the ratio of their relative emission intensities by alternating the λ_{ex}. As a result, the collapse of this pH gradient is monitored over time from changes in the fluorescence of HPTS. After a certain period of data collection, the lipid vesicles are lysed using a lipid soluble detergent, Triton X-100. As a result, HPTS encapsulated inside the vesicles is completely released and the maximum fluorescence exhibited by HPTS can be measured. The measured fluorescence intensity is then converted to a normalized extent of proton permeation (N) using a procedure described previously.[120] N was calculated from the relative emission intensities E_{403}/E_{460} (I) using Eq. 1,

$$N = \frac{(I_t - I_0)}{(I_f - I_0)} \tag{1}$$

where I_t is the relative emission intensity at time t, I_0 is the relative emission intensity at t_0, and I_f is the relative emission intensity when the vesicles are lysed. The N was plotted against time, and the slope of the linear fit represents the rate constant for proton permeation (k_{H+}) (Figure 4.2). Moreover, both k_{H+} and N are used to describe the proton permeation activity of a photochromic compound. In the plot of N versus time, there was always a steep jump in N when the pH gradient was initially formed, followed by slow

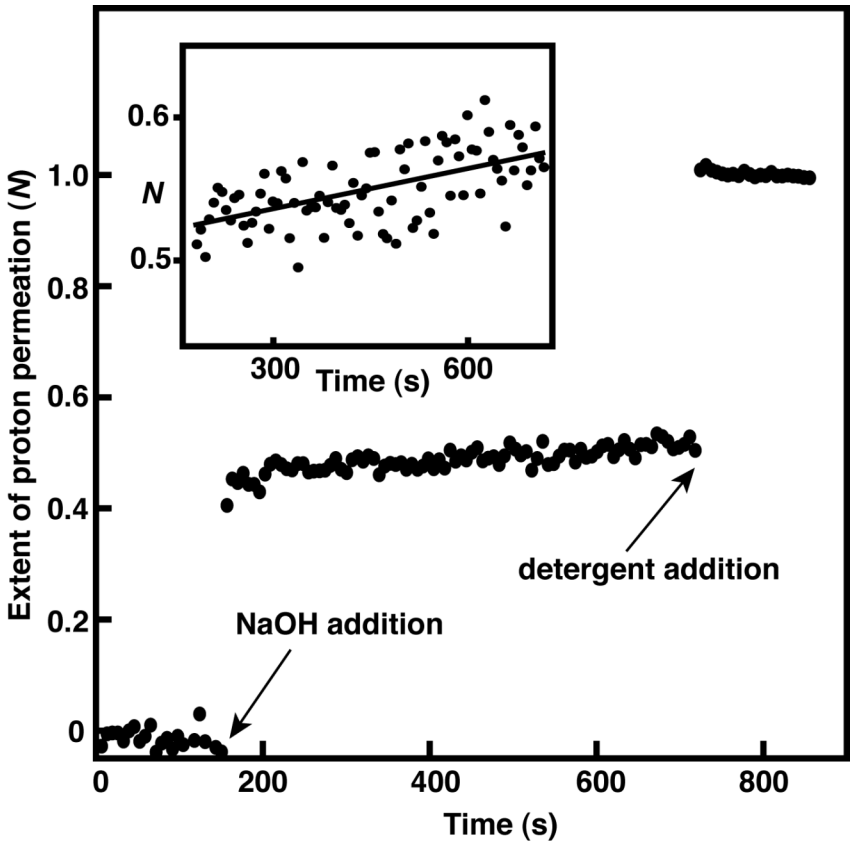

Figure 4.2. Extent of proton permeation as a function of time for **24** in DPPC vesicles. The inset is a linear fit of 200–700 s region.

permeation process. As discussed earlier in the introduction, a sequential two-step mechanism has been proposed to describe the proton permeation across bilayer membranes in lipid vesicles.[122] This proton permeation process begins with a transient-pore mechanism followed by a solubility-diffusion mechanism. The initial fast jump is due to the formation of transient hydrated pores within lipid vesicles to adjust the ionic and osmotic imbalance produced by the pH gradient.[123] This leads to some pH equilibration followed by a slower rate of proton permeation via the solubility–diffusion mechanism. In this process, the permeating protons enter the hydrophobic region from the internal aqueous compartment, diffuse across the hydrophobic region, and finally exit the bilayer into the external bulk aqueous phase.[99] The rate constants reported in these studies were determined from this second part of proton permeation because permeation during this part best represents the effect of inclusion and photoisomerization of photochromic molecules on membrane permeability. This assay was performed in the dark to assess vesicle stability and in the presence of UV light to determine the effect of the photoisomerization of photochromic molecules on membrane permeability. In general, batch-to-batch variation is commonly observed in lipid vesicle assays (i.e., ± 20%).[120] Therefore, it was important to compare vesicles incorporating photochromic compounds with control vesicles composed of only lipids. These comparisons help to ensure that the changes observed in k_{H+} and N are due to the effect of inclusion and photoisomerization of the photochromic compounds on the vesicle permeability. Also, a t-test was used to assess statistical significance in our comparisons. To begin, we will present our analysis of the control vesicles followed by a similar analysis of lipid vesicles incorporating a series of photochromic compounds.

4.1.1. Proton Permeation in Pure Lipid Vesicles

The four lipid systems used in our proton permeation studies are DPPC, DOPC, lecithin, and diPhyPC (Figure 1.7B). The phase state of these lipid systems is dependent on temperature. At room temperature, DPPC vesicles are in the gel phase, whereas DOPC, diPhyPC, and lecithin vesicles are in the fluid phase.[66] The lipid diPhyPC was chosen given this lipid has no detectable gel to liquid crystalline phase transition from −120 to 80 °C due to methyl-branched acyl chains.[67] In addition, lecithin was used to represent a mixture of saturated and unsaturated PC lipids predominantly composed of unsaturated acyl chains (e.g., linoleyl and oleyl). Before incorporating our photochromic compounds into lipid vesicles, the k_{H+} and N were initially determined for pure lipid vesicles with and without UV irradiation. The k_{H+} for these control vesicles increased in the following order: DPPC < DOPC ≈ diPhyPC < lecithin (Table 3.1). Consistent with earlier studies,[65] this trend suggests that DPPC in its gel phase is less permeable to ions than the other lipids in their fluid phase by at least a factor of four, and as high as six fold when compared to lecithin prior to irradiation. A slight decrease in k_{H+} was observed for all lipid vesicles following irradiation, although within the error observed before irradiation. The stability of the lipid systems can also be interpreted from N. As a result, N for the control vesicles with and without UV irradiation was compared. Similar to the rate constant comparisons, DPPC control vesicles were found to be more stable than lipid vesicles in the fluid phase (Table 4.1). The extent of proton permeation increased in the following order: DPPC < DOPC ≈ diphyPC < lecithin. A slight increase in N was observed for all the fluid phase vesicles following irradiation, although within error of those observed before irradiation. Further, a relatively large change in N was observed

Table 4.1. Proton permeation rate constants and normalized extent of proton permeation determined for pure lipid vesicles[a]

Lipid	k_{H+} (10^{-4} s^{-1})		N	
UV	No	Yes	No	Yes
DPPC	0.46 ± 0.26 (46)	0.31 ± 0.28 (40)	0.07 ± 0.06 (46)	0.22 ± 0.07 (40)
DOPC	1.9 ± 0.4 (33)	1.5 ± 0.3 (28)	0.33 ± 0.08 (33)	0.37 ± 0.07 (28)
Lecithin	3.1 ± 1.0 (27)	2.6 ± 1.0 (21)	0.39 ± 0.12 (27)	0.45 ± 0.13 (21)
diPhyPC	1.8 ± 0.4 (23)	1.3 ± 0.4 (23)	0.35 ± 0.08 (23)	0.45 ± 0.09 (23)

[a] The error is the standard deviation of the mean taken from *n* independent measurements. The value of *n* is shown in the parentheses.

for the gel phase DPPC control vesicles following irradiation (Figure 4.3). The magnitude of this change may be due to the higher stability of the non-irradiated DPPC vesicles, which are four fold less permeable than the fluid phase vesicles. As a result, the observed increase for DPPC vesicles following irradiation appears somewhat amplified when compared with the fluid phase control vesicles. In fact, *N* for the irradiated DPPC vesicles is lower than all the irradiated fluid phase vesicles. For the most part, the leakage observed in these control samples is largely due to the pH gradient created by the addition of base and occurs primarily during the transient–pore phase. Nonetheless, comparisons with these control samples will ensure that changes in membrane permeability are related to the presence of DTEs and SpOxs in lipid vesicles. In this way, the HPTS assay will be used to probe the formation of additional pores or defects in bilayer membranes resulting from the inclusion and isomerization of our photochromic molecules.

4.1.2. Proton Permeation in DPPC Lipid Vesicles Incorporating DTEs

DTEs **21**–**23** were incorporated into gel phase DPPC vesicles at 1:20 (DTE/DPPC) mole ratio to assess the effect of their inclusion and photoisomerization on proton permeation. The k_{H+} and *N* were initially examined for **21** and **22** in DPPC vesicles to examine the effect of the alkyl chain length on membrane permeability. Varying the alkyl chain length has been shown to control the embedded position of the photochromic moiety in the bilayer membrane.[93] Prior to UV irradiation, the inclusion of **21** and **22** increases both the k_{H+} and *N* when compared with the control vesicles

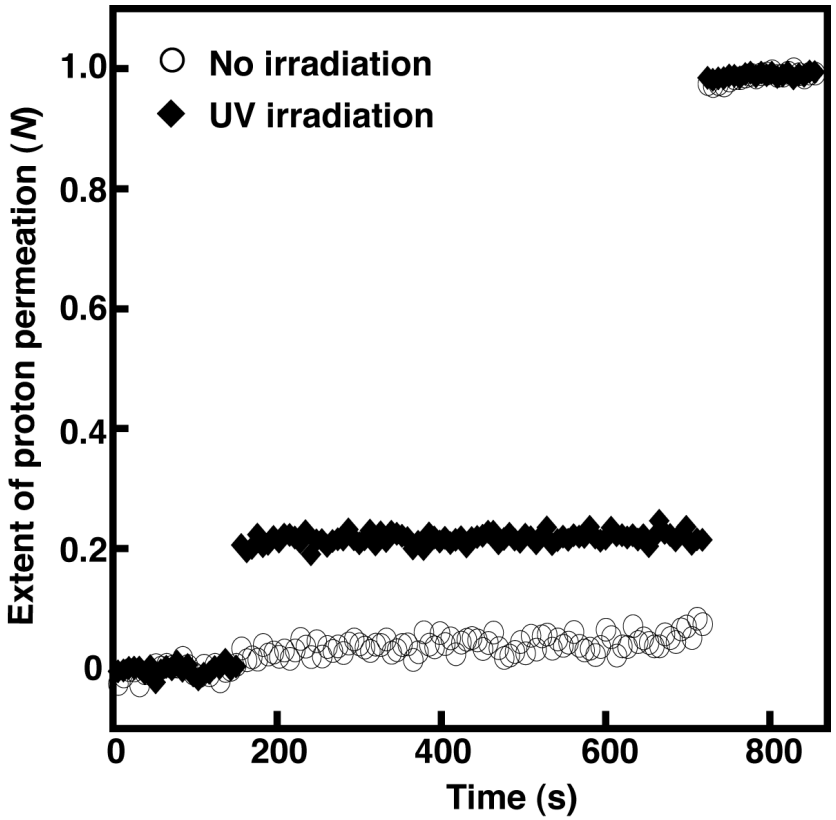

Figure 4.3. Extent of proton permeation as a function of time for DPPC control vesicles.

(Figure 4.4 and Table 4.2). The k_{H+} and N for **21** were nine and eight fold higher than the control vesicles, respectively, whereas the k_{H+} and N for **22** were both ten fold higher than the control vesicles, respectively. Comparing **21** and **22**, the results of k_{H+} and N were within the experimental errors, which suggest that **21** and **22** are equally disruptive irrespective of their chain lengths in DPPC vesicles. Previously, a minimum free volume was reported in the glycerol backbone region of a bilayer membrane.[93] The photochromic moieties of **21** and **22** are most likely positioned closer to the glycerol backbone region of the bilayer membrane. In this view, the presence of photochromic moiety in that region leads to larger disruption to the bilayer membrane, which increases the number of defects in the bilayer and enhances proton permeation through the solubility-diffusion mechanism. Further study is required to assess the relative location of the photochromic moieties of these molecules in the bilayer membrane of lipid vesicles. For example, fluorescent probe molecules incorporated in different regions of bilayer membrane could be used to assess the approximate location of our photochromic molecules.[124] In practice, changes in the fluorescence intensity of these probe molecules in response to the presence of our molecules will report on their relative position in the bilayer membrane of lipid vesicles.

The effect of photoisomerization on membrane permeability was examined by irradiating the vesicles with UV light. Two and three fold reduction in k_{H+} was observed for both **21** and **22** after irradiation, respectively. These results suggest that the closed-ring isomers of **21** and **22** are less disruptive than the open-ring isomers in DPPC vesicles. Although the molecular geometry of the closed-ring isomers is larger, the

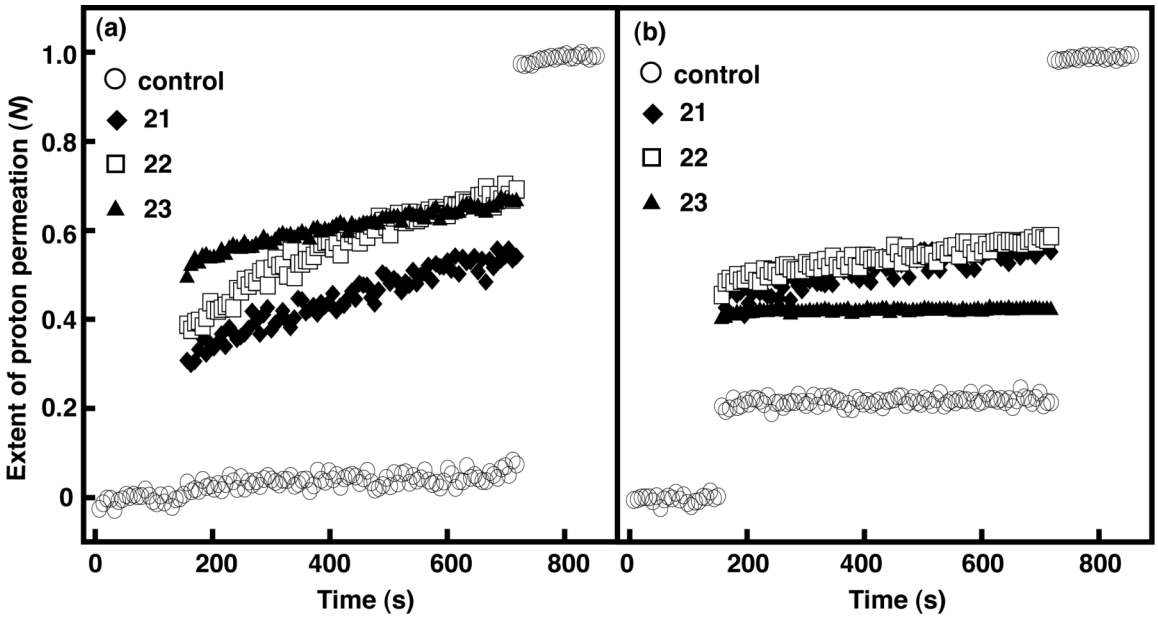

Figure 4.4. Extent of proton permeation as a function of time at 1:20 mole ratio of DTEs **21**–**23** in DPPC vesicles (a) prior to irradiation and (b) after 3 min of UV irradiation. For clarity only the control is shown before the base pulse and after the addition of detergent. Each curve is the average of minimum of three independent measurements.

Table 4.2. Proton permeation rate constants and normalized extent of proton permeation determined for DTEs **21**–**23** in DPPC vesicles at 1:20 mole ratio[a]

1:20 (DTE/DPPC)	k_{H+} (10^{-4} s^{-1})		N	
UV	No	Yes	No	Yes
Control	0.42 ± 0.24 (61)	0.31 ± 0.27 (52)	0.07 ± 0.05 (54)	0.20 ± 0.07 (49)
21	4.2 ± 1.4 (6)	2.3 ± 1.1 (7)	0.54 ± 0.08 (6)	0.56 ± 0.11 (7)
22	4.8 ± 1.0 (9)	1.6 ± 0.5 (8)	0.69 ± 0.04 (9)	0.59 ± 0.07 (8)
23	2.6 ± 0.4 (15)	0.20 ± 0.16 (14)	0.67 ± 0.07 (15)	0.43 ± 0.07 (14)

[a] The error is the standard deviation of the mean taken from *n* independent measurements. The value of *n* is shown in the parentheses.

increased conformational mobility associated with the open-ring isomers and its organization within the membrane appears to promote the formation of a greater number of bilayer defects.

To evaluate the effect of the phenylethynyl substituent on membrane permeability, we examined **23** in DPPC vesicles at 1:20 mole ratio. DTE **23** is an analog of **22** that has methyl substituents at the reactive carbons (Table 4.2). The k_{H+} for **23** was two fold lower than **22**, yet no significant difference in *N* was observed. Thus, in DPPC vesicles, a small steric effect is observed prior to UV irradiation. Following UV irradiation of **23**, a substantial decrease in the k_{H+} was observed, which was 13 fold lower than the non-irradiated vesicles. This suggests that the isomerization to the closed-ring isomer of **23** stabilizes the bilayer membrane to a greater extent than the phenylethynyl derivatives. In fact, the k_{H+} for **23** was 11 fold lower than the k_{H+} for **22** after irradiation and *N* was 30% lower than **22**. Thus, methyl substitution has less of an effect on proton permeation when compared with the bulkier phenylethynyl substituents. Overall, these results suggest that **23** provides better photocontrol of proton permeability in bilayer membranes, given the photoinduced changes are larger than **22** and the vesicles are more stable before and after irradiation. In general, our analysis indicates that substitution at the reactive carbons has a greater effect on proton permeation in DPPC vesicles than the alkyl chain length.

As DTEs are thermally stable in either isomeric state, the reversibility of **23** was examined in DPPC at a mole ratio of 1:20. For that, DPPC vesicles incorporated with closed-ring isomers were prepared and irradiated with visible light. Prior to visible irradiation, the k_{H+} for DPPC vesicles incorporating the closed-ring isomers of **23** was

three fold lower when compared with vesicles incorporating the open-ring isomers**.** That is, the k_{H+} for closed-ring isomer is $(0.97 \pm 0.04)\ 10^{-4}\ s^{-1}$, and the k_{H+} for open-ring isomer is $(2.6 \pm 0.4)\ 10^{-4}\ s^{-1}$ respectively. This was expected given the closed-ring isomers were found to be less disruptive in our previous UV irradiation studies. Upon visible irradiation, the net change in k_{H+} for open-ring isomer was 1.5 fold higher than the closed-ring isomer. Again, this suggests that given the open-ring isomers were found to be more disruptive. As a proof of concept, this preliminary result suggests that ion permeability can be reversibly controlled with light. However, this ion permeation assay is not well suited for monitoring ion permeability while cycling reversible systems because each measurement requires light irradiation prior to establishing the transmembrane pH gradient. As a result, we have also examined these photoresponsive systems using a potassium ion permeation assay (vide infra).

4.1.2.1. Effect of Concentration of DTEs on Vesicle Permeability

DTEs **21**–**23** were also studied at various mole ratios in DPPC vesicles to examine the effect of their concentration on vesicle permeability. In general, we assume that our DTEs act as membrane disruptors rather than membrane transporters. Nevertheless, by monitoring the *N* as a function of DTE concentration, Hill coefficients (n) can be determined to qualitatively assess aggregation behavior.[121,125] For **21o**–**23o** in DPPC vesicles, values for n were ca. 1 which suggests that the active structure is a DTE monomer (Figure A.1, and Table A.1).[125] Following UV irradiation, n values for **21c**–**23c** in DPPC vesicles were within error of the coefficients observed before irradiation

(Table A.1). As a result, these studies suggest that DTE aggregation within the membrane is not significant and not a rate-determining condition of proton permeation. However, varying the concentration of **21**–**23** in DPPC vesicles did affect both the k_{H+} and *N*. Increasing the mole ratio of DTEs in DPPC vesicles from 1:50 to 1:20 (DTE/DPPC) resulted in an increase in k_{H+} and *N* for both non-irradiated and irradiated samples. At 1:10 mole ratio of **23** in DPPC vesicles (**23**/DPPC) resulted in complete disruption of lipid vesicles following the addition of base as clearly seen from *N* before irradiation (Figure 4.5, and Table 4.3). Decreasing the mole ratio to 1:40 significantly lowered *N* five fold, although these vesicles were still three fold more permeable than the control. Still, the largest photoinduced changes were observed at a mole ratio of 1:20. Similar to **23**, vesicle stability was compromised prior to UV irradiation and after the addition of base when **22** was included at a mole ratio of 1:10 (Figure A.2, and Table A.2). Interestingly, DPPC vesicles incorporating **21** were not compromised at the same mole ratio, although they were very permeable. This difference in vesicle stability may be due to the variation in the mechanism through which proton permeation occurs. The inclusion of hexyl derivatives enhances proton permeation during the transient-pore period but provides no significant increase in proton permeation during the solubility-diffusion period (Figure A.2). Conversely, the presence of **21** with a longer dodecyl chain appears to provide moderate stability during the transient-pore period, yet the k_{H+} is three fold higher than **22** during the solubility-diffusion period. This difference in permeability suggests that the inclusion of hexyl derivatives does reduce vesicle stability during the formation of transient-pore compared with the dodecyl derivative. Following UV irradiation, **21** and **22** in DPPC vesicles results in 2–3 fold reduction in the k_{H+} at all

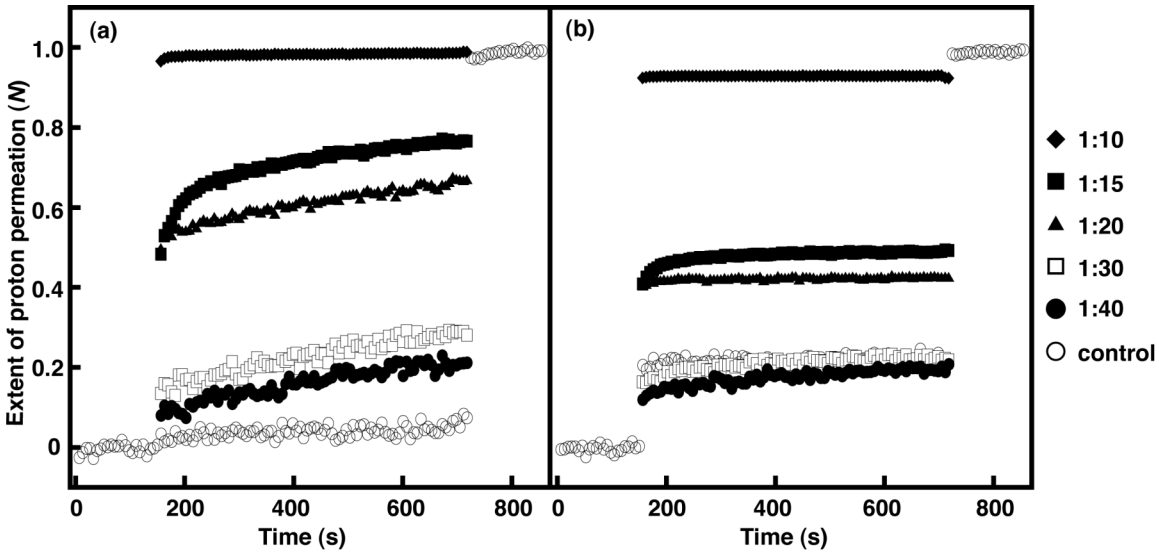

Figure 4.5. Extent of proton permeation as a function of time for various mole ratios of **23** in DPPC vesicles (a) prior to irradiation, and (b) after 3 min of UV irradiation. For clarity only the control is shown before the base pulse and after the addition of detergent. Each curve is the average of minimum of three independent measurements.

Table 4.3. Proton permeation rate constants and normalized extent of proton permeation determined for **23** in DPPC vesicles at various mole ratios[a]

23/DPPC	k_{H+} (10^{-4} s^{-1})		N	
UV	No	Yes	No	Yes
Control	0.46 ± 0.26 (46)	0.31 ± 0.28 (40)	0.07 ± 0.06 (46)	0.22 ± 0.07 (40)
1:10	0.17 ± 0.01 (3)	0.03 ± 0.01 (3)	0.99 ± 0.01 (3)	0.93 ± 0.02 (3)
1:15	2.7 ± 0.5 (6)	0.47 ± 0.30 (6)	0.77 ± 0.03 (6)	0.50 ± 0.05 (6)
1:20	2.6 ± 0.4 (15)	0.20 ± 0.16 (14)	0.67 ± 0.07 (15)	0.43 ± 0.07 (14)
1:30	2.5 ± 0.4 (6)	0.78 ± 0.42 (6)	0.29 ± 0.08 (6)	0.22 ± 0.14 (6)
1:40	2.3 ± 0.5 (6)	0.56 ± 0.41 (6)	0.21 ± 0.05 (6)	0.20 ± 0.14 (6)

[a] The error is the standard deviation of the mean taken from *n* independent measurements. The value of *n* is shown in the parentheses.

mole ratios (Table A.2). Further, the net changes in the k_{H+} were greater for **22** when compared with **21** at all mole ratios but still lower than that observed for **23**. Overall, the concentration of photochromic compound has a significant effect on the stability of the host vesicle and the photocontrol of proton permeability in DPPC vesicles. In the following section, proton permeation studies will be presented for fluid phase vesicles incorporated with DTEs.

4.1.3. Proton Permeation in Fluid Phase Lipid Vesicles Incorporating DTEs

To determine the effect of lipid phase on proton permeation, DTEs **21**–**23** were studied in fluid phase vesicles such as diPhyPC, DOPC, and lecithin and compared with DPPC vesicles. The k_{H+} and N were determined at a mole ratio of 1:20 (DTE/lipid). Prior to UV irradiation, the k_{H+} and N for **21** and **22** were at least two fold higher than their respective controls in all fluid phase vesicles (Tables 4.4 and 4.5). However, the relative change in k_{H+} and N is smaller than that observed in DPPC vesicles. This is most likely due to the change in the phase state of the lipids. The bilayer membrane of fluid phase vesicles is less rigid than the bilayer membrane of gel phase vesicles.[65,88] As a result, the disruption caused by DTEs to the bilayer membrane of fluid phase vesicles is relatively smaller. Thereby, permeation of protons in the fluid phase vesicles is comparatively lower than in gel phase DPPC vesicles. Following UV irradiation, a decrease in the k_{H+} was observed in all fluid phase lipid vesicles, which again suggests that the closed-ring isomers are less disruptive than the open-ring isomers. Further, both DTEs **21** and **22** show similar k_{H+} and N in fluid phase lipid vesicles, irrespective of their

chain length. Consistent with DPPC vesicles, these results suggest that there is also no significant difference caused by differences in alkyl chain length in fluid phase vesicles.

Similar to the DPPC studies, DTE **23** was also investigated in fluid phase vesicles to compare the effect of substitution at the reactive carbons (Tables 4.4 and 4.5). Prior to irradiation, the k_{H+} and N for **23** were three and two fold less permeable than **22** in both DOPC and diPhyPC vesicles. In lecithin, the k_{H+} was similar to **23**, yet, the N values of **23** are lower than **22**. Upon UV irradiation, a reduction in the k_{H+} was observed in DOPC and diPhyPC, whereas for lecithin the change was small and similar to **22**. For the majority of cases, there is a clear steric effect was observed. Similar to DPPC vesicles, the results of k_{H+} and N showed that the methyl derivative **23** is less disruptive than the analogous phenylethynyl derivative **22** in fluid phase vesicles. Overall, fluid phase vesicles incorporating DTEs are less permeable to proton permeation than DPPC vesicles due to the difference in the phase state of the lipid vesicles. For DOPC and diPhyPC vesicles, phenylethynyl substitution does lead to higher proton permeation than the methyl substitution. Moreover, the alkyl chain length in **21** and **22** does not show any difference in proton permeation in fluid phase vesicles.

4.1.4. Proton Permeation in Four Lipid Vesicles Incorporating Neutral DTEs

To evaluate the effect of the amphiphilic structure of **21** and **22** on membrane permeability, the neutral DTEs **51** and **52** were also examined in four lipid vesicles such as DPPC, DOPC, diPhyPC and lecithin (Tables 4.4 and 4.5). The cationic ammonium substituent terminally tethered to the alkyl chain in **21** and **22** resembles the polar head

Table 4.4. Proton permeation rate constants determined in various lipid vesicles at a mole ratio of 1:20 (DTE/lipid)[a]

Lipid	DPPC		Lecithin	
	k_{H+} (10^{-4} s^{-1})		k_{H+} (10^{-4} s^{-1})	
UV	No	Yes	No	Yes
Control	0.46 ± 0.26 (46)	0.31 ± 0.28 (40)	3.1 ± 1.0 (27)	2.6 ± 1.0 (21)
21	4.2 ± 1.4 (6)	2.3 ± 1.1 (7)	6.6 ± 1.2 (16)	3.3 ± 1.4 (14)
22	4.8 ± 1.0 (9)	1.6 ± 0.5 (8)	4.9 ± 0.6 (12)	3.3 ± 0.5 (10)
23	2.6 ± 0.4 (15)	0.20 ± 0.16 (14)	4.5 ± 0.4 (3)	3.2 ± 0.2 (3)
51	4.4 ± 0.4 (7)	2.2 ± 0.4 (10)	1.3 ± 0.2[b] (4)	0.18 ± 0.01[b] (4)
52	3.9 ± 0.3 (8)	1.8 ± 0.4 (8)	1.5 ± 0.2[b] (4)	0.60 ± 0.11[b] (4)
Lipid	DOPC		diPhyPC	
	k_{H+} (10^{-4} s^{-1})		k_{H+} (10^{-4} s^{-1})	
UV	No	Yes	No	Yes
Control	1.9 ± 0.4 (33)	1.5 ± 0.3 (28)	1.8 ± 0.4 (23)	1.3 ± 0.4 (23)
21	3.0 ± 0.6 (7)	2.3 ± 0.5 (7)	3.9 ± 0.5 (7)	2.3 ± 0.6 (8)
22	3.2 ± 0.3 (6)	1.5 ± 0.5 (6)	3.7 ± 0.5 (8)	1.8 ± 0.4 (8)
23	1.7 ± 0.1 (3)	0.76 ± 0.14 (3)	2.4 ± 0.7 (5)	0.47 ± 0.14 (5)
51	5.4 ± 0.3[b] (4)	4.5 ± 0.1[b] (3)	4.4 ± 0.2 (8)	2.4 ± 0.2 (8)
52	6.6 ± 0.3[b] (4)	5.5 ± 0.4[b] (4)	3.4 ± 0.2 (9)	1.7 ± 0.3 (8)

[a] The error is the standard deviation of the mean taken from *n* independent measurements. The value of *n* is shown in the parentheses.
[b] A mole ratio of 1:30 DTE/lipid was used.

Table 4.5. Normalized extent of proton permeation determined in various lipid vesicles at a mole ratio of 1:20 (DTE/lipid)[a]

Lipid	DPPC		Lecithin	
	N		*N*	
UV	No	Yes	No	Yes
Control	0.07 ± 0.06 (46)	0.22 ± 0.07 (40)	0.39 ± 0.12 (27)	0.45 ± 0.13 (21)
21	0.54 ± 0.08 (6)	0.56 ± 0.11 (7)	0.68 ± 0.10 (16)	0.66 ± 0.10 (14)
22	0.69 ± 0.04 (9)	0.59 ± 0.07 (8)	0.58 ± 0.12 (12)	0.55 ± 0.14 (10)
23	0.67 ± 0.07 (15)	0.43 ± 0.07 (14)	0.42 ± 0.01 (3)	0.50 ± 0.03 (3)
51	0.56 ± 0.07 (7)	0.53 ± 0.04 (10)	0.54 ± 0.03[b] (4)	0.50 ± 0.06[b] (4)
52	0.56 ± 0.07 (8)	0.51 ± 0.13 (8)	0.90 ± 0.01[b] (4)	0.83 ± 0.02[b] (4)
Lipid	DOPC		diPhyPC	
	N		*N*	
UV	No	Yes	No	Yes
Control	0.33 ± 0.08 (33)	0.37 ± 0.07 (28)	0.35 ± 0.08 (23)	0.45 ± 0.09 (23)
21	0.60 ± 0.02 (7)	0.66 ± 0.04 (7)	0.54 ± 0.07 (7)	0.56 ± 0.04 (8)
22	0.69 ± 0.09 (6)	0.69 ± 0.09 (6)	0.66 ± 0.05 (8)	0.64 ± 0.07 (8)
23	0.23 ± 0.06 (3)	0.23 ± 0.02 (3)	0.49 ± 0.07 (5)	0.31 ± 0.05 (5)
51	0.90 ± 0.02[b] (4)	0.81 ± 0.03[b] (3)	0.89 ± 0.01 (8)	0.71 ± 0.04 (8)
52	0.94 ± 0.02[b] (4)	0.89 ± 0.02[b] (4)	0.79 ± 0.02 (9)	0.62 ± 0.05 (8)

[a] The error is the standard deviation of the mean taken from *n* independent measurements. The value of *n* is shown in the parentheses.
[b] A mole ratio of 1:30 DTE/lipid was used.

group of phospholipids. Therefore, it was hypothesized that **21** and **22** linked to a charged tether would have better organization in the bilayer membrane. Neutral DTEs **51** and **52** without charged group would be less organized and primarily reside in the hydrophobic aliphatic region of the bilayer. However, the tertiary amino substituents of **51** and **52** are ionizable and presumably protonated in the presence of phosphate buffer given the p*K*a for a similar tertiary amine is ca. 9.8. Nonetheless, a significant effect on proton permeability in fluid phase lipid vesicles was observed, particularly in DOPC and lecithin. At a mole ratio of 1:20, these vesicles were not stable after the addition of base as the N was essentially unity. As a result, **51** and **52** were examined at a lower mole ratio of 1:30. In DOPC vesicles, before and after irradiation, the k_{H+} for **51** and **52** were two fold higher when compared with **21** and **22** at mole ratios of 1:20. However, the magnitude of change in the k_{H+} and N after UV irradiation was relatively similar to **21** and **22**. In lecithin vesicles, the k_{H+} for **51** and **52** were two fold lower than the controls and a minimum of three fold lower than **21** and **22** prior to irradiation. Upon UV irradiation, the k_{H+} for **51** and **52** decreased by at least seven and three fold, respectively, when compared with the non-irradiated vesicles including **51** and **52**. This decrease in k_{H+} again suggests a slight preference for the closed-ring isomers. In diPhyPC, non-irradiated vesicles at a 1:20 mole ratio were also more permeable in the presence of **51** and **52**. While in DPPC, the changes in the rate constants and N were similar to **21** and **22**. These results suggest that the moderate increase in hydrophobicity of the ionizable derivatives reduces the overall lipid order within the membrane of fluid phase lipid vesicles to a greater extent than DTEs with a cationic substituent. To further evaluate the effect of DTE hydrophobicity on the stability of fluid phase vesicles, asymmetrical DTE

derivatives like **51** and **52** without terminal amino substituents will need to be prepared and examined. From these studies, it is clear that the lack of a quaternary ammonium cation, the neutral DTEs in fluid phase vesicles have shown higher proton permeation than the cationic DTEs. While in DPPC vesicles, both cationic and neutral DTEs have shown similar membrane permeability. The next few sections describe the effect of inclusion and photoisomerization of SpOx derivatives on vesicle permeability. Proton permeation studies were also carried out for SpOxs incorporated in DPPC and DOPC vesicles. The main difference between SpOxs and DTEs is their thermal reversibility. As described earlier, the isomers of DTE derivatives are thermally stable, whereas the open-ring or MC form of SpOxs are not. In the dark and at room temperature, the MC form will revert back to the SP form. The purpose of studying two different photochromic compounds is to identify the photoresponsive system that has the most potential for photocontrolling ion permeability in lipid vesicles. Two phenanthryl-based SpOx monomers **24** with a longer dodecyl chain and **25** with a shorter hexyl chain, and a bolaamphiphilic SpOx dimer **26** will be examined in lipid vesicles at a mole ratio of 1:30 (SpOx/lipid).

4.1.5. Proton Permeation in DPPC Vesicles Incorporating SpOxs

The k_{H+} and N were initially examined for SpOx derivatives **24** and **25** in DPPC vesicles to assess the effect of the relative position of the photochromic moiety on membrane permeability. Varying the alkyl chain length has been shown to be an effective approach for controlling the embedding depth of the photochromic moiety in

bilayer membranes.[93] Upon the inclusion of **24** and **25** in DPPC vesicles, the k_{H+} was at least three fold higher than the control vesicles (Figure 4.6, and Table 4.6). In addition, *N* was nine and three fold higher for **24** and **25**, respectively, than the control vesicles. As the k_{H+} for **24** and **25** are within experimental error of one another, the significant difference in *N* suggests that the inclusion of **24** with a longer dodecyl chain enhances proton permeation in DPPC vesicles immediately following the addition of base, via transient-pore mechanism. Thus, dodecyl derivative **24** appears to be a more effective membrane disruptor than hexyl derivative **25** in DPPC vesicles. This suggests that the relative positioning of the photochromic moiety of **24** and **25** in the bilayer membrane are different because of variation in the alkyl chain length. The photochromic moiety of **24** is presumably more deeply embedded in the bilayer membrane, where the largest available free volume was reported.[93,110]

The bolaamphiphilic dimer **26** was also examined in DPPC vesicles to determine if the inclusion of a larger dimer is a more disruptive to a bilayer membrane than a monomer like **24**. Assuming, **26** spans a bilayer membrane by positioning charged tethers within the hydrophilic headgroup region of the inner and outer leaflets. However, it is possible that the dimer may adopt a U-shaped or folded conformation in lipid vesicles where both charged tethers resides in a single leaflet. Nonetheless, the inclusion of **26** should cause greater disruption than a monomer that resides in only one leaflet. Prior to irradiation, **26** also exhibited a significant increase in proton permeation but it was similar to that observed for the monomers. Specifically, both the k_{H+} and *N* for **26** were similar to **24**. This result suggests that **26** follows the mechanism similar to **24** in DPPC vesicles even though the structure of dimer is larger, and possibly the dimer may

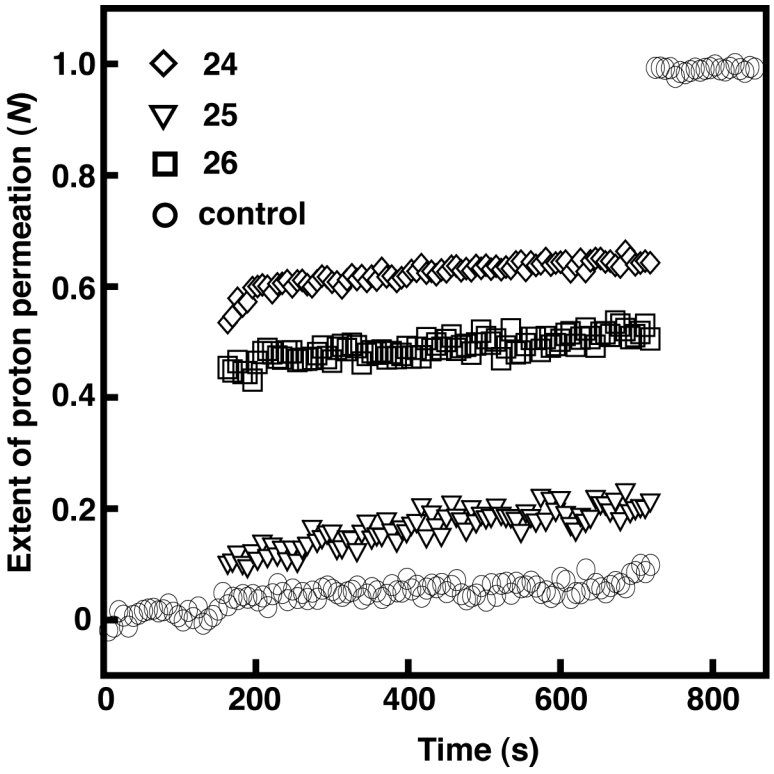

Figure 4.6. Extent of proton permeation as a function of time at 1:30 mole ratio of SpOx derivatives **24**–**26** in DPPC vesicles, prior to irradiation. For clarity only the control is shown before the base pulse and after the addition of detergent. Each curve is the average of minimum of three independent measurements.

Table 4.6. Proton permeation rate constants and normalized extent of proton permeation determined for SpOx derivatives **24**–**26** in DPPC vesicles at 1:30 mole ratio[a]

1:30 (SpOx/DPPC)	k_{H+} (10^{-4} s^{-1})		N	
UV	No	Yes	No	Yes
Control	0.42 ± 0.24 (61)	0.31 ± 0.27 (52)	0.07 ± 0.05 (54)	0.20 ± 0.07 (49)
24	1.1 ± 0.3 (6)	0.99 ± 0.50 (6)	0.65 ± 0.05 (6)	0.71 ± 0.07 (6)
25	1.7 ± 0.6 (6)	1.4 ± 0.6 (6)	0.22 ± 0.06 (6)	0.40 ± 0.09 (6)
26	1.0 ± 0.3 (6)	0.83 ± 0.35 (6)	0.53 ± 0.11 (6)	0.62 ± 0.09 (6)

[a] The error is the standard deviation of the mean taken from *n* independent measurements. The value of *n* is shown in parentheses.

have U-shaped organization located in a single leaflet of the bilayer membrane. Overall, in DPPC vesicles, the k_{H+} was similar for all three SpOx molecules. Like DTEs, there is no correlation between k_{H+} and the molecular size of the SpOxs in DPPC vesicles. Comparatively, the DTE derivatives showed at least two fold higher k_{H+} than the SpOx derivatives at 1:30 mole ratio. This comparison showed that the incorporation of DTEs **21**–**23** in DPPC vesicles is more permeable to protons than the SpOxs **24**–**26**. The increased membrane permeability of DTEs is possibly due to the increased conformational flexibility associated with the open-ring isomers and its organization within the membrane may promote the formation of a greater number of bilayer defects. Also, the permeation of protons in DPPC vesicles incorporating SpOxs is mainly through the transient-pore mechanism, whereas DTEs allow proton permeation via the solubility-diffusion mechanism.

Next, to determine the effect of photoisomerization of SpOx derivatives in DPPC vesicles the samples were irradiated with UV light. There was no significant change in k_{H+} following UV irradiation for all three SpOx derivatives. Due to the efficient thermal reversibility of these SpOxs[1,40], rapid isomerization of the MC form to the SP form is likely upon turning off the UV lamp prior to the addition of base pulse. As a result, the similarity between the non-irradiated and irradiated SpOx is not completely unexpected. However, there was a two fold increase in N for **25** but no significant change was observed for **24** and **26** upon UV irradiation. From this, it appears as though the photoisomerization of the hexyl chain analogue disrupts the bilayer membrane to a greater extent than the dodecyl analogue in DPPC. Interestingly, at lower concentrations of **25** in DPPC vesicles (i.e., 1:40 (**25**/DPPC); Figure A.3 and Table A.3) a substantial

increase in *N* was observed following irradiation, whereas at higher concentrations (i.e., 1:20) no significant difference was observed. This concentration dependence on *N* again suggests that these changes are more a reflection of the higher stability of non-irradiated DPPC vesicles and those incorporating low concentrations of SpOxs than the photoisomerization of the photochromic compounds. To support this proposal further, the *N* for both **24** and the dimer **26** in DPPC at 1:50 was two fold higher following irradiation (Tables A.4 and 3.8, and Figures A.4 and 3.8, respectively). Yet, at 1:30 both SpOxs had similar *N*. Thus, increase in *N* for **25** in DPPC vesicles following UV irradiation excludes the possibility of hexyl derivative having higher membrane permeability than **24** and **26**. Overall, the photoisomerization of SpOxs appears to have no effect on proton permeation in DPPC vesicles when monitored using this assay due to the rapid thermal ring-closure of SpOxs. As will be discussed in later sections, the assay used in these studies may not be appropriate for thermally reversible photoresponsive systems. The following section deals with proton permeation of SpOxs in fluid phase DOPC vesicles at 1:30 mole ratio.

4.1.6. Proton Permeation in DOPC Vesicles Incorporating SpOxs

Like DPPC vesicles, to assess the effect of alkyl chain length on proton permeation in DOPC vesicles, the k_{H+} and *N* were initially compared to the monomers (Figure 4.7 and Table 4.7). Prior to UV irradiation, the k_{H+} observed for **24** was two fold larger than the non-irradiated control, whereas the k_{H+} for **25** was similar to the control. Further, *N* for **24** and **25** was at least two fold higher than the non-irradiated control.

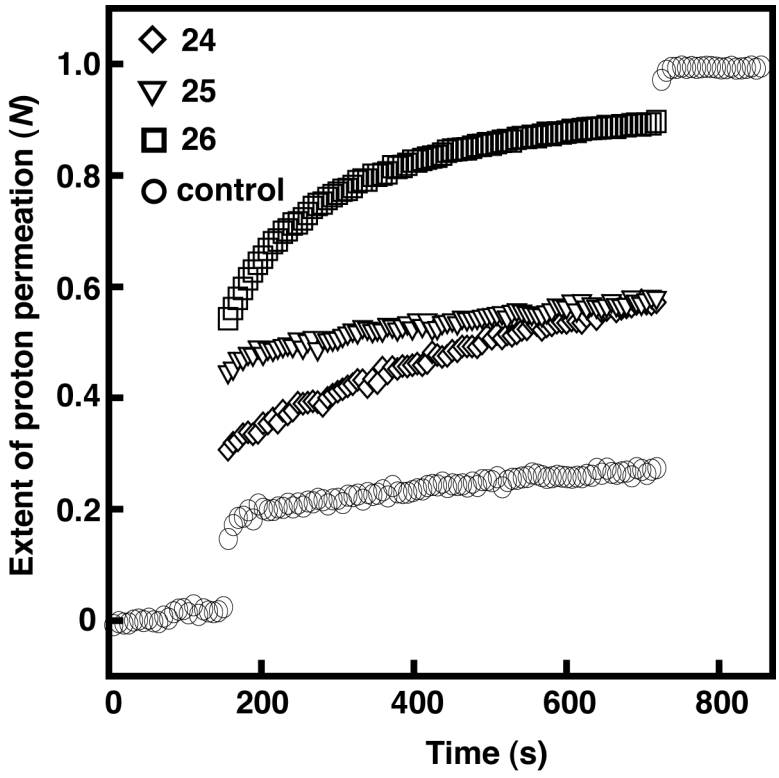

Figure 4.7. Extent of proton permeation as a function of time at 1:30 mole ratio of SpOx derivatives **24**–**26** in DOPC vesicles, prior to irradiation. For clarity only the control is shown before the base pulse and after the addition of detergent. Each curve is the average of minimum of three independent measurements.

Table 4.7. Proton permeation rate constants and normalized extent of proton permeation determined for SpOx derivatives **24**–**26** in DOPC vesicles at 1:30 mole ratio[a]

1:30 (SpOx/DOPC)	k_{H+} (10^{-4} s^{-1})		*N*	
UV	No	Yes	No	Yes
Control	1.8 ± 0.5 (57)	1.4 ± 0.6 (52)	0.31 ± 0.07 (47)	0.37 ± 0.06 (45)
24	4.3 ± 0.4 (6)	4.1± 0.2 (6)	0.57 ± 0.02 (6)	0.62 ± 0.05 (6)
25	1.8 ± 0.1 (6)	1.7 ± 0.4 (6)	0.57 ± 0.03 (6)	0.61 ± 0.03 (6)
26	8.9 ± 0.6 (6)	8.7 ± 0.2 (6)	0.89 ± 0.01 (7)	0.90 ± 0.01 (6)

[a] The error is the standard deviation of the mean taken from *n* independent measurements. The value of *n* is shown in the parentheses.

However, the relative change in k_{H+} and N for both monomers is lower in DOPC vesicles than DPPC vesicles. As described previously, this is most likely due to the lipid bilayer phase state. The gel phase vesicles are more rigid than fluid phase vesicles and therefore reorganization of vesicles after the photoinduced disturbance is slow in gel phase vesicles.[88,110,126] In the plot of N versus time, **24** and **25** shows difference in the proton permeation process after the addition of base pulse (Figure 4.7). A gradual increase in N was observed for **24**, which suggests that the incorporation of **24** with a longer dodecyl chain in DOPC vesicles increases the permeation of the protons during solubility-diffusion period. Whereas, the presence of **25** with a shorter hexyl chain most likely enhances the proton permeation during the transient-pore period. Consistent with DPPC vesicles, **24** exhibits larger effect on proton permeation than **25** in DOPC vesicles. Again, this suggests that the position of photochrome in the bilayer membrane is important for vesicle permeability.

Similar to DPPC studies, SpOx dimer **26** was also examined in DOPC vesicles to determine the structural effect on proton permeation. As anticipated, due to the large molecular volume of **26** both the k_{H+} and N were higher than the monomers in DOPC vesicles (Table 3.7). Specifically, the k_{H+} for **26** was five fold higher than **25,** and two fold higher than **24**. Similarly, the N for **26** was also 50% greater than both monomers. In fact, proton permeation observed for **26** in DOPC vesicles following the addition of base is more pronounced than all other photochromic systems, which qualitatively indicates that the higher k_{H+}. Thus, **26** disrupts the bilayer membrane more efficiently than **24** and **25** in DOPC vesicles. In contrast to the DPPC vesicles, the molecular size of these SpOxs is positively correlated with k_{H+} in DOPC vesicles. This correlation

suggests that a structure–activity relationship does exist within this series of SpOx molecules. The fluid nature of DOPC lipids possibly allows **26** to span the entire bilayer membrane. Consequently, the charged groups on both ends of dimer could anchor within the hydrophilic head group regions of a bilayer membrane, unlike monomers, which most likely reside in a single leaflet. As a result, the dimer may create a greater number of transient defects within the membrane that allows for enhanced permeation of protons across the bilayer membrane. Therefore, SpOx structure is important for proton permeation in fluid phase lipid vesicles. Interestingly, the k_{H+} for **26** was at least three fold higher than the DTE monomers in DOPC vesicles, which also suggests that molecular size is correlated with vesicle permeability. Overall, the inclusion of the SpOx dimer has the greatest effect on proton permeation in DOPC vesicles than both the DTE and SpOx monomers.

The effect of SpOx photoisomerization on vesicle permeability was also examined in DOPC vesicles. Consistent with DPPC vesicles, the k_{H+} and N values did not show any significant difference between the irradiated and non-irradiated DOPC vesicles containing **24**–**26** (Table 4.7). As discussed earlier, this assay was determined to be inappropriate for thermally reversible photoresponsive systems. Nonetheless, it is useful for describing the effect of inclusion on the permeability of lipid vesicles. Therefore, in the following section, the effect of SpOx concentration on proton permeation will be presented.

4.1.7. Effect of Concentration of SpOxs on Membrane Permeability

SpOxs **24**–**26** in DPPC and DOPC vesicles were examined at various mole ratios to measure the effect of SpOx concentration on membrane permeability. As expected, the SpOx concentration in DPPC and DOPC vesicles do affect both k_{H+} and N. However, the magnitude of these changes was dependent on the SpOx and the lipid system studied. Increasing the concentration of **26** in lipid vesicles increases the k_{H+} and N in both DPPC and DOPC vesicles (Figure 4.8, and Table 4.8). At 1:20 mole ratio, the inclusion of **26** in both DPPC and DOPC resulted in the disruption of lipid vesicles and complete collapse of the pH gradient as clearly seen from N values approaching unity (Figure 4.8). Decreasing the mole ratio to 1:50 significantly lowered the proton leakage by three fold in DPPC vesicles, but had a relatively small effect in DOPC vesicles. In DOPC vesicles, the k_{H+} for **26** increased by 50% when increasing the mole ratio from 1:60 to 1:30, whereas in DPPC vesicles the k_{H+} was constant over the same concentration range. Again, this highlights the importance of lipid bilayer phase on the observed behavior. Overall, in DPPC vesicles, N was dependent on concentration, whereas k_{H+} is not. Conversely, in DOPC vesicles, k_{H+} is dependent on concentration, but N is moderately dependent. These trends suggest that lipid bilayer phase affects the predominant mechanism that governs permeation through a bilayer membrane. That is, the inclusion of the SpOx dimer primarily affects proton permeation during the solubility-diffusion period in fluid phase vesicles, whereas in gel phase vesicles permeation is largely altered during the transient-pore period.

Increasing the concentration of **24** in lipid vesicles increases the k_{H+} and N in both DPPC and DOPC vesicles (Figure A.3, and Table A.3). Interestingly, the highest mole

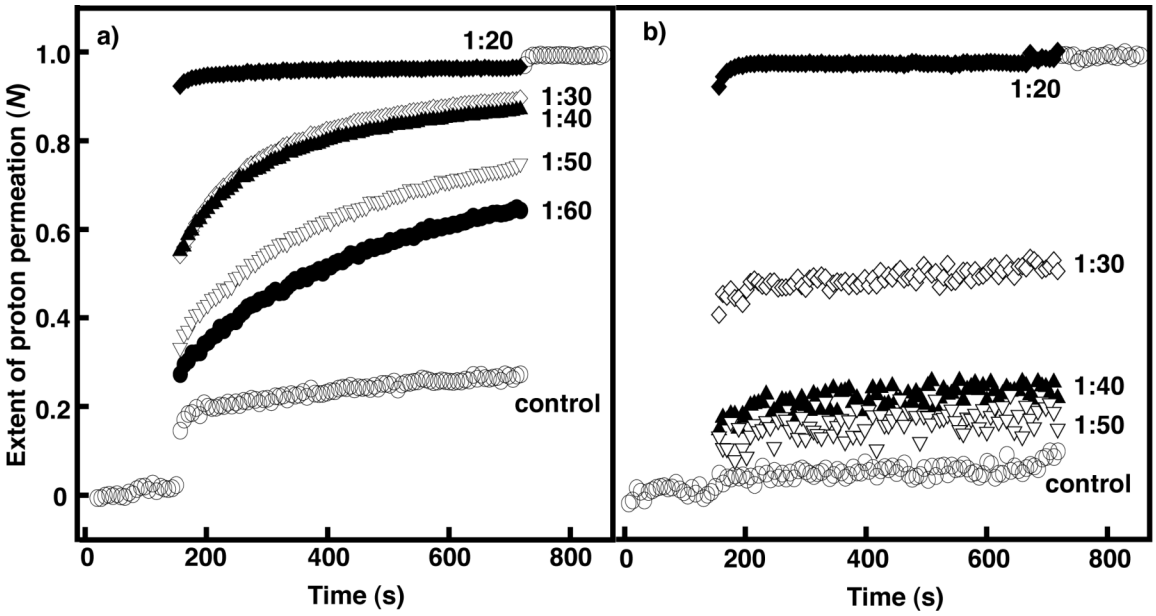

Figure 4.8. Extent of proton permeation as a function of time at various mole ratios of **26** in (a) DOPC and (b) DPPC vesicles, prior to irradiation. For clarity only the control is shown before the base pulse and after the addition of detergent. Each curve is the average of minimum of three independent measurements.

Table 4.8. Proton permeation rate constants and normalized extent of proton permeation determined for SpOx **26** in DOPC and DPPC vesicles at various mole ratios[a]

26/DOPC	k_{H+} (10^{-4} s^{-1})		*N*	
UV	No	Yes	No	Yes
Control	1.8 ± 0.5 (57)	1.4 ± 0.6 (52)	0.31 ± 0.07 (47)	0.37 ± 0.06 (45)
1:20	0.83 ± 0.11 (4)	0.71 ± 0.37 (4)	0.97 ± 0.01 (4)	0.98 ± 0.01 (4)
1:30	8.9 ± 0.6 (6)	8.7 ± 0.2 (6)	0.89 ± 0.01 (7)	0.90 ± 0.01 (6)
1:40	7.3 ± 0.5 (7)	6.9 ± 1.1 (6)	0.87 ± 0.01 (7)	0.88 ± 0.03 (6)
1:50	5.9 ± 0.2 (7)	5.5 ± 0.2 (7)	0.73 ± 0.02 (7)	0.74 ± 0.06 (7)
1:60	5.7 ± 0.2 (6)	5.2 ± 0.4 (6)	0.64 ± 0.05 (6)	0.66 ± 0.04 (6)
26/DPPC	k_{H+} (10^{-4} s^{-1})		*N*	
UV	No	Yes	No	Yes
Control	0.42 ± 0.24 (61)	0.31 ± 0.27 (52)	0.07 ± 0.05 (54)	0.20 ± 0.07 (49)
1:20	0.15 ± 0.06 (6)	0.38 ± 0.12 (4)	0.98 ± 0.01 (6)	0.97 ± 0.01 (4)
1:30	1.0 ± 0.3 (6)	0.83 ± 0.35 (6)	0.53 ± 0.11 (6)	0.62 ± 0.10 (6)
1:40	0.95 ± 0.57 (6)	0.75 ± 0.40 (6)	0.25 ± 0.05 (6)	0.34 ± 0.08 (6)
1:50	0.94 ± 0.45 (6)	0.64 ± 0.37 (6)	0.17 ± 0.04 (6)	0.30 ± 0.09 (6)

[a] The error is the standard deviation of the mean taken from *n* independent measurements. The value of *n* is shown in parentheses.

ratio at which lipid vesicles incorporating **24** were not compromised was dependent on the lipid bilayer phase state. Similar to **26**, vesicle stability was compromised when **24** was included in DPPC vesicles at a mole ratio of 1:20. Conversely, vesicle stability was not compromised when **24** was included in DOPC vesicles at a mole ratio of 1:10, although they were very permeable. Increasing the mole ratio from 1:40 to 1:20 significantly increased the k_{H+} and N by 30% and 40%, respectively, in DOPC vesicles. While in DPPC vesicles, increasing the mole ratio from 1:50 to 1:30 significantly increased the proton leakage by five fold but the k_{H+} was constant over the same concentration range. Consistent with **26**, the inclusion of **24** largely affects the proton permeation during the transient-pore period in DPPC vesicles and the proton permeation increased during the solubility-diffusion period in DOPC vesicles. Once again, this suggests the lipid bilayer phase have an effect on the vesicle permeability.

Incorporation of **25** in both DOPC and DPPC vesicles increased the k_{H+} by 30% when increasing the mole ratio from 1:40 to 1:20 (Figure A.4, and Table A.4). Decreasing the mole ratio to 1:40 significantly lowered the proton leakage by ten fold in DPPC vesicles, but had a relatively small effect in DOPC vesicles. Unlike **26**, DPPC and DOPC vesicle stability was compromised only when **25** was incorporated at a higher mole ratio of 1:10. Overall, in DPPC vesicles, N was dependent on concentration, whereas k_{H+} is not. While in DOPC vesicles, k_{H+} and N is moderately dependent on concentration. The inclusion of **25** in both DPPC and DOPC vesicles increase the proton permeation most likely through the transient-pore mechanism. At all mole ratios, the effect of **25** on proton permeation was more pronounced in DPPC vesicles when comparing the net changes of both k_{H+} and N to DOPC vesicles. This result indicates that

the presence of **25** disrupts the membrane organization of gel phase vesicles to a greater extent than fluid phase vesicles. In general, increasing the concentration of all SpOxs in both DOPC and DPPC vesicles have a significant effect on the stability of the host vesicles.

4.2. Summary

In summary, DTE **21**–**23** and SpOx **24**–**26** were included in lipid vesicles and the effect of their inclusion and photoisomerization on proton permeation was studied. In total, DTEs were examined in four different lipid systems, namely DPPC, DOPC, diPhyPC, and lecithin. The proton permeation studies showed that the open-ring isomers of these DTEs are more disruptive than the closed-ring isomers in all lipid systems, regardless of their lamellar phase at room temperature. In all cases, UV irradiation led to a reduction in proton permeability. Specifically, the methyl analog showed a significant decrease in proton permeability in gel phase lipid vesicles upon UV exposure. Furthermore, an apparent steric effect was observed as the methyl-substituted DTE **23** showed lower rates of proton permeation than the bulkier phenylethynyl-substituted DTEs **21** and **22**. Also, increasing the concentration of DTEs in DPPC vesicles has a significant effect on the vesicle stability. Considering both k_{H+} and N together, the amphiphilic DTEs in lipid vesicles increases the proton permeation in the following order of **23** < **22** ≈ **21**. Additionally, a preliminary investigation on photocontrol of proton permeation by incorporating the closed-ring isomer of **23** in DPPC vesicles shows that proton permeation can be reversibly controlled with light using photochromic DTEs. The

increase in the relative magnitude of k_{H+} for DTEs is higher in gel phase vesicles when compared with fluid phase vesicles.

SpOxs **24**–**26** were also examined in DOPC and DPPC vesicles. The incorporation of SpOxs at a 1:30 mole ratio significantly increases the membrane permeability of both DPPC and DOPC vesicles. After irradiation with UV light, there was no significant difference in k_{H+} and N values from the non-irradiated samples. The photoisomerization and the subsequent rapid thermal isomerization back to the closed-ring isomers of SpOxs before the addition of base pulse is the primary reason for the apparent lack of photoactivity. However, the molecular size of these SpOxs is positively correlated with k_{H+} in DOPC vesicles prior to irradiation. Thus, a structure–activity relationship does exist within this series of photochromic molecules. By contrast, this relationship is not observed in DPPC vesicles, as k_{H+} was similar for all three molecules. Thus, DPPC vesicles are less sensitive to the change in structure of SpOxs for proton permeation because inclusion of SpOxs primarily altered the proton permeation during the transient-pore period and not during the solubility-diffusion period. As a result, this lack of selectivity implies that the inclusion of SpOxs exhibits an 'all-or-nothing' activity in gel phase lipid vesicles, whereas SpOx structure is important to activity in fluid phase lipid vesicles. Proton permeation studies showed that the permeability of DOPC vesicles incorporating these amphiphilic SpOx derivatives increases in the order of **25** ≤ **24** < **26** when one considers both k_{H+} and N collectively. For DPPC vesicles, permeability increases in the order of **25** < **24** ≈ **26**. These differences in relative permeability indicate that both lipid bilayer phase and SpOx structure are important to vesicle integrity. Moreover, increasing the concentration of SpOx derivatives in lipid vesicles have a

significant effect on the stability of the host vesicles.

In general, the membrane permeability for DTEs and SpOxs in DPPC and DOPC vesicles were compared to identify the best photoresponsive system for controlling proton permeation in lipid vesicles. However, given the limitations of the proton permeation assay for monitoring thermally reversible systems, this assay was primarily used to assess the effect of the inclusion of these photochromic compounds on membrane permeability. Considering both k_{H+} and N together, the membrane permeability of DPPC vesicles incorporating **21**–**26** increases in the following order of **25** < **24** ≈**26** < **23** < **22** ≈ **21**. This ranking shows that DPPC vesicles incorporating DTEs, especially **21** and **22**, exhibit higher membrane permeability than vesicles incorporating SpOxs. Thus, the predominant mechanism that governs proton permeation in DPPC vesicles differs for these two photochromic families because of the differences in the conformational flexibility in their structures. As a result, the open-ring isomer of DTEs with more fluxionality is most likely creating greater number of bilayer defects and enhancing ion permeation than the more rigid closed-ring isomer of SpOxs. In DOPC vesicles, incorporating these photochromic compounds increases membrane permeability in the order of **23** < **25** < **22** ≈ **21** < **24** < **26** when one considers both k_{H+} and N collectively. This trend suggests that DOPC vesicles incorporating SpOx dimer **26** are most permeable to protons than all other photochromic compounds. Further, in all cases proton permeation is predominantly altered during the solubility-diffusion period. The large molecular structure of dimer most likely disrupts the hydrocarbon chain packing to a greater extent in DOPC vesicles. Overall, these comparisons reveal that DTEs **21** and **22** in DPPC vesicles, and SpOx **26** in DOPC vesicles are the best photoresponsive systems

for controlling proton permeation among the other systems studied above. Among these photoresponsive systems, DOPC vesicles incorporating SpOx dimer exhibits good photocontrol of proton permeation. Further study will be required to assess the activity of these photoresponsive systems as membrane disruptors for the delivery of small molecules from lipid vesicles.

CHAPTER 5

PHOTOCONTROL OF POTASSIUM ION PERMEATION IN LIPID VESICLES

In this chapter, the photocontrol of potassium ion permeation in lipid vesicles incorporated with DTEs and SpOxs is discussed. At first, the assay used for potassium ion permeation studies will be described. Then, the rate constant of potassium ion permeation and the % release of potassium ion obtained for the pure lipid vesicles will be discussed. This will be followed by a discussion on the effect of inclusion and reversible photoisomerization of DTEs and SpOxs on potassium ion permeation in DPPC and DOPC vesicles. Finally, these series of photochromic compounds will be compared to identify the photoresponsive system that exhibits good photocontrol of potassium ion permeation.

5.1. Potassium Ion Permeation Assay

In the previous chapter, the proton permeation assay was used to examine the permeability of lipid vesicles incorporated with photochromic molecules. However, in this assay, the reversibility of ion permeation could not be examined within the same experiment. In particular, the thermal reversibility of SpOxs did not allow for an examination of membrane permeability in the presence of the transient open-ring isomers. Even for thermally irreversible systems, the introduction of an irradiation source (i.e., UV or visible) during data collection would produce a substantial amount of background, scattered light, which would be easily detected by the photomultiplier tube

of the fluorescence spectrometer, interfering with the measurement. Therefore, the fluorescence measurement would need to be stopped while the irradiation source is illuminated. In addition, interchanging the optical filters within the sample chamber is cumbersome and would require additional time to complete. In order to follow changes in permeability in both isomeric states uninterrupted, an assay that is not sensitive to the irradiation source is required. As a result, an assay that uses an ion-selective electrode was chosen to monitor changes in ion permeability across the bilayer membrane of lipid vesicles.[37,74,83] Specifically, potassium ion permeation from lipid vesicles incorporating DTEs and SpOxs was continuously monitored under UV and visible irradiation using a potassium ion-selective electrode (Figure 5.1). Since the electrode potential measurements are not sensitive to light, the release of encapsulated potassium ions from lipid vesicles can be monitored continuously without interference from light sources. Further, these light sources can be easily interchanged during the course of the experiment. This assay was used to determine the rate constant for potassium ion permeation (k_{K+}) and the percentage of potassium ion release (% release).

5.1.1. Potassium Ion Permeation in Pure Lipid Vesicles

The k_{K+} and % release were initially measured for DPPC and DOPC control vesicles before and during irradiation with UV and visible light (Table 5.1). Similar to the results from the proton permeation assay, DOPC vesicles are more permeable than DPPC vesicles. The k_{K+} and % release were at least two fold higher in DOPC than DPPC vesicles before and during irradiation. In general, the leakage observed in these control

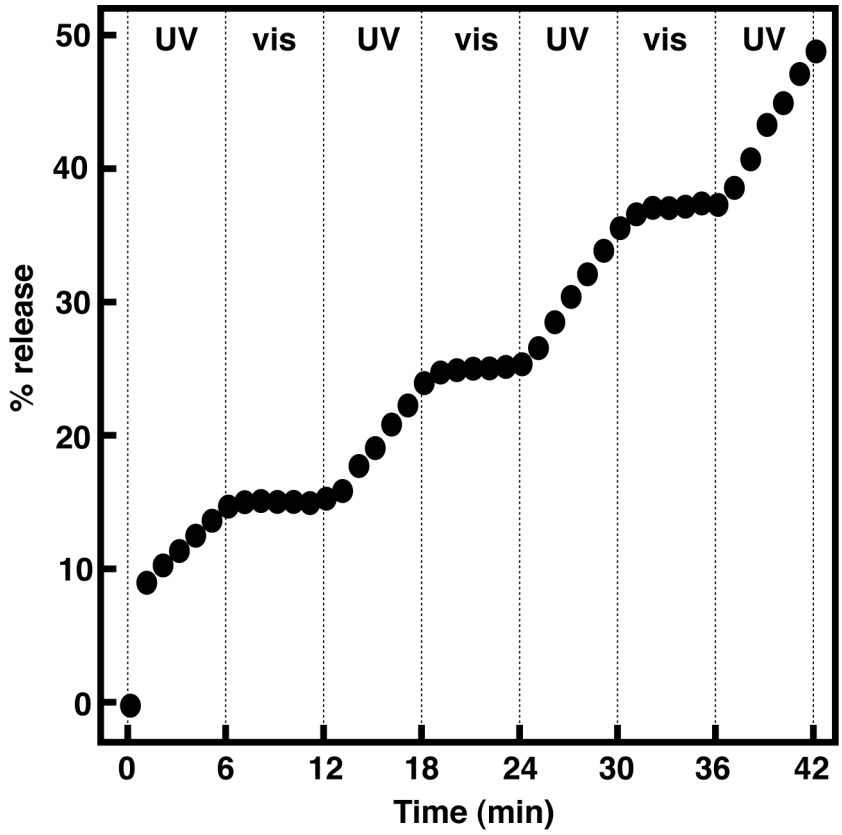

Figure 5.1. Normalized percentage of potassium ion release as a function of time for **24** in DOPC vesicles at a mole ratio of 1:20 at alternating periods of continuous UV and visible irradiation.

Table 5.1. Potassium ion permeation rate constants and normalized percentage of potassium ion release for DPPC and DOPC control vesicles[a]

Lipid vesicles	k_{K+} (10^{-8} M s^{-1})			% release	
Light	No	UV	Visible	No	UV and Visible[b]
DPPC	0.7 ± 0.1 (3)	0.8 ± 0.1 (8)	0.6 ± 0.1 (8)	6 ± 1 (3)	7 ± 1 (8)
DOPC	1.4 ± 0.1 (3)	2.1 ± 0.1 (9)	1.9 ± 0.1 (9)	15 ± 1 (3)	21 ± 2 (9)

[a] The error is the standard deviation of the mean taken from *n* independent measurements. The value of *n* is shown in the parentheses.
[b] The percentage of potassium ion release was determined after 3.5 cycles of UV and visible light irradiation.

vesicles is largely due to the potassium ion concentration gradient and occurs primarily via the solubility-diffusion mechanism.[37] Irradiation of DOPC vesicles with alternating periods of UV and visible light showed a 50% increase in k_{K+} and % release when compared with the non-irradiated DOPC vesicles. For DPPC vesicles, irradiation did not show any significant change in k_{K+} or % release when compared with non-irradiated DPPC vesicles, as these values were within the experimental error of one another. The increase observed in k_{K+} and % release in DOPC vesicles during UV irradiation could be due to the photooxidation of unsaturated double bonds present in the lipid tails. Previously, the photochemical generation of free radicals in unsaturated lipids and their subsequent reaction with molecular oxygen to produce a lipid peroxide radical has been observed.[127] As a result, vesicular properties such as permeability, packing order and head group hydration were altered.[128] Although, we have not tested this hypothesis, the increase in k_{K+} and % release observed for UV irradiated DOPC vesicles could be attributed to photooxidation.

5.1.2. Potassium Ion Permeation in DPPC and DOPC Vesicles Incorporating DTEs

Thermally irreversible DTEs **21** and **22** were incorporated into DPPC and DOPC vesicles to determine the k_{K+} and % release for both non-irradiated and irradiated samples. As previously described, the results obtained were compared with control vesicles to ensure that changes in membrane permeability are related to the inclusion and photoisomerization of photochromic compounds in lipid vesicles. In general, these studies will assist us to establish structure-activity relationships for our series of

photochromic compounds in two lipid systems with different phase states at room temperature. Initially, **21** and **22** were examined in DPPC vesicles at a mole ratio of 1:20 (DTE/DPPC). The incorporation of **21** and **22** in DPPC vesicles results in two fold increase in k_{K+} and three fold increase in % release than the DPPC control (Figure 5.2a, and Table 5.2). However the magnitude of increase in potassium ion permeation for **21** and **22** was lower than the proton permeation. The nine fold increase in k_{H+} was observed for **21** and **22**, respectively. This variation in ion permeability suggests that DPPC bilayer membranes are less permeable to potassium ions than protons. As described previously, protons permeation occurs through a bilayer membrane via both the transient-pore and solubility-diffusion mechanisms, whereas potassium ions are limited to the solubility-diffusion mechanism.[98,99] Also, another mechanism which increases the proton permeation in the bilayer membrane is the Grotthuss mechanism. This mechanism proposes that protons can cross the membrane by hopping along hydrogen-bonded chains of water, which is a pathway not possible for potassium ions.[129] In general, the incorporation of DTEs does disrupt bilayer packing in DPPC vesicles and increases the membrane permeability.

Photoisomerization to the closed-ring isomers of DTE lead to an increase in k_{K+} of 45% and 30% for **21** and **22**, respectively, when compared with the non-irradiated DPPC vesicles containing **21** and **22**. These increases show that closed-ring isomers are more disruptive than the open-ring isomers. This is in contrast to proton permeation studies, where open-ring isomers were more disruptive than the closed-ring isomers. In addition, % release for these systems was also measured after several cycles of alternating UV and

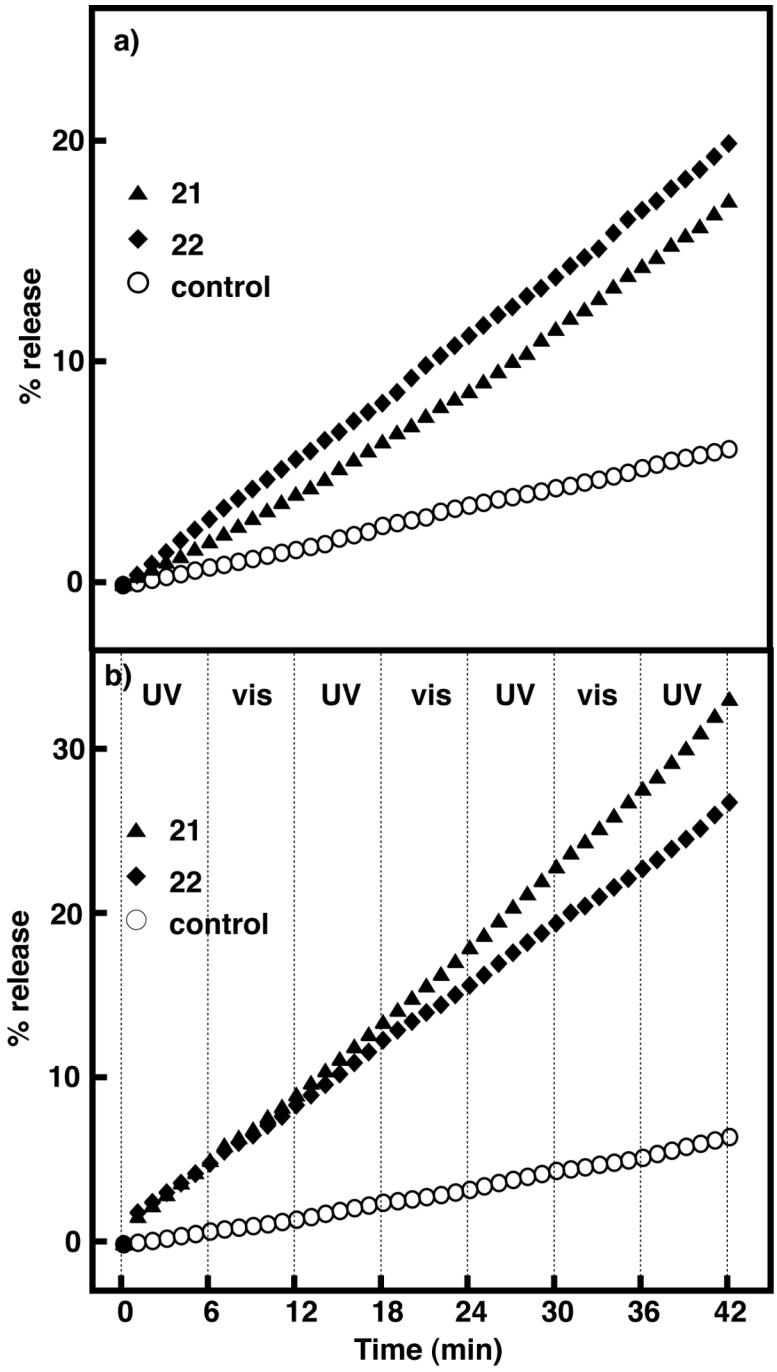

Figure 5.2. Normalized percentage of potassium ion release as a function of time for **21** and **22** in DPPC vesicles at a mole ratio of 1:20 (a) prior to irradiation, and (b) alternating periods of continuous UV and visible irradiation. Each plot is an average of three independent measurements.

Table 5.2. Potassium ion permeation rate constants and normalized percentage of potassium ion release for DPPC and DOPC vesicles incorporating DTEs at a mole ratio of 1:20 (DTE/lipid)[a]

DTE/lipid	k_{K+} (10^{-8} M/s)			% Release[b]	
Light	No	UV	Visible	No	UV and Visible
DPPC control	0.7 ± 0.1 (3)	0.8 ± 0.1 (8)	0.6 ± 0.1 (8)	6 ± 1 (3)	7 ± 1 (8)
21/DPPC	1.5 ± 0.1 (3)	2.7 ± 0.4 (3)	2.4 ± 0.3 (3)	17 ± 1 (3)	33 ± 1 (3)
22/DPPC	1.6 ± 0.1 (3)	2.3 ± 0.2 (3)	1.9 ± 0.1 (3)	20 ± 1 (3)	27 ± 1 (3)
DOPC control	1.4 ± 0.1 (3)	2.1 ± 0.1 (9)	1.9 ± 0.1 (9)	15 ± 1 (3)	21 ± 2 (9)
21/ DOPC	1.9 ± 0.1 (3)	2.8 ± 0.4 (3)	2.8 ± 0.3 (3)	22 ± 1 (3)	37 ± 1 (3)
22/ DOPC	1.6 ± 0.1 (3)	2.1 ± 0.4 (3)	1.8 ± 0.4 (3)	20 ± 1 (3)	29 ± 3 (3)

[a] The error is the standard deviation of the mean taken from *n* independent measurements. The value of *n* is shown in the parentheses.
[b] The percentage of potassium ion release was determined after 3.5 cycles of UV and visible light irradiation.

visible irradiation. The net change in % release for **21** and **22** was 16 and 7 fold higher than the control vesicles, respectively (Figure 5.2b). After photoisomerization, **21** with a longer dodecyl chain shows higher k_{K+} and % release than **22** with a shorter hexyl chain. The difference in alkyl chain length between **21** and **22** does appear to have an effect on potassium ion permeation in DPPC vesicles. This difference is possibly due to the relative position of the photochromic moiety in the bilayer membrane. DTE **21** is most likely embedded the photochromic moiety more deeply in the hydrocarbon region of bilayer membrane where larger free volume is reported.[93] Thus, upon irradiation, **21** creates greater number of bilayer defects and increases the potassium ion permeation in DPPC vesicles when compared to **22**. As discussed earlier, further studies are required to assess the relative positioning of the photochromic moieties of these molecules within the bilayer membrane. The reversible isomerization of these systems with visible light shows no significant difference in k_{K+} from UV irradiation. The reason expected for not showing any significant difference in k_{K+} between UV and visible irradiation may due to the gel phase nature of DPPC vesicles. Previously, Song et al. studied the photocontrolled release of a fluorescent dye from DPPC vesicles incorporating an azobenzene derivative.[88] Upon irradiation with UV light, these vesicles released dye by a fast process. They hypothesized that the fast release was due to a loss in membrane integrity, as the rigid nature of DPPC vesicles did not allow for a reorganization of the bilayer membrane structure following disruption by the azobenzene moiety.[88] Consistent with this view, the lack of a significant change in the k_{K+} upon irradiation with visible light may also signify an irreversible change in membrane structure of DPPC vesicles.

Another possible reason could be the change in molecular volume of DTE isomers upon photoisomerization was not significant that alters the potassium ion permeation.

The k_{K+} and % release was also determined for **21** and **22** in DOPC vesicles to assess the effect of potassium ion permeation on fluid phase vesicles. The incorporation of **21** and **22** in DOPC vesicles showed 30 and 15% increase in k_{K+} than the control vesicles, respectively, (Figure 5.3, and Table 5.2). In addition, % release for **21** and **22** was 30 and 25% higher than the control vesicles, respectively (Figure 5.3a). The results suggest that inclusion of **21** and **22** disrupts the bilayer membrane and enhances the potassium ion permeation through solubility-diffusion mechanism. In the proton permeation studies, a 40% increase in k_{H+} was observed in DOPC vesicles, which again suggests that the bilayer membrane is less permeable to potassium ions than the protons. The photoisomerization of **21** and **22** to its closed-ring isomer in DOPC vesicles resulted in increase in k_{K+} to 30 and 25%, respectively, when compared to non-irradiated vesicles containing DTEs. In addition, 40 and 30% increase in % release was observed for **21** and **22**, respectively, when compared with the non-irradiated samples (Figure 5.3b). Consistent with DPPC vesicles, the dodecyl derivative appears to be a more disruptive than the hexyl derivative in DOPC vesicles. Similar to DPPC vesicles, the reversible isomerization of **21** and **22** back to its open-ring form had similar k_{K+} of closed-ring isomer. Overall, these results suggest that inclusion and photoisomerization of **21** and **22** in DOPC vesicles increases the vesicle permeability. However, the relative magnitude of changes in k_{K+} and % release in DOPC vesicles were lower than in the DPPC vesicles. This is consistent with proton permeation studies, where DPPC vesicles are more

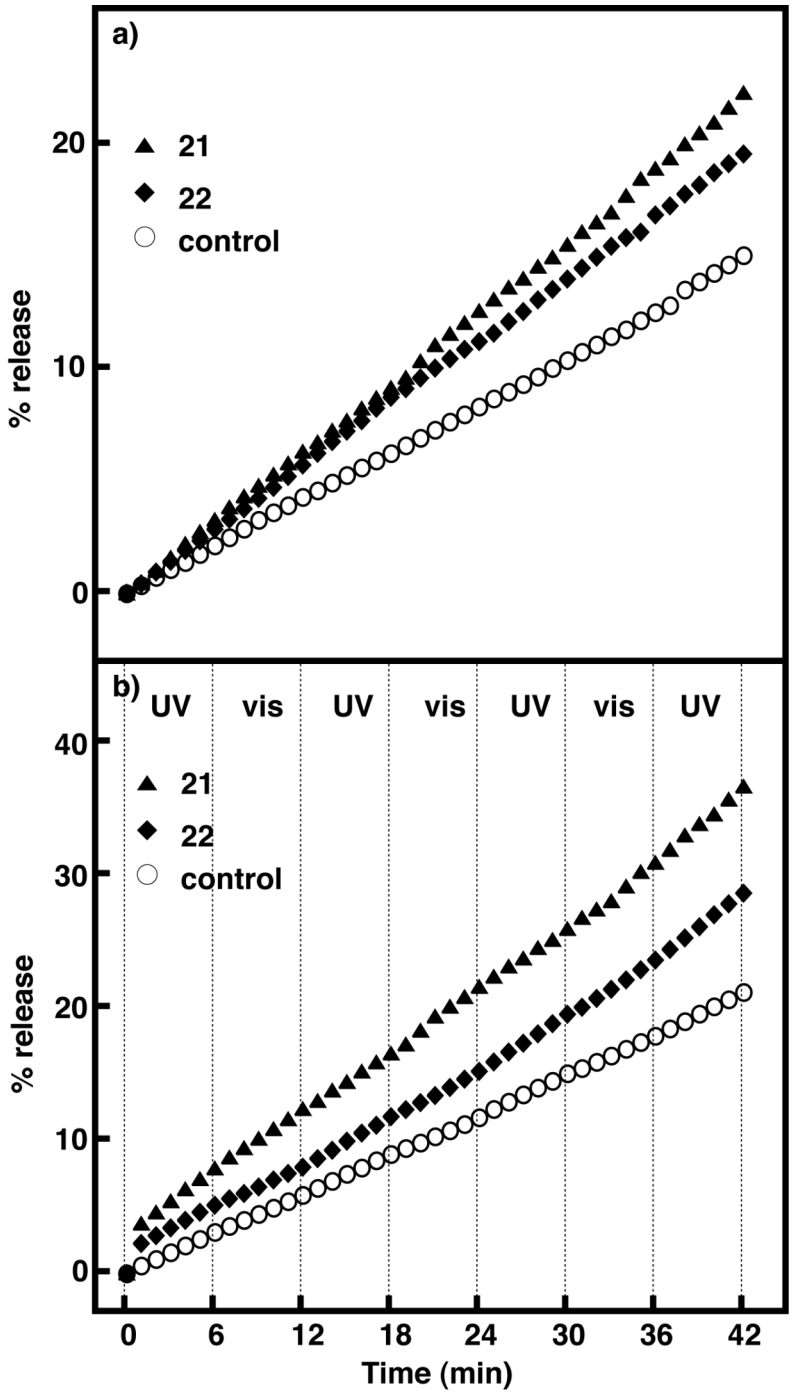

Figure 5.3. Normalized percentage of potassium ion release as a function of time for **21** and **22** in DOPC vesicles at a mole ratio of 1:20 (a) prior to irradiation, and (b) alternating periods of continuous UV and visible irradiation. Each plot is an average of three independent measurements.

permeable to protons than DOPC vesicles. Once again, this suggests that the presence of DTEs in bilayer membrane causes more disruption to the gel phase vesicles than the fluid phase vesicles. The subsequent section discusses the effect of SpOxs **24**–**26** on potassium ion permeation in DPPC vesicles.

5.1.3. Potassium Ion Permeation in DPPC Vesicles Incorporating SpOxs

The inclusion of **24**–**26** in DPPC vesicles at a mole ratio of 1:20 lead to a minimum of three fold increase in k_{K+} when compared with the DPPC control (Figure 5.4, and Table 5.3). The % release for these systems was also a minimum of three fold higher than the control (Figure 5.4a). The results of this assay are consistent with the proton permeation assay in that the inclusion of all SpOx derivatives disrupts the bilayer membrane and increased the vesicle permeability when compared with the control vesicles. The effect of photoisomerization of **24**–**26** on membrane permeation was assessed. In all systems, the presence of the MC form lead to an increase in both k_{K+} and % release when compared with the non-irradiated DPPC vesicles containing SpOxs (Table 5.3). Specifically, the k_{K+} was 40, 30, and 60% larger for **24**, **25**, and **26**, respectively, whereas the % release was 50, 30, and 70% larger for **24**, **25**, and **26**, respectively, than the non-irradiated vesicles (Figure 5.4b). These statistically significant increases in k_{K+} and % release suggest that the photoisomerization of SpOxs to their more polar ring-opened MC form causes greater disruption to the bilayer membrane than the SP form. It appears that the more polar MC form allows for increased free volume in the bilayer membrane, which enhances potassium ion permeation through solubility-

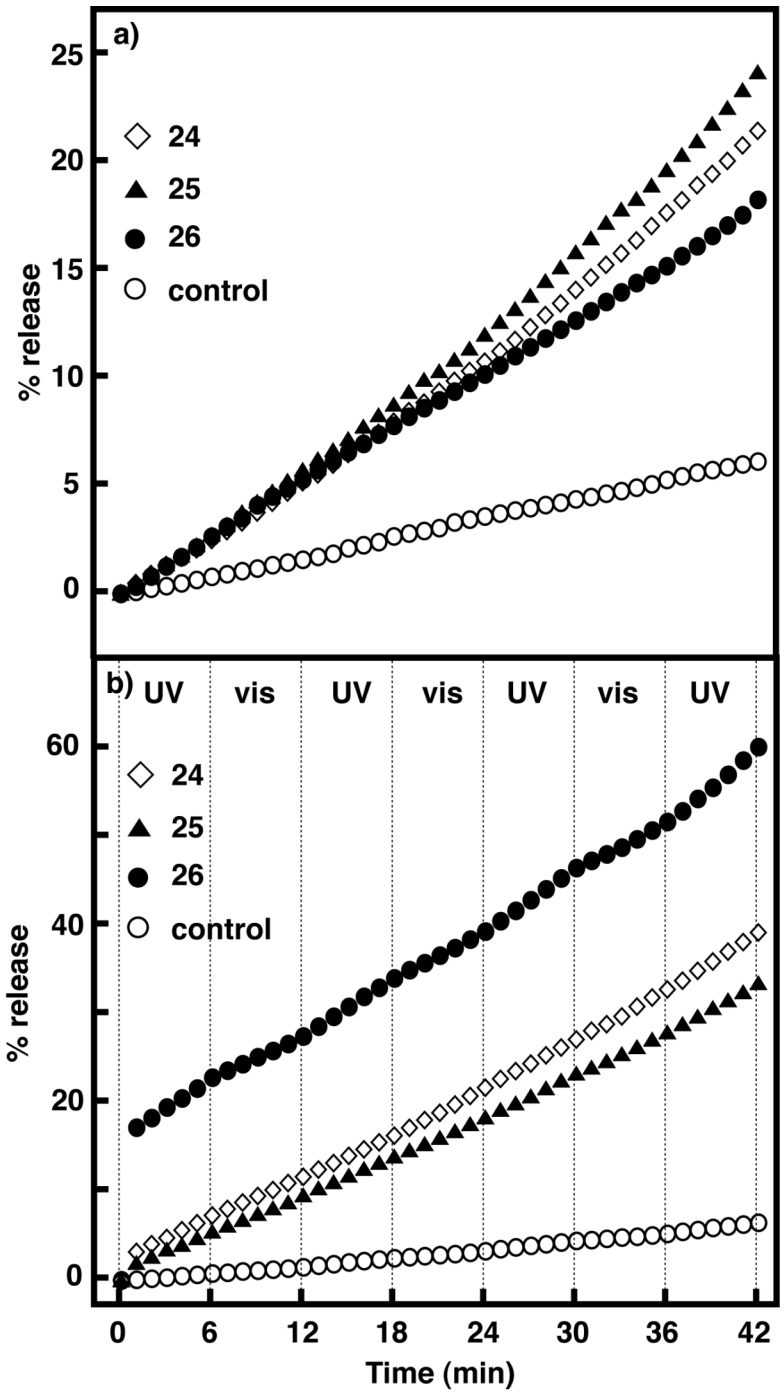

Figure 5.4. Normalized percentage of potassium ion release as a function of time for **24**–**26** in DPPC vesicles at a mole ratio of 1:20 (a) prior to irradiation, and (b) alternating periods of continuous UV and visible irradiation. Each plot is an average of three independent measurements.

Table 5.3. Potassium ion permeation rate constants and normalized percentage of potassium ion release for DPPC vesicles incorporating SpOxs at a mole ratio of 1:20 (SpOx/DPPC)[a]

DPPC	k_{K+} (10^{-8} M s^{-1})			% release	
Light	No	UV	Visible	No	UV and Visible[b]
Control	0.7 ± 0.1 (3)	0.8 ± 0.1 (8)	0.6 ± 0.1 (8)	6 ± 1 (3)	7 ± 1 (8)
24	1.8 ± 0.1 (3)	2.8 ± 0.4 (3)	2.7 ± 0.4 (3)	21 ± 1 (3)	39 ± 3 (3)
25	1.9 ± 0.1 (3)	2.6 ± 0.3 (3)	2.4 ± 0.2 (3)	24 ± 1 (3)	34 ± 1 (3)
26	1.6 ± 0.1 (3)	4.0 ± 0.5 (3)	2.8 ± 0.2 (3)	18 ± 3 (3)	60 ± 5 (3)

[a] The error is the standard deviation of the mean taken from *n* independent measurements. The value of *n* is shown in the parentheses.
[b] The percentage of potassium ion release was determined after 3.5 cycles of UV and visible light irradiation.

diffusion mechanism. To examine the reversibility of SpOxs in DPPC vesicles, the samples were irradiated with visible light, which photochemically isomerizes the MC form back to the SP form. The k_{K+} for **24** and **25** were relatively unchanged, whereas a slight decrease in k_{K+} was observed for **26** when compared with the UV irradiated samples in DPPC vesicles. These results are consistent with DPPC vesicles incorporating DTEs in potassium ion permeation where no significant difference in k_{K+} was observed between UV and visible irradiation. Again, this implies that irreversible change in membrane structure of gel phase DPPC vesicles upon irradiation.

To compare the effect of alkyl chain length on vesicle permeability, the k_{K+} and % release for **24** and **25** were compared before and during irradiation. The k_{K+} observed for **24** and **25** were not significantly different, as the results were within the experimental error. However, there is a significant increase in % release after irradiation was observed for **24**. Consistent with the proton permeation studies, this could be due to the difference in the relative positioning of the photochromic moiety of **24** and **25** in the lipid bilayer, although further studies are required to evaluate their relative position in the bilayer membrane as described previously. This result suggests that **24** with a longer dodecyl chain is more disruptive than **25** with a shorter hexyl chain in DPPC vesicles.

To further understand the effect of molecular size on potassium ion permeation in DPPC vesicles, the bolaamphiphilic dimer **26** was compared to the monomer systems. Ideally, **26** would span the entire lipid bilayer by anchoring its charged moieties in the polar head group regions of each leaflet of the bilayer membrane. The k_{K+} and % release for the inclusion of **26** and monomers prior to irradiation were not significantly different, as the results were within the experimental error. Consistent with the proton permeation

studies, the inclusion of dimer does not show any significant difference in membrane permeation from monomers in DPPC vesicles. Upon UV irradiation, the k_{K+} obtained for **26** was a minimum of 30% higher than the monomers. In addition, the % release was two fold higher than the monomers after several cycles of alternating UV and visible irradiation. These increases suggest that the photoisomerization of SpOx dimer to its more polar ring-opened form leads to greater disruption of the local bilayer membrane than the monomers. Further, the permeability is found to increase in the order of **25** < **24** < **26**. As a result, molecular size is positively correlated with net change in % release of irradiated samples, whereas a similar correlation was not observed for non-irradiated samples.

5.1.4. Potassium Ion Permeation in DOPC Vesicles Incorporating SpOxs

Like DPPC vesicles, **24**–**26** were studied in DOPC vesicles at the same mole ratio of 1:20. The inclusion of **24**–**26** showed that there was a minimum of 50% increase in k_{K+} for all SpOxs (Figure 5.5a, and Table 5.4). Also, the % release was minimum of two fold larger for **24**–**26** in DOPC vesicles. Consistent with the proton permeation studies, the relative magnitude of change in k_{K+} and % release for all SpOxs in DOPC vesicles when compared with control was lower than in the DPPC vesicles. This again suggests that the number of bilayer defects occurred in DOPC vesicles incorporating SpOxs are lesser because of more fluidic nature of the bilayer membrane. In addition, the two fold difference observed in k_{H+} between **24** and **25** in DOPC vesicles was not evident in this

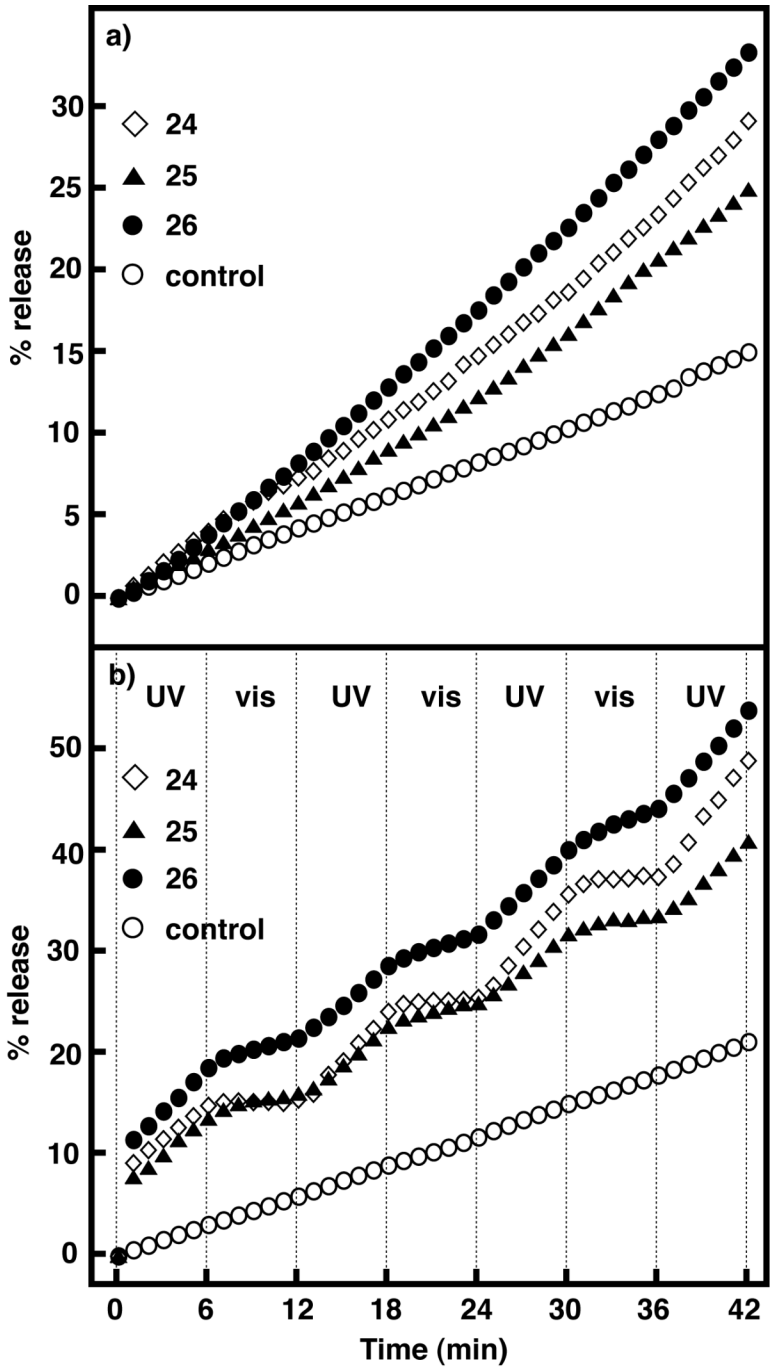

Figure 5.5. Normalized percentage of potassium ion release as a function of time for **24**–**26** in DOPC vesicles at a mole ratio of 1:20 (a) prior to irradiation, and (b) alternating periods of continuous UV and visible irradiation. Each plot is an average of three independent measurements.

Table 5.4. Potassium ion permeation rate constants and normalized percentage of potassium ion release for DOPC vesicles incorporating SpOxs at a mole ratio of 1:20 (SpOx/DOPC)[a]

DOPC	k_{K+} (10^{-8} M s^{-1})			% release	
Light	No	UV	Visible	No	UV and Visible[b]
Control	1.4 ± 0.1 (3)	2.1 ± 0.1 (9)	1.9 ± 0.1 (9)	15 ± 1 (3)	21 ± 2 (9)
24	2.1 ± 0.1 (3)	4.7 ± 1.1 (3)	0.3 ± 0.2 (3)	29 ± 4 (3)	49 ± 1 (3)
25	2.0 ± 0.1 (3)	4.0 ± 0.2 (3)	0.9 ± 0.2 (3)	25 ± 3 (3)	41 ± 2 (3)
26	2.7 ± 0.1 (3)	3.9 ± 0.5 (3)	1.4 ± 0.3 (3)	33 ± 1 (3)	54 ± 3 (3)

[a] The error is the standard deviation of the mean taken from *n* independent measurements. The value of *n* is shown in the parentheses.
[b] The percentage of potassium ion release was determined after 3.5 cycles of UV and visible light irradiation.

assay. This variance highlights the increased sensitivity of the proton permeation assay to changes in structure because proton permeation can also occur by the Grotthuss mechanism. This mechanism proposes that protons can cross the membrane by hopping along hydrogen-bonded chains of water, which is a pathway not possible for potassium ions.[129]

To examine the effect of photoisomerization of the SpOx derivatives on membrane permeation, DOPC vesicles containing **24**–**26** was irradiated with UV light. The MC form of SpOxs had an increase in k_{K+} when compared with the non-irradiated DOPC vesicles containing SpOx derivatives. Specifically, the k_{K+} was 50% higher for monomers, and 30% higher for dimer (Table 5.4). The % release was also 40% higher for irradiated vesicles. Like DPPC vesicles, the increases in k_{K+} and % release suggest that the more polar ring-opened MC form causes greater disruption to the bilayer membrane than the SP form. Following irradiation with visible light, SpOxs isomerizes back to the SP form. Unlike DPPC vesicles, a significant decrease in k_{K+} was observed for **24**–**26** when compared with the UV irradiated SpOxs in DOPC vesicles. The k_{K+} was 15 fold lower for **24**, four fold lower for **25** and three fold lower for **26** than the UV irradiated samples (Table 5.4 and Figure 5.5b). The large changes observed in these rate constants suggest that isomerization to the less polar closed-ring isomers restores the normal bilayer membrane structure, which significantly reduces the rate of permeation. The photocontrol of potassium ion permeation from lipid vesicles has been reported previously for an alkylated spiropyran.[37] The isomeric state of this spiropyran, that disrupted the organization of bilayer membrane was reversed when compared with our systems. For the spiropyran, the rate of potassium ion permeation increased when the

spiropyran was in its SP form and decreased when it was in the MC form. In fact, the difference in permeability between these two isomeric forms of spiropyran was shown to be within the experimental error in PC vesicles. This contrasting result suggests that the inclusion of a terminally charged 'tether' improves the organization of our SpOx derivatives, as closed-ring isomers, within the bilayer membrane, enhancing membrane stability. Consequently, this comparison clearly shows that the order of disturbance to the bilayer membrane can be conveniently controlled through the insertion or deletion of this structural feature. In addition, the differences in potassium ion permeation under UV and visible irradiation are significantly greater for SpOxs than the previously reported spiropyran derivative. Interestingly, the k_{K+} for SpOx samples irradiated with visible light was lower than the non-irradiated SpOx samples, which are seven fold lower for **24** and two fold lower for **25** and **26**. This suggests that an equilibrium mixture of both isomers exists prior to irradiation. This thermal equilibrium is a consequence of the thermochromic behavior of these SpOxs,[47] which explains the higher permeability of potassium ion prior to the irradiation. Overall, these results demonstrate that changes in membrane permeability can be reversibly photocontrolled with SpOx derivatives in DOPC vesicles.

Similar to the DPPC studies, the k_{K+} and % release for **24** and **25** were compared to determine the effect of alkyl chain length on vesicle permeability. The k_{K+} for the inclusion of **24** and **25** prior to irradiation were not significantly different, as the results were within the experimental error. However, the k_{K+} upon UV and visible irradiation underwent the largest changes for **24** in DOPC vesicles. Also, the % release of **24** is higher than **25** before and during irradiation. Once again, the dodecyl derivative appears

to be a more disruptive than the hexyl derivative. Consistent with the proton permeation studies, this could be due the difference in the relative positioning of the photochromic moiety of **24** and **25** in the lipid bilayer.

To assess the effect of molecular size on potassium ion permeation in DOPC vesicles, **26** was compared to the monomers. The k_{K+} obtained for the inclusion of **26** was 30% higher than both monomers. Following UV irradiation, the dimer showed a 50% increase in k_{K+} than the controls but similar to monomers. A three fold decrease in k_{K+} was observed for **26** upon visible irradiation, which is also similar to the monomer systems. This highlights the lower sensitivity of this assay to changes in molecular structure, as the large differences in k_{H+} between dimer and the monomers in DOPC vesicles were not apparent. However, this assay is beneficial in examining the effect of photoisomerization on membrane permeability. The % releases of **26** before and after several cycles of continuous irradiation were significantly higher than both monomers. The increase in % releases of dimer correlates with the larger molecular size of **26** disrupts the bilayer membrane to a greater extent than the monomers in DOPC vesicles. Overall, the photoinduced changes in potassium ion permeation from DOPC vesicles incorporating these SpOx derivatives was found to increase in the order of **25** < **24** < **26**.

5.2. Summary

DTEs **21** and **22** and SpOxs **24**–**26** were studied in DPPC and DOPC vesicles to examine the effect of inclusion and photoisomerization of photochromic compounds on the vesicle permeability. The inclusion of both DTEs increased the k_{K+} and % release in

DPPC and DOPC vesicles when compared with the control vesicles. Also, the k_{K+} and % release of UV and visible irradiated vesicles containing DTEs were higher than the non-irradiated vesicles containing DTEs. The relative magnitude of the changes in the k_{K+} was larger for DPPC vesicles than DOPC vesicles, due to the difference in the lipid phase state. In addition, lipid vesicles incorporating the longer dodecyl derivative **21** appears to be more permeable to potassium ions than the shorter hexyl derivative **22**. Thus, the potassium ion permeation is clearly sensitive to both the lipid bilayer phase state and the relative position of the photochromic moiety in the bilayer membrane.

The inclusion of **24**–**26** showed significantly larger k_{K+} and % release when compared with the control vesicles for both lipid systems. The results of this assay are consistent with the proton permeation assay in that the inclusion of SpOxs does disrupt bilayer packing in DPPC and DOPC vesicles and increases their permeability. The photoisomerization of SpOxs to their more polar open-ring MC form leads to greater disruption of the bilayer membrane structure, and enhances permeability in DOPC vesicles. Upon irradiation with visible light, the k_{K+} for the closed-ring SP forms was significantly lower than the MC forms in DOPC vesicles. As a result, the changes in membrane permeability can be reversibly photocontrolled with (bola)amphiphilic SpOxs in DOPC vesicles. The k_{K+} for the closed-ring SP forms in DPPC vesicles were relatively unchanged with visible irradiation. There is a strong correlation exists between the membrane permeability and the phase state of the lipids. Among the SpOx monomers, the dodecyl derivative **24** appears to be a more disruptive than the hexyl derivative **25** in both lipid systems because the photochromic moiety of **24** is presumably more deeply embedded in the bilayer membrane. Also, SpOx dimer has shown a relatively larger

effect on vesicle permeability than the monomers in both lipid vesicles. The differences in the relative permeability of lipid vesicles indicate that SpOx structures are important for vesicle permeability. Considering the changes in k_{K+} upon UV and visible irradiation and the net change in % release, the membrane permeability of lipid vesicles incorporating **24**–**26** increases in the following order of **25** < **24** < **26**. This ranking shows that the molecular sizes of these SpOxs are positively correlated with the membrane permeability in both DPPC and DOPC vesicles.

Overall, the photoinduced changes in potassium ion permeation from both DPPC and DOPC vesicles incorporating these photochromic compounds is found to increase in the order of **22** < **21** < **25** < **24** < **26**. Moreover, the lipid vesicles incorporating photochromic compounds are most likely follow the solubility-diffusion mechanism for the permeation of potassium ions. By comparison, vesicles incorporating SpOxs produce better photoresponsive systems for controlling potassium ion permeation than DTEs. The more polar and ionic nature of SpOxs, and their large change in molecular volume during photoisomerization are the possible reasons for why SpOxs exhibit higher rate constants for potassium ion permeation in lipid vesicles than DTEs. Also, this ranking suggests that the SpOx dimer in both lipid systems is more permeable to potassium ions than all other photoresponsive systems. Further, the differences in potassium ion permeability under UV and visible irradiation are considerably more pronounced for the dimer in DOPC vesicles than the dimer in DPPC vesicles. Consistent with proton permeation studies, the potassium ion permeation studies suggest that the SpOx dimer in DOPC vesicles exhibits the best photocontrol of ion permeation. As a result, we propose that the

SpOx dimer in DOPC vesicles would be the best candidate, from those examined in this study, for the delivery of small molecules.

CHAPTER 6

FUTURE WORK

Since SpOx dimer **26** in DOPC vesicles has shown better photocontrol of ion permeation than the respective monomer, DTE dimer **27** is also expected to enhance the membrane permeability than its monomer. Similar to the SpOx dimer, the DTE dimer may also disrupt the bilayer membrane more efficiently to enhance the ion permeation. Previously, I and one of our research group members have made attempts to synthesize **27** using the synthetic routes shown in A.1 and A.2 (Appendix B).[111] However, our attempts were unsuccessful, as the final coupling step did not work in our hands. Therefore, an alternate synthetic route as shown in Scheme 6.1 will be tried to complete the synthesis of **27**.[130] Upon completion of the synthesis of **27**, a photophysical characterization of **27** will be performed. This includes measuring the absorption spectra for open and closed-ring isomers, the photoinduced cyclization and cycloreversion quantum yields, and the photoconversion yields. Also, the fatigue resistance of **27** will be investigated to determine the photostability of **27**. Finally, **27** will be incorporated into lipid vesicles, and its photocontrol of ion permeation in lipid vesicles will be examined and compared to systems studied in this research. Further, to advance our understanding in the photocontrolled release of small molecules, DOPC vesicles with smaller diameters that incorporate **26** and lipophilic fluorescent molecules will be investigated.

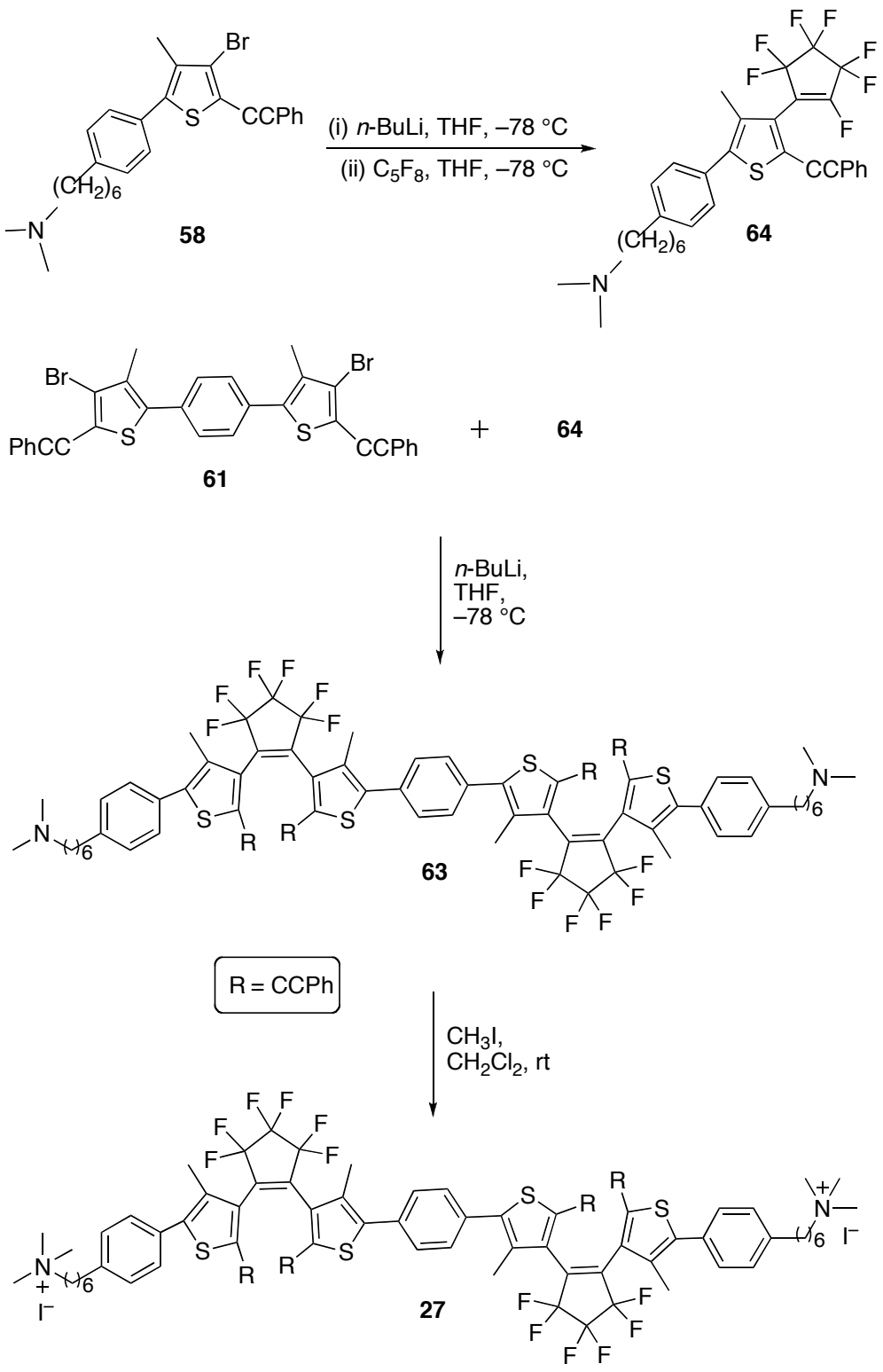

Scheme 6.1. Alternate method for the synthesis of **27**.

REFERENCES

(1) Dürr, H.; Bouas-Layrent, H. *Photochromism-Molecules and Systems*; Elsevier: Amsterdam, 1990.

(2) Tian, H.; Feng, Y. *J. Mater. Chem.* **2008**, *18*, 1617-1622.

(3) Tian, H.; Yang, S. *Chem. Soc. Rev.* **2004**, *33*, 85-97.

(4) Irie, M. *Chem. Rev.* **2000**, *100*, 1685-1716.

(5) Patel, P. D.; Mikhailov, I. A.; Belfield, K. D.; Masunov, A. E. *Int. J. Quantum Chem.* **2009**, *109*, 3711-3722.

(6) Turro, N. J. *Modern Molecular Photochemistry*; University Science Books: Sausalito, CA, 1991.

(7) Carroll, F. A. *Perspectives on Structure and Mechanism in Organic Chemistry*; Brooks/Cole: London, 1998.

(8) Hoffmann, R.; Woodward, R. B. *J. Am. Chem. Soc.* **1965**, *87*, 2046-2048.

(9) Higashiguchi, K.; Matsuda, K.; Matsuo, M.; Yamada, T.; Irie, M. *J. Photochem. Photobiol., A* **2002**, *152*, 141-146.

(10) Yam, V. W. W.; Ko, C. C.; Zhu, N. Y. *J. Am. Chem. Soc.* **2004**, *126*, 12734-12735.

(11) Irie, M.; Sakemura, K.; Okinaka, M.; Uchida, K. *J. Org. Chem.* **1995**, *60*, 8305-8309.

(12) Nakamura, S.; Irie, M. *J. Org. Chem.* **1988**, *53*, 6136-6138.

(13) Uchida, K.; Tsuchida, E.; Aoi, Y.; Nakamura, S.; Irie, M. *Chem. Lett.* **1999**, *28*, 63-64.

(14) Irie, M.; Lifka, T.; Uchida, K.; Kobatake, S.; Shindo, Y. *Chem. Commun.* **1999**, 747-750.

(15) Higashiguchi, K.; Matsuda, K.; Yamada, T.; Kawai, T.; Irie, M. *Chem. Lett.* **2000**, 1358-1359.

(16) Higashiguchi, K.; Matsuda, K.; Kobatake, S.; Yamada, T.; Kawai, T.; Irie, M. *Bull. Chem. Soc. Jpn.* **2000**, *73*, 2389-2394.

(17) de Jong, J. J. D.; Lucas, L. N.; Hania, R.; Pugzlys, A.; Kellogg, R. M.; Feringa, B. L.; Duppen, K.; van Esch, J. H. *Eur. J. Org. Chem.* **2003**, *2003*, 1887-1893.

(18) Morimitsu, K.; Kobatake, S.; Irie, M. *Tetrahedron Lett.* **2004**, *45*, 1155-1158.

(19) Cai, J. X.; Farhat, A.; Tsitovitch, P. B.; Bodani, V.; Toogood, R. D.; Murphy, R. S. *J. Photochem. Photobiol., A* **2010**, *212*, 176-182.

(20) Fan, C.; Pu, S.; Liu, G.; Yang, T. *J. Photochem. Photobiol., A: Chem.* **2008**, *194*, 333-343.

(21) Liu, G.; Liu, M.; Pu, S.; Fan, C.; Cui, S. *Dyes Pigm.* **2012**, *95*, 553-562.

(22) Pu, S.; Wang, R.; Liu, G.; Liu, W.; Cui, S.; Yan, P. *Dyes Pigm.* **2012**, *94*, 195-206.

(23) Sevez, G.; Pozzo, J.-L. *Dyes Pigm.* **2011**, *89*, 246-253.

(24) Endtner, J. M.; Effenberger, F.; Hartschuh, A.; Port, H. *J. Am. Chem. Soc.* **2000**, *122*, 3037-3046.

(25) Al-Atar, U.; Fernandes, R.; Johnsen, B.; Baillie, D.; Branda, N. R. *J. Am. Chem. Soc.* **2009**, *131*, 15966-15967.

(26) Wang, H.; Xu, W.; Zhu, D. *Tetrahedron* **2012**, *68*, 8719-8723.

(27) Perrier, A. l.; Maurel, F. o.; Jacquemin, D. *Acc. Chem. Res.* **2012**, *45*, 1173-1182.

(28) Areephong, J.; Browne, W. R.; Feringa, B. L. *Org. Biomol. Chem.* **2007**, *5*, 1170-1174.

(29) Gilat, S. L.; Kawai, S. H.; Lehn, J.-M. *Chem. Eur. J.* **1995**, *1*, 275-284.

(30) Pu, S.; Fan, C.; Miao, W.; Liu, G. *Dyes Pigm.* **2010**, *84*, 25-35.

(31) Lucas, Linda N.; Jong, Jaap J. D. d.; Esch, Jan H. v.; Kellogg, Richard M.; Feringa, Ben L. *Eur. J. Org. Chem.* **2003**, *2003*, 155-166.

(32) Lucas, L. N.; van Esch, J.; Kellogg, R. M.; Feringa, B. L. *Tetrahedron Lett.* **1999**, *40*, 1775-1778.

(33) Hermes, S.; Dassa, G.; Toso, G.; Bianco, A.; Bertarelli, C.; Zerbi, G. *Tetrahedron Lett.* **2009**, *50*, 1614-1617.

(34) Kobatake, S.; Terakawa, Y. *Chem. Commun.* **2007**, 1698-1700.

(35) Minkin, V. I. *Chem. Rev.* **2004**, *104*, 2751-2776.

(36) Lokshin, V. A.; Samat, A.; Metelitsa, A. V. *Russ. Chem. Rev.* **2002**, *71*, 893-916.

(37) Khairutdinov, R. F.; Hurst, J. K. *Langmuir* **2001**, *17*, 6881-6886.

(38) Tong, R.; Hemmati, H. D.; Langer, R.; Kohane, D. S. *J. Am. Chem. Soc.* **2012**, *134*, 8848-8855.

(39) Klajn, R. *Chem. Soc. Rev.* **2014**, *43*, 148-184.

(40) Khairutdinov, R. F.; Giertz, K.; Hurst, J. K.; Voloshina, E. N.; Voloshin, N. A.; Minkin, V. I. *J. Am. Chem. Soc.* **1998**, *120*, 12707-12713.

(41) Yam, V. W.-W.; Ko, C.-C.; Wu, L.-X.; Wong, K. M.-C.; Cheung, K.-K. *Organometallics* **2000**, *19*, 1820-1822.

(42) Kumar, S.; Watkins, D. L.; Fujiwara, T. *Chem. Commun.* **2009**, 4369-4371.

(43) Bletz, M.; Pfeifer-Fukumura, U.; Kolb, U.; Baumann, W. *J. Phys. Chem. A* **2002**, *106*, 2232-2236.

(44) Wohl, C. J.; Kuciauskas, D. *J. Phys. Chem. B* **2005**, *109*, 21893-21899.

(45) Feringa, B. L.; Browne, W. R. *Molecular Switches*; 2nd ed.; Wiley-VCH: Germany, 2011; Vol. 1.

(46) Zelichenok, A.; Buchholtz, F.; Ratner, J.; Fischer, E.; Krongauz, V. *J. Photochem. Photobiol., A* **1994**, *77*, 201-206.

(47) Louis, K. M.; Kahan, T.; Morley, D.; Peti, N.; Murphy, R. S. *J. Photochem. Photobiol., A* **2007**, *189*, 224-231.

(48) Li, X.; Li, J.; Wang, Y.; Matsuura, T.; Meng, J. *J. Photochem. Photobiol., A* **2004**, *161*, 201-213.

(49) Watkins, D. L.; Fujiwara, T. *J. Photochem. Photobiol., A* **2012**, *228*, 51-59.

(50) Fuhrhop, J.-H.; Wang, T. *Chem. Rev.* **2004**, *104*, 2901-2937.

(51) Jin, L. M.; Li, Y.; Ma, J.; Li, Q. *Org. Lett.* **2010**, *12*, 3552-3555.

(52) Bahri, M. A.; Heyne, B. J.; Hans, P.; Seret, A. E.; Mouithys-Mickalad, A. A.; Hoebeke, M. D. *Biophys. Chem.* **2005**, *114*, 53-61.

(53) Malic, N.; Campbell, J. A.; Ali, A. S.; York, M.; D'Souza, A.; Evans, R. A. *Macromolecules* **2010**, *43*, 8488-8501.

(54) Zhou, W.; Zhang, H.; Li, H.; Zhang, Y.; Wang, Q.-C.; Qu, D.-H. *Tetrahedron* **2013**, *69*, 5319-5325.

(55) Watkins, D. L.; Fujiwara, T. *J. Mater. Chem. C* **2013**, *1*, 506-514.

(56) Fihey, A.; Perrier, A.; Browne, W. R.; Jacquemin, D. *Chem. Soc. Rev.* **2015**, *44*, 3719-3759.

(57) Yoshida, K.; Fujii, Y.; Nishio, I. *J. Phys. Chem. B* **2014**, *118*, 4115-4121.

(58) Samad, A.; Sultana, Y.; Aqil, M. *Curr. Drug Deliv.* **2007**, *4*, 297-305.

(59) Lasic, D. D. *Trends Biotechnol.* **1998**, *16*, 307-321.

(60) Lian, T.; Ho, R. J. Y. *J. Pharm. Sci.* **2001**, *90*, 667-680.

(61) Shum, P.; Kim, J.-M.; Thompson, D. H. *Adv. Drug Delivery Rev.* **2001**, *53*, 273-284.

(62) Çirli, Ö. Ö.; Hasirci, V. *J. Controlled Release* **2004**, *96*, 85-96.

(63) Guo, X.; Szoka, F. C. *Acc. Chem. Res.* **2003**, *36*, 335-341.

(64) Fomina, N.; Sankaranarayanan, J.; Almutairi, A. *Adv. Drug Delivery Rev.* **2012**, *64*, 1005-1020.

(65) Lasic, D. D. *Liposomes: From Physics to Applications*; Elsevier: New York, 1993.

(66) Marsh, D. *Handbook of Lipid Bilayers*; 2nd ed.; CRC Press: Boca Raton, 2013.

(67) Lindsey, H. P., N. O.; Chan, S. I. *Biochim. Biophys. Acta* **1979**, *555*, 147-167.

(68) Ahmad, M. U.; Xu, X. *Polar Lipids: Biology, Chemistry, and Technology*; AOCS Press: Urbana, Illinois, 2015.

(69) Fyles, T. M. *Chem. Soc. Rev.* **2007**, *36*, 335-347.

(70) Saier, M. H. *J. Membr. Biol.* **2000**, *175*, 165-180.

(71) Madhavan, N.; Robert, E. C.; Gin, M. S. *Angew. Chem. Int. Ed.* **2005**, *44*, 7584-7587.

(72) Sidorov, V.; Kotch, F. W.; Kuebler, J. L.; Lam, Y.-F.; Davis, J. T. *J. Am. Chem. Soc.* **2003**, *125*, 2840-2841.

(73) Das, G.; Talukdar, P.; Matile, S. *Science* **2002**, *298*, 1600-1602.

(74) Khairutdinov, R. F.; Hurst, J. K. *Langmuir* **2004**, *20*, 1781-1785.

(75) Song, J.; Fang, Z.; Wang, C.; Zhou, J.; Duan, B.; Pu, L.; Duan, H. *Nanoscale* **2013**, *5*, 5816-5824.

(76) Liu, T.; Bao, C.; Wang, H.; Lin, Y.; Jia, H.; Zhu, L. *Chem. Commun.* **2013**, *49*, 10311-10313.

(77) Alvarez-Lorenzo, C.; Bromberg, L.; Concheiro, A. *Photochem. Photobiol.* **2009**, *85*, 848-860.

(78) Ercole, F.; Davis, T. P.; Evans, R. A. *Polym. Chem.* **2010**, *1*, 37-54.

(79) Velema, W. A.; Szymanski, W.; Feringa, B. L. *J. Am. Chem. Soc.* **2014**, *136*, 2178-2191.

(80) Dong, J.; Wang, Y. N.; Zhang, J.; Zhan, X. W.; Zhu, S. Q.; Yang, H.; Wang, G. J. *Soft Matter* **2013**, *9*, 370-373.

(81) Yavlovich, A. S., B.; Gupta, K.; Blumenthal, R.; Puri, A. *Mol. Membr. Biol.* **2010**, *27*, 364-381.

(82) Kuiper, J. M.; Stuart, M. C. A.; Engberts, J. *Langmuir* **2008**, *24*, 426-432.

(83) Lei, Y.; Hurst, J. K. *Langmuir* **1999**, *15*, 3424-3429.

(84) Liu, X. M.; Yang, B.; Wang, Y. L.; Wang, J. Y. *Biochim. Biophys. Acta, Biomembr.* **2005**, *1720*, 28-34.

(85) Matsumura, A.; Tsuchiya, K.; Torigoe, K.; Sakai, K.; Sakai, H.; Abe, M. *Langmuir* **2011**, *27*, 1610-1617.

(86) Morgan, C. G.; Bisby, R. H.; Johnson, S. A.; Mitchell, A. C. *FEBS Lett.* **1995**, *375*, 113-116.

(87) Song, B. L.; Zhao, J. X.; Wang, B. X.; Jiang, R. *Colloids Surf., A.* **2009**, *352*, 24-30.

(88) Song, X. D.; Perlstein, J.; Whitten, D. G. *J. Am. Chem. Soc.* **1997**, *119*, 9144-9159.

(89) Bisby, R. H.; Mead, C.; Morgan, C. G. *Biochem. Biophys. Res. Commun.* **2000**, *276*, 169-173.

(90) Jog, P. V.; Gin, M. S. *Org. Lett.* **2008**, *10*, 3693-3696.

(91) Yagi, S.; Karatsu, T.; Kitamura, A. *Chem. Eur. J.* **2005**, *11*, 4054-4063.

(92) Takumi, K.; Sakamoto, H.; Uda, R. M.; Sakurai, Y.; Kume, H.; Kimura, K. *Colloids Surf., A* **2007**, *301*, 100-105.

(93) Wohl, C. J.; Helms, M. A.; Chung, J. O.; Kuciauskas, D. *J. Phys. Chem. B* **2006**, *110*, 22796-22803.

(94) Koçer, A.; Walko, M.; Meijberg, W.; Feringa, B. L. *Science* **2005**, *309*, 755-758.

(95) Ohya, Y.; Okuyama, Y.; Fukunaga, A.; Ouchi, T. *Supramol. Sci.* **1998**, *5*, 21-29.

(96) Xie, X.; Bakker, E. *ACS Appl. Mater. Interfaces* **2014**, *6*, 2666-2670.

(97) Falck, E.; Patra, M.; Karttunen, M.; Hyvönen, M. T.; Vattulainen, I. *J. Chem. Phys.* **2004**, *121*, 12676-12689.

(98) Baker, R. W. In *Membrane Technology and Applications*; 2nd ed.; John Wiley & Sons: Menlo Park, CA, 2004, p 15-88.

(99) Paula, S.; Volkov, A. G.; VanHoek, A. N.; Haines, T. H.; Deamer, D. W. *Biophys. J.* **1996**, *70*, 339-348.

(100) Paula, S.; Volkov, A. G.; Deamer, D. W. *Biophys. J.* **1998**, *74*, 319-327.

(101) Brodbelt, J. S.; Liou, C.-C. *Pure Appl. Chem.* **1993**, *65*, 409-414.

(102) Volkov, A. G.; Paula, S.; Deamer, D. W. *Bioelectrochem. Bioenerg.* **1997**, *42*, 153-160.

(103) Fyles, T. M.; van Straaten-Nijenhuis, W. F. In *Comprehensive Supramolecular Chemistry*; Reinhoudt, D. N., Ed.; Elsevier Science: Amsterdam/New York, 1996; Vol. 10, p 53-77.

(104) Han, J.; Burgess, K. *Chem. Rev.* **2010**, *110*, 2709-2728.

(105) Ramos, C.; Bonato, D.; Winterhalter, M.; Stegmann, T.; Teissié, J. *FEBS Lett.* **2002**, *518*, 135-138.

(106) Lakowich, J. R. In *Principles of Fluorescence Spectroscopy*; 2nd ed.; Kluwer Academic/Plenum Publishers: New York, 1999, p 531-572.

(107) Jeon, Y. J.; Kim, H.; Jon, S.; Selvapalam, N.; Oh, D. H.; Seo, I.; Park, C.-S.; Jung, S. R.; Koh, D.-S.; Kim, K. *J. Am. Chem. Soc.* **2004**, *126*, 15944-15945.

(108) Yili, B.; Louis, K. M.; Murphy, R. S. *J. Photochem. Photobiol., A: Chem.* **2007**, *192*, 130-141.

(109) Irie, M.; Miyatake, O.; Uchida, K.; Eriguchi, T. *J. Am. Chem. Soc.* **1994**, *116*, 9894-9900.

(110) Kandasamy, Y. S.; Cai, J.; Ottaviano, J. G.; Smith, K. A.; Williams, A. N.; Moore, J.; Louis, K. M.; Selzler, L.; Beler, A.; Okwuonu, T.; Murphy, R. S. *Org. Biomol. Chem.* **2016**, *14*, 296-308.

(111) Cai, J. M.Sc. Thesis, University of Regina, Regina, SK, 2011.

(112) Harris, D. C. In *Quantitative Chemical Analysis*; 3rd ed.; W. H. Freeman: New York, 1991.

(113) Irie, M.; Lifka, T.; Kobatake, S.; Kato, N. *J. Am. Chem. Soc.* **2000**, *122*, 4871-4876.

(114) Peters, A.; Branda, N. R. *Adv. Mater. Opt. Electron.* **2000**, *10*, 245-249.

(115) Celani, P.; Ottani, S.; Olivucci, M.; Bernardi, F.; Robb, M. A. *J. Am. Chem. Soc.* **1994**, *116*, 10141-10151.

(116) Calvert, J. G.; Pitts, J. N., Jr. *Photochemistry*; Wiley & Sons: New York, 1966.

(117) Perrin, D. D.; Armarego, W. L. *Purification of Laboratory Chemicals*; Elsevier Science: New York, 1988.

(118) Glaze, A. P.; Heller, H. G.; Whittall, J. *J. Chem. Soc.-Perkin Trans. 2* **1992**, 591-594.

(119) Heller, H. G.; Langan, J. R. *J. Chem. Soc.-Perkin Trans. 2* **1981**, 341-343.

(120) Fyles, T. M.; Luong, H. *Org. Biomol. Chem.* **2009**, *7*, 733-738.

(121) Matile, S.; Sakai, N. In *Analytical Methods in Supramolecular Chemistry*; Schalley, C., Ed.; Wiley-VCH: Weinheim, 2007, p 391-418.

(122) Kuyper, C. L.; Kuo, J. S.; Mutch, S. A.; Chiu, D. T. *J. Am. Chem. Soc.* **2006**, *128*, 3233-3240.

(123) Moszynski, J. M.; Fyles, T. M. *Org. Biomol. Chem.* **2010**, *8*, 5139-5149.

(124) Sheynis, T.; Sykora, J.; Benda, A.; Kolusheva, S.; Hof, M.; Jelinek, R. *Eur. J. Biochem.* **2003**, *270*, 4478-4487.

(125) Hennig, A.; Fischer, L.; Guichard, G.; Matile, S. *J. Am. Chem. Soc.* **2009**, *131*, 16889-16895.

(126) Leonenko, Z. V.; Finot, E.; Ma, H.; Dahms, T. E. S.; Cramb, D. T. *Biophys. J.* **2004**, *86*, 3783-3793.

(127) Porter, N. A.; Caldwell, S. E.; Mills, K. A. *Lipids* **1995**, *30*, 277-290.

(128) Mertins, O.; Bacellar, I. O. L.; Thalmann, F.; Marques, C. M.; Baptista, M. S.; Itri, R. *Biophys. J.* **2014**, *106*, 162-171.

(129) Paula, S.; Deamer, D. W. In *Membrane Permeability* Deamer, D. W., Kleinzeller, A., Fambrough, D. M., Eds.; Academic Press: San Diego, 1999, p 77-96.

(130) Kobatake, S.; Irie, M. *Tetrahedron* **2003**, *59*, 8359-8364.

APPENDICES

Table of Contents

Appendix A: Supporting Results of Proton Permeation in Lipid Vesicles Incorporating DTEs and SpOxs

Table A.1. The values of EC_{50} and Hill coefficients (n) of **21**–**23**[a]

DTEs	EC_{50} (μM)	n
21o	72	0.9 ± 0.3
22o	72	1.1 ± 0.4
23o	78	1.4 ± 0.2
21c	78	1.2 ± 0.4
22c	80	0.9 ± 0.4
23c	78	2.2 ± 0.9

[a] The error is the standard deviation of the mean taken from a minimum of three independent measurements.

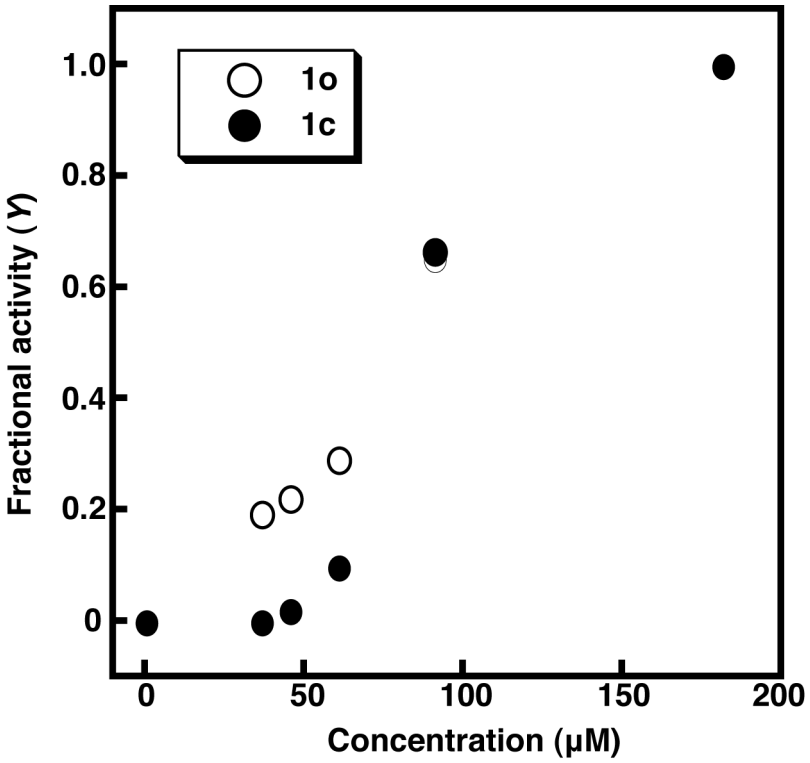

Figure A.1. Fractional activity as a function of concentration of **21** in DPPC vesicle.

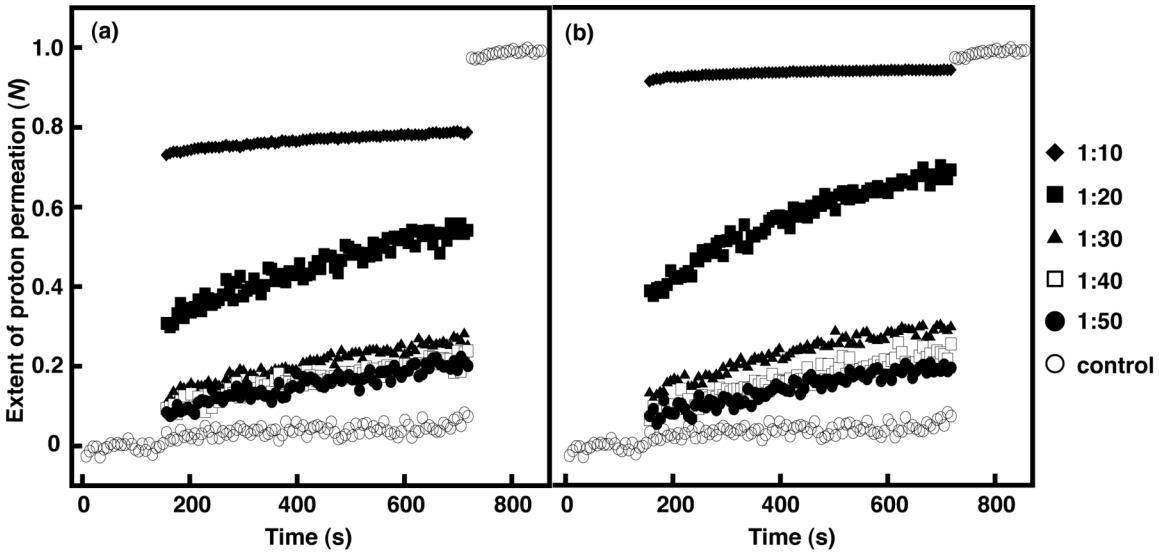

Figure A.2. Extent of proton permeation as a function of time for various mole ratios of (a) **21** and (b) **22** in DPPC vesicles prior to irradiation. For clarity only the control is shown before the base pulse and after the addition of detergent. Each curve is the average of minimum of three independent measurements.

Table A.2. Proton permeation rate constants and normalized extent of proton permeation determined for **21** and **22** in DPPC vesicles at various mole ratios[a]

21/DPPC	k_{H+} (10^{-4} s^{-1})		*N*	
UV	No	Yes	No	Yes
Control	0.46 ± 0.26 (46)	0.31 ± 0.28 (40)	0.07 ± 0.06 (46)	0.22 ± 0.07 (40)
1:10	0.85± 0.13 (6)	0.20 ± 0.06 (6)	0.79 ± 0.03 (6)	0.73 ± 0.03 (6)
1:20	4.2 ± 1.4 (6)	2.3 ± 1.1 (7)	0.54 ± 0.08 (6)	0.56 ± 0.11 (7)
1:30	2.4 ± 0.2 (7)	0.56 ± 0.10 (7)	0.28 ± 0.05 (7)	0.27 ± 0.04 (7)
1:40	2.1 ± 0.1 (6)	0.54 ± 0.15 (6)	0.23 ± 0.02 (6)	0.23 ± 0.04 (6)
1:50	2.0 ± 0.05 (6)	0.52 ± 0.15 (6)	0.21 ± 0.02 (6)	0.22 ± 0.04 (6)
22/DPPC	k_{H+} (10^{-4} s^{-1})		*N*	
UV	No	Yes	No	Yes
Control	0.46 ± 0.26 (46)	0.31 ± 0.28 (40)	0.07 ± 0.06 (46)	0.22 ± 0.07 (40)
1:10	0.34± 0.06 (7)	0.04 ± 0.04 (7)	0.95 ± 0.01 (7)	0.84 ± 0.03 (7)
1:20	4.8 ± 1.0 (9)	1.6 ± 0.5 (8)	0.69 ± 0.04 (9)	0.59 ± 0.07 (8)
1:30	2.9 ± 0.5 (8)	0.61 ± 0.22 (8)	0.30 ± 0.06 (8)	0.29 ± 0.07 (8)
1:40	2.6 ± 0.5 (7)	0.55 ± 0.18 (7)	0.24 ± 0.07 (7)	0.27 ± 0.15 (7)
1:50	2.3 ± 0.5 (8)	0.43 ± 0.13 (7)	0.20 ± 0.08 (8)	0.25 ± 0.13 (7)

[a] The error is the standard deviation of the mean taken from *n* independent measurements. The value of *n* is shown in the parentheses.

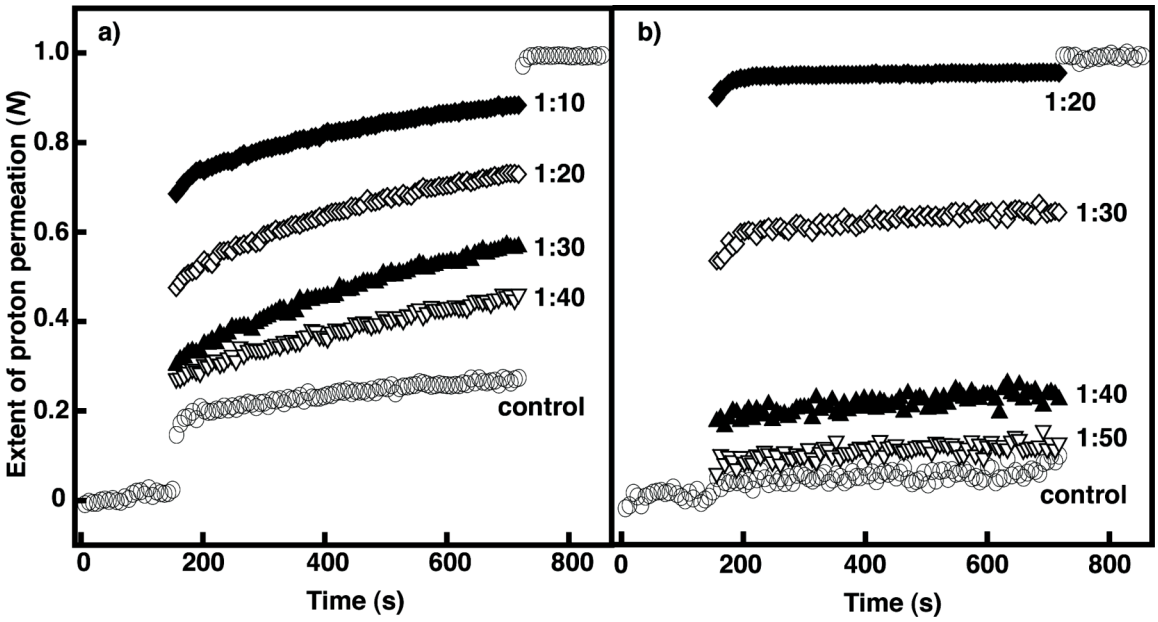

Figure A.3. Extent of proton permeation as a function of time at various mole ratios of **24** in (a) DOPC and (b) DPPC vesicles, prior to irradiation. For clarity only the control is shown before the base pulse and after the addition of detergent. Each curve is the average of minimum of three independent measurements.

Table A.3. Proton permeation rate constants and normalized extent of proton permeation determined for SpOx **24** in DOPC and DPPC vesicles at various mole ratios[a]

24/DOPC	k_{H+} (10^{-4} s^{-1})		*N*	
UV	No	Yes	No	Yes
Control	1.8 ± 0.5 (57)	1.4 ± 0.6 (52)	0.31 ± 0.07 (47)	0.37 ± 0.06 (45)
1:10	2.8 ± 0.4 (6)	2.4 ± 0.1 (6)	0.88 ± 0.02 (6)	0.88 ± 0.02 (6)
1:20	4.3 ± 0.1 (6)	3.8 ± 0.3 (6)	0.73 ± 0.01 (6)	0.78 ± 0.01 (6)
1:30	4.3 ± 0.4 (6)	4.1± 0.2 (6)	0.57 ± 0.02 (6)	0.62 ± 0.05 (6)
1:40	3.1 ± 0.2 (6)	2.5 ± 0.1 (6)	0.45 ± 0.02 (6)	0.48 ± 0.02 (6)
24/DPPC	k_{H+} (10^{-4} s^{-1})		*N*	
UV	No	Yes	No	Yes
Control	0.42 ± 0.24 (61)	0.31 ± 0.27 (52)	0.07 ± 0.05 (54)	0.20 ± 0.07 (49)
1:20	0.25 ± 0.10 (6)	0.22 ± 0.15 (6)	0.96 ± 0.01 (6)	0.96 ± 0.01 (6)
1:30	1.1 ± 0.3 (6)	0.99 ± 0.50 (6)	0.65 ± 0.05 (6)	0.71 ± 0.07 (6)
1:40	1.0 ± 0.4 (6)	0.57 ± 0.16 (6)	0.28 ± 0.02 (6)	0.55 ± 0.01 (6)
1:50	0.67 ± 0.20 (6)	0.45 ± 0.16 (6)	0.12 ± 0.04 (6)	0.22 ± 0.04 (6)

[a] The error is the standard deviation of the mean taken from *n* independent measurements. The value of *n* is shown in parentheses.

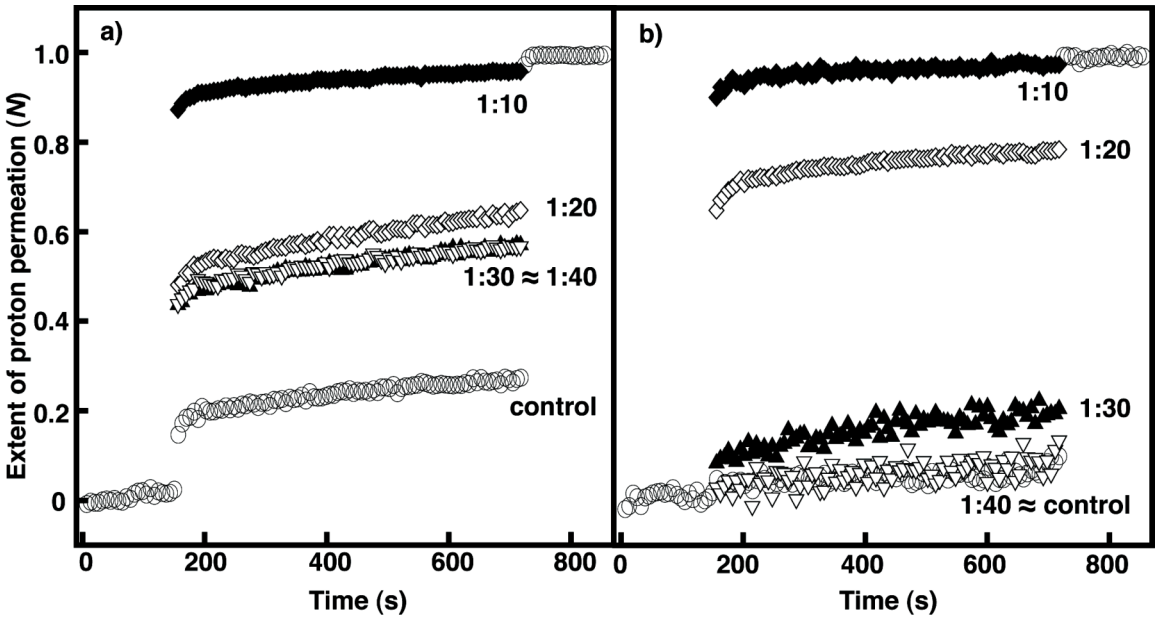

Figure A.4. Extent of proton permeation as a function of time at various mole ratios of **25** in (a) DOPC and (b) DPPC vesicles, prior to irradiation. For clarity only the control is shown before the base pulse and after the addition of detergent. Each curve is the average of minimum of three independent measurements.

Table A.4. Proton permeation rate constants and normalized extent of proton permeation determined for SpOx **25** in DOPC and DPPC vesicles at various mole ratios[a]

25/DOPC	k_{H+} (10^{-4} s^{-1})		N	
UV	No	Yes	No	Yes
Control	1.8 ± 0.5 (57)	1.4 ± 0.6 (52)	0.31 ± 0.07 (47)	0.37 ± 0.06 (45)
1:10	0.89 ± 0.10 (4)	1.3 ± 0.1 (4)	0.96 ± 0.01 (4)	0.96 ± 0.03 (4)
1:20	2.2 ± 0.2 (6)	2.2 ± 0.4 (6)	0.65 ± 0.02 (6)	0.70 ± 0.02 (6)
1:30	1.8 ± 0.1 (6)	1.7 ± 0.4 (6)	0.57 ± 0.03 (6)	0.61 ± 0.03 (6)
1:40	1.6 ± 0.2 (6)	1.1 ± 0.1 (6)	0.56 ± 0.02 (6)	0.59 ± 0.01 (6)
25/DPPC	k_{H+} (10^{-4} s^{-1})		N	
UV	No	Yes	No	Yes
Control	0.42 ± 0.24 (61)	0.31 ± 0.27 (52)	0.07 ± 0.05 (54)	0.20 ± 0.07 (49)
1:10	0.77 ± 0.07 (3)	0.36 ± 0.05 (3)	0.98 ± 0.01 (3)	0.99 ± 0.01 (3)
1:20	1.6 ± 0.2 (6)	1.2 ± 0.3 (6)	0.78 ± 0.03 (6)	0.75 ± 0.05 (6)
1:30	1.7 ± 0.6 (6)	1.4 ± 0.6 (6)	0.22 ± 0.06 (6)	0.40 ± 0.09 (6)
1:40	1.1 ± 0.3 (6)	0.84 ± 0.28 (6)	0.08 ± 0.09 (6)	0.30 ± 0.04 (6)

[a] The error is the standard deviation of the mean taken from *n* independent measurements. The value of *n* is shown in parentheses.

Appendix B: Schemes and Procedures for the Attempted Synthesis of Dimer 27

Synthesis of DTE Dimer 27

Synthetic schemes for DTE dimer **27** are shown in Schemes A.1 and A.2. The synthesis of compound **58** starting from 2,4-dibromo-3-methylthiophene followed a similar synthetic route as described for the synthesis of **46**. A Suzuki coupling reaction was used to couple one mole of 1,4-phenyldiboronic acid with two moles of 2-bromo-3-methylthiophene to form the product **59**. The coupled product **59** on bromination with excess NBS produced **60** in low yield. A Sonogashira coupling reaction of **60** with phenylacetylene gave **61**. This product was then reacted with excess of OFCP using *n*-BuLi to form **62**. The synthesis of **27** was successfully completed up to this step. There are two more steps remaining for the completion of dimer, (i) coupling of lithiated compound **62** with **58** to give precursor **63** of the final dimer, and (ii) conversion of tertiary amine in **63** to its respective quaternary ammonium group using iodomethane to give the final product **27**. Attempts to couple lithiated **62** with **58** to form **63** have resulted in a mixture of unidentifiable products. Therefore, an alternate method for coupling reaction has to be chosen to form **27** in future.

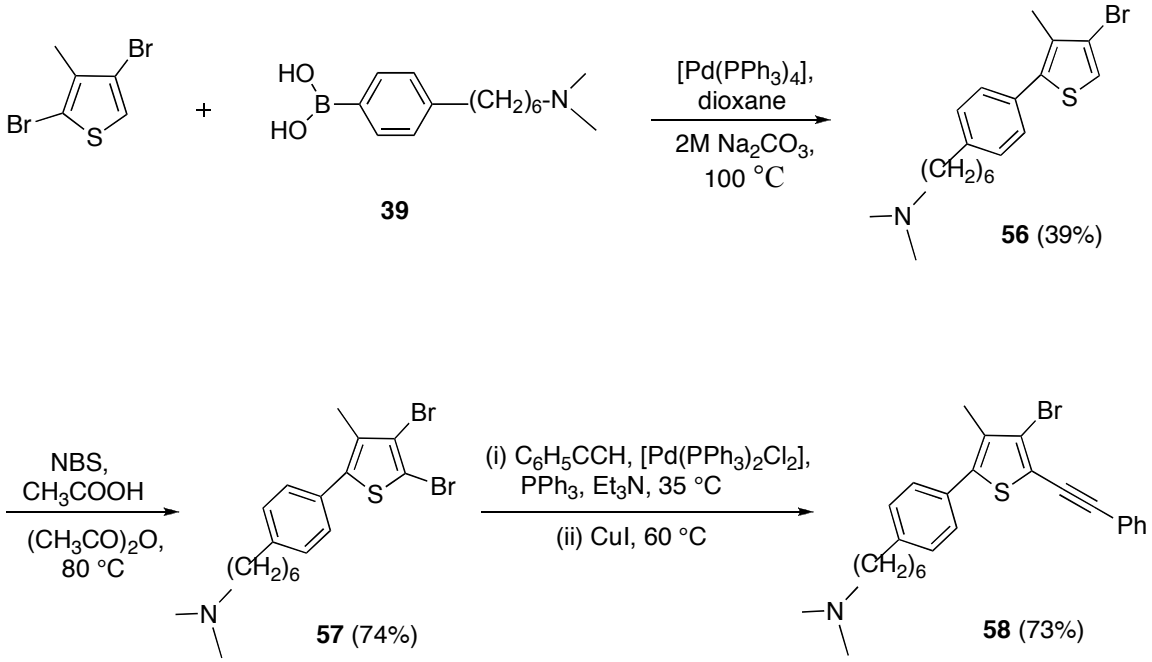

Scheme A.1. Synthesis of **58**.

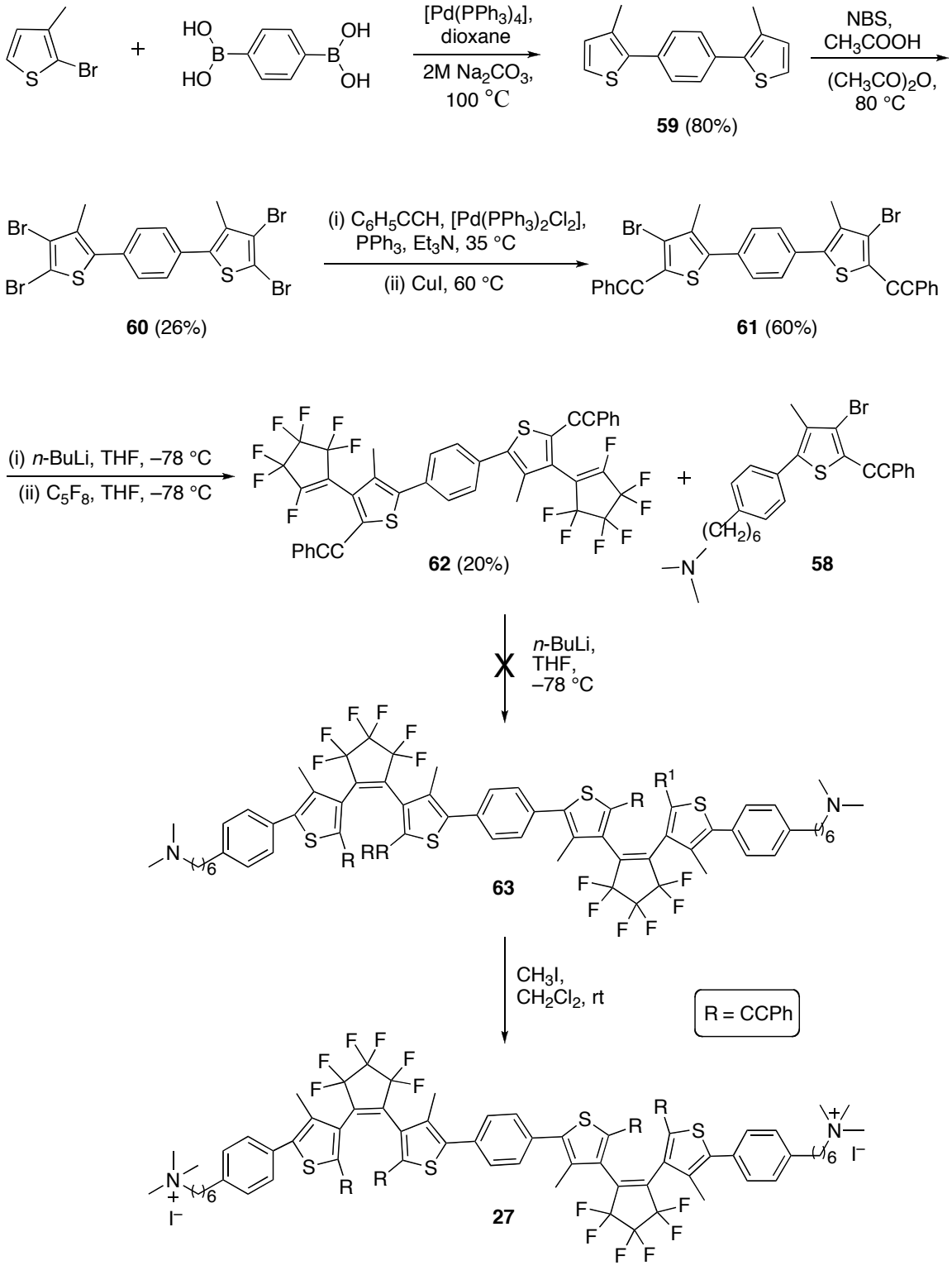

Scheme A.2. Synthesis of dimer **27**.

Procedures for the Attempted Synthesis of Dimer 27

The synthesis of **27** has been adapted from previously reported procedures.[111]

6-(4-(4-Bromo-3-methylthiophen-2-yl)phenyl)-*N*,*N*-dimethylhexan-1-amine (56)

This method is similar to that used for **41**. Purification of the crude product by flash column chromatography (10:1:0.1 ethyl acetate/methanol/triethylamine) gave pure compound **56** as pale yellow oil (39%). ^{1}H NMR ($CDCl_3$, δ): 1.36 (m, 4H, CH_2), 1.46 (m, 2H, CH_2), 1.64 (m, 2H, CH_2), 2.21 (s, 6H, CH_3), 2.24 (t, J = 7.3 Hz, 2H, CH_2), 2.27 (s, 3H, CH_3), 2.64 (t, J = 7.5 Hz, 2H, CH_2), 7.19–7.25 (m, 3H, Ar H), 7.29–7.35 (m, 2H, Ar H). ^{13}C NMR ($CDCl_3$, δ): 15.0, 27.5, 28.0, 29.5, 31.6, 35.8, 45.8, 60.1, 114.3, 120.9, 128.9, 129.2, 131.9, 132.3, 138.9, and 143.0. HRMS-EI (*m*/*z*): $[M]^+$ calcd for $C_{19}H_{26}{}^{79}BrNS$, 379.0964; found 379.0973.

6-(4-(4,5-Dibromo-3-methylthiophen-2-yl)phenyl)-*N*,*N*-dimethylhexan-1-amine (57)

This method is similar to that used for **43**. Purification of the crude product by flash column chromatography (5:1:0.2 ethyl acetate/methanol/triethylamine) gave pure compound **57** as pale yellow oil (74%). ^{1}H NMR ($CDCl_3$, δ): 1.36 (m, 4H, CH_2), 1.43 (m, 2H, CH_2), 1.66 (m, 2H, CH_2), 2.22 (s, 6H, CH_3), 2.25 (t, J = 7.3 Hz, 2H, CH_2), 2.29 (s, 3H, CH_3), 2.64 (t, J = 7.3 Hz, 2H, CH_2), 7.19–7.25 (m, 2H, Ar H), 7.26–7.32 (m, 2H, Ar H). ^{13}C NMR ($CDCl_3$, δ): 18.1, 27.6, 27.8, 29.5, 31.5, 35.9, 45.8, 60.1, 108.9, 118.2, 129.0, 129.1, 131.1, 132.9, 139.3, and 143.4. HRMS-ESI (*m*/*z*): $[M+H]^+$ calcd for $C_{19}H_{25}{}^{79}Br_2NS$, 457.006; found 457.0078.

6-(4-(4-Bromo-3-methyl-5-(phenylethynyl)thiophen-2-yl)phenyl)-*N,N*-dimethylhexan-1-amine (58)

This method is similar to that used for **45**. Purification of the crude product by flash column chromatography (10:1 chloroform/methanol) gave pure compound **58** as pale yellow oil (73%). ^{1}H NMR ($CDCl_3$, δ): 1.37 (m, 4H, CH_2), 1.48 (m, 2H, CH_2), 1.66 (m, 2H, CH_2), 2.23 (s, 6H, CH_3), 2.27 (t, J = 7.3 Hz, 2H, CH_2), 2.29 (s, 3H, CH_3), 2.65 (t, J = 7.6 Hz, 2H, CH_2), 7.19–7.28 (m, 2H, Ar H), 7.30–7.42 (m, 5H, Ar H), 7.52–7.61 (m, 2H, Ar H). ^{13}C NMR ($CDCl_3$, δ): 15.7, 27.5, 27.9, 29.5, 31.5, 35.9, 45.7, 60.1, 82.1, 97.3, 118.5, 120.4, 123.1, 128.6, 128.8, 129.0, 129.2, 131.3, 131.7, 132.7, 139.6, and 143.4. HRMS-EI (*m*/*z*): $[M]^+$ calcd for $C_{32}H_{20}{}^{79}Br_2S_2$, 625.9367; found 625.9355.

1,4-Bis(3-methylthiophen-2-yl)benzene (59)

Sodium carbonate (52 mL of a 2 M aqueous solution) was added dropwise to a stirred mixture of 2-bromo-3-methylthiophene (4.57 g, 25.81 mmol), 1,4-phenyldiboronic acid (2.14 g, 95%, 12.9 mmol) and $Pd(PPh_3)_4$ (0.745 g, 0.644 mmol) in 1,4-dioxane (260 mL) under an atmosphere of argon. After stirring at 100 °C for 3.5 h, the reaction mixture was allowed to cool to room temperature, diluted with diethyl ether (100 mL), poured into water (150 mL) and extracted with diethyl ether (2 × 100 mL). The combined the organic extracts were washed with a saturated aqueous solution of sodium chloride (100 mL), dried over anhydrous sodium sulfate, filtered and concentrated under reduced pressure. Purification of the crude product by flash column chromatography (petroleum ether) gave pure **59** as a colorless solid (2.65 g, 80 %, mp157–158 °C). ^{1}H NMR ($CDCl_3$, δ): 2.38 (s, 6H, CH_3), 6.95 (d, 2H), 6.77 (d, J = 5.1 Hz, Ar H), 7.23 (d, 2H,

J = 5.1 Hz, Ar H), 7.52 (s, 4H, Ar H). ^{13}C NMR ($CDCl_3$, δ): 15.3, 123.7, 129.2, 131.5, 133.6, 133.8, and 137.7. HRMS-ESI (*m*/*z*): $[M+H]^+$ calcd for $C_{16}H_{14}S_2$, 270.0531; found 270.0542.

1,4-Bis(4,5-dibromo-3-methylthiophen-2-yl)benzene (60)

NBS (17.5 g, 98.0 mmol) was added to the suspension of **59** (2.65 g, 9.8 mmol) in acetic anhydride (150 mL) and glacial acetic acid (24 mL). After stirring at 80 °C for 80 min, the reaction mixture was allowed to cool to room temperature, diluted with water (50 mL), neutralized with a saturated aqueous solution of sodium carbonate and extracted with dichloromethane (3 × 100 mL). The combined organic extracts were washed with a saturated aqueous solution of sodium chloride (2 x 100 mL), dried over anhydrous sodium sulfate, filtered and concentrated under reduced pressure. Purification of the crude product by flash column chromatography (4:1 petroleum ether/dichloromethane) gave pure **60** as an off-white solid (1.51 g, 26%, mp 211–212 °C). ^{1}H NMR ($CDCl_3$, δ): 2.34 (s, 6H, CH_3), 7.44 (s, 4H, Ar H). ^{13}C NMR ($CDCl_3$, δ): 16.4, 109.9, 118.6, 129.5, 133.6, 133.7, and 138.3. HRMS-ESI (*m*/*z*): $[M+H]^+$ calcd for $C_{16}H_{10}{}^{79}Br_4S_2$, 581.6952; found 581.6950.

1,4-Bis(4-bromo-3-methyl-5-(phenylethynyl)thiophen-2-yl)benzene (61)

A solution of ethynylbenzene (0.354 g, 5.29 mmol) in triethylamine (7.0 mL) was added dropwise to a stirred solution of **60** (0.964 g, 1.645 mmol) in triethylamine (10.0 mL) followed by the addition of $PdCl_2(PPh_3)_2$ (11.6 mg, 0.0165mmol) and PPh_3 (5.6 mg, 0.0213 mmol) under an atmosphere of argon. After stirring at 35 °C for 15 min, copper

iodide (10 mg, 0.0533mmol) was added to the reaction mixture and stirred at 60 °C for 3.5 h. After allowing the reaction mixture to cool to room temperature, it was neutralized with hydrochloric acid (2.0 M aqueous solution) and extracted with chloroform (3 × 50 mL). The combined organic extracts were washed with a saturated aqueous solution of sodium chloride (80 mL), dried over anhydrous sodium sulfate, filtered and concentrated under reduced pressure. Purification of the crude product by flash column chromatography (5:1 petroleum ether/chloroform followed by neat chloroform) gave pure **61** as a yellow solid (0.615 g, 60%, mp 258–259 °C). ^{1}H NMR ($CDCl_3$, δ): 2.35 (s, 6H, CH_3), 7.35–7.40 (m, 6H, Ar H), 7.51 (s, 4H, Ar H), 7.55–7.61 (m, 4H, Ar H). ^{13}C NMR ($CDCl_3$, δ): 15.9, 119.3, 120.6, 122.9, 128.6, 129.0, 129.5, 131.8, 133.5, 133.8, and 138.5. HRMS-ESI (*m*/*z*): $[M+H]^+$ calcd for $C_{32}H_{20}{}^{79}Br_2S_2$, 625.9367; found 625.9355.

1,4-Bis(3-methyl-4-(perfluorocyclopent-1-enyl)-5-(phenylethynyl)thiophen-2-yl)benzene (62)

n-BuLi (0.46 mL of a 2.5 M solution in hexanes, 0.450 mmol) was added dropwise to a solution of **61** (0.330 g, 0.525 mmol) in THF (25 mL) at –78 °C and under an atmosphere of argon. After stirring for 20 min, the reaction mixture was added dropwise via cannula to a solution of OFCP (2.2 g, 10.47 mmol) in THF (5 mL) at –78 °C. The mixture was stirred for another 5 h at –78 °C and then allowed to warm to room temperature. After 2 h, hydrochloric acid (4.5 mL of a 1.0 M aqueous solution) was added. Following 10 min of vigorous stirring, THF was removed under reduced pressure and the residue was diluted with 50 ml of water and extracted with dichloromethane (3 × 50 mL). The combined organic extracts were washed by a saturated aqueous solution of

sodium bicarbonate (50 mL) followed by a saturated aqueous solution of sodium chloride (60 mL), dried over anhydrous sodium sulfate, filtered and concentrated under reduced pressure. Purification of the crude product by flash column chromatography (1:20 petroleum ether/dichloromethane) gave pure compound **62** as a yellow solid (90 mg, 20%). ^{1}H NMR ($CDCl_3$, δ): 2.26 (s, 6H, CH_3), 7.32–7.41 (m, 6H, Ar H), 7.43–7.50 (m, 4H, Ar H), 7.56 (s, 4H, Ar H). ^{19}F NMR ($CDCl_3$, δ): –107.9 (d, *J*=5.2Hz, 4F), –119.4 (d, *J*=5.2Hz, 4F), –124.4 (m, 2F), –130.8 (d, *J*=5.2Hz, 4F). ^{13}C NMR ($CDCl_3$, δ): 14.3, 80.3, 98.7, 122.3, 124.9, 127.8, 128.8, 129.3, 129.9, 131.6, 133.0, 133.3, and 140.2. HRMS-ESI (*m*/*z*): $[M+H]^+$ calcd for $C_{42}H_{20}F_{14}S_2$, 854.0777; found 854.0782.